Cross-Layer Performance Analysis of Resource Allocation Mechanisms in Emerging Wireless Networks

by

Abdulaziz Alorainy

A THESIS SUBMITTED IN PARTIAL FULFILLMENT OF
THE REQUIREMENTS FOR THE DEGREE OF

DOCTOR OF PHILOSOPHY

in

THE COLLEGE OF GRADUATE STUDIES

(Electrical Engineering)

THE UNIVERSITY OF BRITISH COLUMBIA

(Okanagan)

August 2017

The undersigned certify that they have read, and recommend to the College of Graduate Studies for acceptance, a thesis entitled: Cross-Layer Performance Analysis of Resource Allocation Mechanisms in Emerging Wireless Networks submitted by Abdulaziz Alorainy in partial fulfilment of the requirements of the degree of Doctor of Philosophy

Jahangir Hossain, School of Engineering
Supervisor

Julian Cheng, School of Engineering
Supervisory Committee Member

Jonathan Holzman, School of Engineering
Supervisory Committee Member

Long Le, University of Quebec
External Examiner, Professor

August 08, 2017
(Date Submitted to Grad Studies)

Abstract

Due to rapidly increasing contribution of information and communication technology (ICT) industry to global energy consumption and increasing popularity of wireless communications, it is essential to further improve energy efficiency, cellular coverage, and network capacity of emerging wireless networks. Moreover, these improvements must be achieved in a cost-efficient manner. Various solutions are being considered to address these issues and some of these solutions have already been deployed. Examples of these solutions include small cell networks (SCNs), cell sleeping, and carrier aggregation (CA). Different services transmitted over wireless networks have different quality of service (QoS) requirements in terms of delay constraint and packet loss probability (PLP). In order to maintain these QoS requirements, resource allocation mechanisms of radio resources such as power and bandwidth play an important role. More importantly, analytical models, which enable the system designer to compare data link layer QoS performance measures of different resource allocation mechanisms and to determine various design parameters, are highly desirable.

In this thesis, we mainly focus on development of analytical models via cross-layer design approach. In particular, we develop queuing analytical models that capture various aspects of emerging wireless networks. These models assist the system designer to gauge data link layer QoS performance measures beforehand for various operating and system parameters. As such QoS requirements of user equipments (UEs) can be ensured by tuning/selecting design parameters.

Preface

I am the primary researcher for this thesis. I have identified and formulated the research problems. Mathematical analysis and formulation of the problems were totally carried out by me. I wrote the computer programs for implementing the mathematical models and for simulating performances of considered resource allocation mechanisms. Also, I have materialized the ideas and prepared manuscripts for scholarly publication. Prof. Mohammed-Slim Alouini is a co-author for his contribution in Chapter 4. He provided access to computational facilities at King Abdullah University of Science and Technology (KAUST) that were necessary for implementing our developed models.

The following is a list of publications during my PhD program.

- Journal articles:

  J1. A. Alorainy and Md. Jahangir Hossain, "Cross-layer performance analysis of channel scheduling mechanisms in small cell networks with non-line-of-sight wireless backhaul links," *IEEE Trans. Wireless Commun.*, vol. 14, no. 9, pp. 4907-4922, Sep. 2015.

  J2. E. Bedeer, A. Alorainy, Md. Hossain, O. Amen, and M.-S. Alouini "Fairness-aware energy-efficient resource allocation for AF cooperative OFDMA networks," *IEEE Journal on Selected Areas in Commun.*, vol. 33, no. 12, pp. 2478-2493, Dec. 2015.

  J3. A. Alorainy and Md. Jahangir Hossain, "Cross-layer performance of downlink dynamic cell selection with random packet scheduling and partial CQI feedback in wireless networks with cell sleeping," *IEEE Trans. Wireless Commun.* (pending minor revision).

  J4. A. Alorainy and Md. Jahangir Hossain, "Cross-layer performance of downlink multi-flow carrier aggregation in heterogeneous networks," *IEEE Trans. Commun.* (to revise and resubmit).

- Conference articles:

  C1. A. Alorainy, S. M. Tanzil, and Md. Hossain, "Cross-layer performance of channel scheduling mechanisms in small cell networks," in Proc. of the *IEEE Wireless Comm. and Networking Conf. (WCNC'14)*, Istanbul, Turkey, pp. 1727-1732, Apr. 2014.

  C2. A. Alorainy and Md. Hossain "Dynamic cell selection in wireless networks with cell sleeping: cross-layer performance analysis," in Proc. of the *IEEE Global Commun. Conf. (Globecom)*, San Diego, CA, USA, pp. 1-7, Dec. 2015.

  C3. A. Alorainy, Md. Hossain, and M.-S. Alouini "Multi-flow carrier aggregation in heterogeneous networks: cross-layer performance analysis," in Proc. of the *IEEE Globecom workshops (GC Wkshps)*, Washington, DC, USA, pp. 1-7, Dec. 2016.

Table of Contents

Abstract . . . . . **iii**

Preface . . . . . **iv**

Table of Contents . . . . . **viii**

List of Tables . . . . . **ix**

List of Figures . . . . . **xiii**

List of Acronyms . . . . . **xiv**

Acknowledgment . . . . . **xvi**

Chapter 1: Introduction and Overview **1**

1.1 Introduction 1

1.2 Motivation, Objective and Contributions 3

1.3 Background and Literature Review 4

1.3.1 Small cell networks with non-line-of-sight wireless backhaul links . . 4

1.3.2 DL DCS in wireless networks with cell sleeping 5

1.3.3 DL multi-flow CA in HetNets 6

1.4 Queuing Models 8

Chapter 2: Cross-Layer Performance of Channel Scheduling Mechanisms in Small Cell Networks with Non-Line-of-Sight Wireless Backhaul Links **10**

2.1 Synopsis 10

2.2 System Model and Operating Assumptions 11

2.2.1 Overall system description 11

2.2.2 Channel model and adaptive transmission 13

2.2.3 Channel scheduling mechanisms 15

2.3 Development of the Queueing Model 16
2.3.1 Packet arrival and buffer dynamics 16
2.3.2 System's state space and transition probability 17
2.3.3 Derivation of performance measures 25
2.4 Numerical Results and Discussions 27
2.4.1 Effect of number of interfering small cells 27
2.4.2 Effect of the size of the small cells 28
2.4.3 Effect of average SNR in the backhaul link 29
2.4.4 Effect of target bit error rate 30
2.4.5 Effect of varying the number of UEs 30
2.4.6 Example applications of the developed queuing model 31

Chapter 3: DL Dynamic Cell Selection in Wireless Networks with Cell Sleeping 36
3.1 Synopsis 36
3.2 System Model and Operating Assumptions 37
3.2.1 Overall system description 37
3.2.2 Channel model and adaptive transmission 38
3.2.3 Channel scheduling and cell selection 40
3.2.4 Packet arrival and scheduling 41
3.3 Formulation of the Queueing Model 42
3.3.1 Tagged UE's joint cell selection and sum transmission rate 42
3.3.2 System's overall state space and transition probability 45
3.3.3 Steady state solution and derivation of performance measures 48
3.4 Numerical Results and Example Applications 51
3.4.1 Effect of the packet forwarding probability 52
3.4.2 Effect of varying the number of channels 54
3.4.3 Effect of varying the location of the tagged UE 56
3.4.4 Effect of varying the number of UEs in the sleeping cell 57
3.4.5 Comparison with state-of-the-art DCS 59
3.4.6 Example applications of the developed queuing model 69

Chapter 4: DL Multi-Flow CA in Heterogeneous Networks 71
4.1 Synopsis 71
4.2 System Model and Operating Assumptions 72
4.2.1 Overall system description 72

4.2.2 Channel model, adaptive transmission, channel scheduling and partial CQI feedback . . . 73
4.2.3 Packet arrival model and packet scheduling . . . 75
4.3 Formulation of the Queueing Model . . . 76
4.3.1 Tagged MUE joint sum transmission rate . . . 76
4.3.2 System's state space and transition probability . . . 80
4.3.3 Steady state solution and derivation of performance measures . . . 82
4.4 Numerical Results and Example Applications . . . 86
4.4.1 Effect of the packet forwarding probability . . . 87
4.4.2 Effect of varying the number of small cells . . . 88
4.4.3 Effect of varying the number of MUEs . . . 89
4.4.4 Effect of varying the ER of the reference small cell . . . 90
4.4.5 Example applications of the developed queuing model . . . 91

Chapter 5: Conclusion . . . 97

Bibliography . . . 99

Appendices . . . 105
Appendix A: Derivation of Block Sub-Matrices of $\mathbf{P}$ in Chapter 2 . . . 106
Appendix B: Derivation of Block Sub-Matrices $\mathbf{B2}_{\delta 2}^{(q2)}(\lambda)$ in Chapter 2 . . . 108
Appendix C: Derivation of Block Sub-Matrices of $\mathbf{P}$ in Chapter 3 . . . 110
Appendix D: Proof of Eq. (3.6) . . . 113
Appendix E: Proof of Eq. (3.7) . . . 115
Appendix F: Proof of Eq. (3.10) . . . 116
Appendix G: Proof of Eq. (3.17) . . . 117
Appendix H: Derivation of Block Sub-Matrices of $\mathbf{P}$ in Chapter 4 . . . 119
Appendix I: Derivation of Block Sub-Matrices $\mathbf{B}_{\delta_S}^{(q_S)}(i)$ in Chapter 4 . . . 121
Appendix J: Proof of Eq. (4.6) . . . 123
Appendix K: Proof of Eq. (4.7) . . . 125

List of Tables

Table 2.1 Summary of parameter values. 28

Table 3.1 Summary of parameter symbols and values. 51

Table 4.1 Summary of parameter symbols and values. 86

List of Figures

Figure 2.1 An example of a two-tier cellular network with macrocells and small cells (darker areas show the coverage of SBSs) 12
Figure 2.2 A typical SBS connected to the CN via NLOS wireless backhaul link. For clarity the CN buffer and the SBS buffer of a particular UE are shown in this figure. 12
Figure 2.3 Packet loss rate vs. number of interfering SBSs. 29
Figure 2.4 Average delay vs. number of interfering SBSs. 30
Figure 2.5 Packet loss probability vs. the radius of the small cells. 31
Figure 2.6 Average queuing delay vs. the radius of the small cells. 32
Figure 2.7 Packet loss probability for different values of the average received SNR in the backhaul link. 33
Figure 2.8 Average delay for different values of the average received SNR in the backhaul link. 33
Figure 2.9 Packet loss probability for different values of target bit error rate, BER_0. 34
Figure 2.10 Average queuing delay for different values of target bit error rate, BER_0. 34
Figure 2.11 Packet loss probability vs. number of UEs in the reference small cell. 35
Figure 2.12 Average queuing delay vs. number of UEs in the reference small cell. 35

Figure 3.1 An example of first tier of a cellular network with a sleeping cell (green cell corresponds to the sleeping cell). 38
Figure 3.2 A flow chart of the considered DCS scheme. 40
Figure 3.3 The resulting F/J queuing system. 43
Figure 3.4 Packet loss probability vs. packet forwarding probability (markers correspond to Monte Carlo simulation results. $m_2 = 0$ corresponds to fixed cell selection with BS_1 and $m_1 = 0$ corresponds to fixed cell selection with BS_2). 52

Figure 3.5 Average queuing delay vs. packet forwarding probability (markers correspond to Monte Carlo simulation results. $m_2 = 0$ corresponds to fixed cell selection with BS_1 and $m_1 = 0$ corresponds to fixed cell selection with BS_2). 53
Figure 3.6 Delay CDF of various packet scheduling, CQI feedback and packet arrival scenarios (markers correspond to Monte Carlo simulation results). 54
Figure 3.7 Packet loss probability vs. the number of outer band channels (markers correspond to Monte Carlo simulation results. $m_2 = 0$ corresponds to fixed cell selection with BS_1 and $m_1 = 0$ corresponds to fixed cell selection with BS_2). 55
Figure 3.8 Average queuing delay vs. the number of outer band channels (markers correspond to Monte Carlo simulation results. $m_2 = 0$ corresponds to fixed cell selection with BS_1 and $m_1 = 0$ corresponds to fixed cell selection with BS_2). 56
Figure 3.9 Delay CDF for various number of outer band channels, packet scheduling, CQI feedback and packet arrival scenarios (markers correspond to Monte Carlo simulation results). 57
Figure 3.10 Packet loss probability vs. tagged UE's location (markers correspond to Monte Carlo simulation results. $m_2 = 0$ corresponds to fixed cell selection with BS_1 and $m_1 = 0$ corresponds to fixed cell selection with BS_2). 58
Figure 3.11 Average queuing delay vs. tagged UE's location (markers correspond to Monte Carlo simulation results. $m_2 = 0$ corresponds to fixed cell selection with BS_1 and $m_1 = 0$ corresponds to fixed cell selection with BS_2). 59
Figure 3.12 Delay CDF of various locations, packet scheduling, CQI feedback and packet arrival scenarios (markers correspond to Monte Carlo simulation results). 60
Figure 3.13 Packet loss probability vs. number of UEs in the sleeping cell (markers correspond to Monte Carlo simulation results. $m_2 = 0$ corresponds to fixed cell selection with BS_1 and $m_1 = 0$ corresponds to fixed cell selection with BS_2). 61
Figure 3.14 Average queuing delay vs. number of UEs in the sleeping cell (markers correspond to Monte Carlo simulation results. $m_2 = 0$ corresponds to fixed cell selection with BS_1 and $m_1 = 0$ corresponds to fixed cell selection with BS_2). 62

Figure 3.15 Delay CDF of various packet scheduling, number of UEs in the sleeping cell, CQI feedback and packet arrival scenarios (markers correspond to Monte Carlo simulation results). 63
Figure 3.16 Packet loss probability vs. the number of outer band channels (Non-solid lines correspond to various CQI feedback scenarios and markers correspond to simulation results of the considered DCS scheme) . . 63
Figure 3.17 Average queuing delay vs. the number of outer band channels (Non-solid lines correspond to various CQI feedback scenarios and markers correspond to simulation results of the considered DCS scheme). . 64
Figure 3.18 Delay CDF for various number of outer band channels, packet scheduling, CQI feedback and packet arrival scenarios (Non-solid lines correspond to various CQI feedback scenarios and markers correspond to simulation results of the considered DCS scheme). 64
Figure 3.19 Packet loss probability vs. X2 interface delay (Non-solid lines correspond to various CQI feedback scenarios and markers correspond to simulation results of the considered DCS scheme) 65
Figure 3.20 Average queuing delay vs. X2 interface delay (Non-solid lines correspond to various CQI feedback scenarios and markers correspond to simulation results of the considered DCS scheme). 65
Figure 3.21 Packet loss probability vs. tagged UE's location (Non-solid lines correspond to various CQI feedback scenarios and markers correspond to simulation results of the considered DCS scheme) 66
Figure 3.22 Average queuing delay vs. tagged UE's location (Non-solid lines correspond to various CQI feedback scenarios and markers correspond to simulation results of the considered DCS scheme). 66
Figure 3.23 Delay CDF for various locations, packet scheduling, CQI feedback and packet arrival scenarios (Non-solid lines correspond to various CQI feedback scenarios and markers correspond to simulation results of the considered DCS scheme). 67
Figure 3.24 Packet loss probability vs. number of UEs in the sleeping cell (Non-solid lines correspond to various CQI feedback scenarios and markers correspond to simulation results of the considered DCS scheme) . . 68
Figure 3.25 Average queuing delay vs. number of UEs in the sleeping cell (Non-solid lines correspond to various CQI feedback scenarios and markers correspond to simulation results of the considered DCS scheme). . 68

Figure 3.26 Delay CDF for various number of UEs in the sleeping cell, packet scheduling, CQI feedback and packet arrival scenarios (Non-solid lines correspond to various CQI feedback scenarios and markers correspond to simulation results of the considered DCS scheme). . . . 69

Figure 4.1 An example of a two-tier cellular network with CRE of the small cells. 73
Figure 4.2 The resulting F/J queuing system (for clarity only tagged MUE and its serving SBS and MBS are shown). 76
Figure 4.3 PLP vs. packet forwarding probability (markers correspond to simulation results). 87
Figure 4.4 Average queuing delay vs. packet forwarding probability (markers correspond to simulation results). 88
Figure 4.5 Delay CDF of various cases of packet arrival, amount of CQI feedback and packet scheduling parameter (markers correspond to simulation results). 89
Figure 4.6 Packet loss probability vs. the number of interfering small cells (markers correspond to simulation results). 90
Figure 4.7 Average queuing delay vs. the number of interfering small cells (markers correspond to simulation results). 91
Figure 4.8 Delay CDF for several cases of packet arrival, amount of CQI feedback and number of interfering small cells (markers correspond to simulation results). 92
Figure 4.9 Packet loss probability vs. number of MUEs (markers correspond to simulation results). 93
Figure 4.10 Average queuing delay vs. number of MUEs (markers correspond to simulation results). 93
Figure 4.11 Delay CDF for several cases of packet arrival, amount of CQI feedback and number of MUEs (markers correspond to simulation results). 94
Figure 4.12 Packet loss probability vs. the ER of the reference small cell (markers correspond to simulation results). 94
Figure 4.13 Average queuing delay vs. the ER of the reference small cell (markers correspond to simulation results). 95
Figure 4.14 Delay CDF for several cases of packet arrival, amount of CQI feedback and ER of the reference small cell (markers correspond to simulation results). 95

List of Acronyms

BS	Base station
CA	Carrier aggregation
CAC	Call admission control
CDF	Cumulative distribution function
CF	Characteristic function
CN	Connector node
CoMP	Coordinated multi point
CQI	Channel quality information
CRE	Cell range expansion
DCS	Dynamic cell selection
DL	Downlink
DTMC	Discrete time Markov chain
ER	Expanded range
F/J	Fork/join
HetNets	Heterogeneous networks
ICIC	Inter-cell interference coordination
ICT	Information and communications technologies
LTE-A	Long term evolution advanced
MBS	Macro base station
MUE	Macro user equipment
NLOS	Non-line-of-sight
OFDMA	Orthogonal frequency division multiple access
OSI	Open systems interconnection
PLP	Packet loss probability
PSG	Packet serving gateway
QBD	Quasi birth and death
QoS	Quality of service
RAT	Radio access technology
SBS	Small cell base station

SCN	Small cell network
SINR	Signal-to-interference-plus-noise-ratio
SNR	Signal-to-noise-ratio
SUE	Small cell user equipment
UE	User equipment

Acknowledgment

I reserve my thanks to Allah the Almighty for his countless blessings.

I would like to express my deepest gratitude to my supervisor, Dr. Jahangir Hossain for his guidance and support. I thank him for his encouragement and helpful advices, which made this endeavour productive and enriching. My gratitude and thanks are extended to Dr. Mohamed Alkanhal, Director of Communications and Information Technology Research Institute at King Abdulaziz City for Science and Technology (KACST), for his unequivocal support. I thank Prof. Mohammed-Slim Alouini for his helpful advices and for hosting me at his lab. I also thank Dr. Ebrahim Bedeer for his helpful advices and fruitful collaboration.

My appreciation goes to all my family members for their support. I am especially thankful to my parents for their love and support. I thank my wife for her encouragement, support and sacrifice.

I would like to thank Khaled Alqahtani, a former colleague and a dear friend, for his help, which had a lasting impact on my career. I also thank members of my research group for their encouragement.

Chapter 1

Introduction and Overview

1.1 Introduction

One key design challenge that the emerging wireless networks are facing is to meet the rapidly increasing demand for high data rate and low latency services. For example, current long term evolution advanced (LTE-A) specifications can support up to 1Gbps peak data rate, 10Mpbs user equipment (UE) experienced data rate and 50ms latency [1]. However, emerging wireless networks are expected to support up to 20Gbps peak data rate, 100Mpbs UE experienced data rate and latency below 10ms [1]. So, peak data rates are expected to increase 20 times, UE experienced data rates are expected to increase 10 times and latencies are expected to reduce by a factor of 5. Another design challenge is to reduce the contribution of information and communications technologies (ICT) industry to energy consumption and global CO_2 emission. It is estimated that ICT industry today is responsible for 2% of global CO_2 emission [2]. With the increasing demand for high data rates and current energy efficiency trends, ICT based emissions are expected to grow. Therefore, it is necessary to significantly improve the energy efficiency of emerging wireless networks. Moreover, these improvements in the supported data rates and energy consumption of emerging wireless networks must be achieved in a cost-efficient manner due to flattening-out revenue per UE and revenue per bit [3].

One of the main features of emerging wireless networks that addresses the aforementioned challenges is the utilization of multi radio access technologies (multi-RATs). For example, low-power access nodes, also referred to as small cells, are densely deployed in an unplanned manner forming so-called small cell networks (SCNs). These SCNs coexist with the existing macrocellular networks, resulting in multi-tier cellular networks, which are referred to as heterogeneous networks (HetNets) [4]. HetNets play an important role to meet the ever-increasing demand for high data rates and to improve energy efficiency with low deployment and operational cost [4].

Another promising technology that is implemented in emerging wireless networks is the utilization of multiple component carriers to achieve high data rates, which is known as carrier aggregation (CA). In CA, several component carriers are used simultaneously for data transmission. These component carriers can be in contiguous band of the spectrum,

or they can be in different bands. For instance, CA of up to five component carriers has been discussed for LTE-A [5], [6]. CA can be classified into two types based on the UE association criteria, namely, single-flow CA and multi-flow CA. In single-flow CA, a UE is served by a single base station (BS) from a given tier using multiple component carriers, whereas multiple BSs from different tiers using distinct component carriers serve a UE in multi-flow CA [7], [5]. Multi-flow CA results in significant performance improvement compared to single-flow CA [7].

In order to improve the overall power consumption, under-utilized BSs are inactivated. This process is referred to as cell sleeping. Recent studies have shown that BSs can be largely under-utilized as the traffic load varies over time and location. Traffic load remaining below 10% is estimated to be 30% in week days and 45% at weekends [8]. Also, it is estimated that BSs are responsible for 90% of the total energy consumption while UEs consume only 10% [8]. Moreover, static energy consumption constitutes $60\% - 80\%$ of the total energy consumed by a given BS [9]. In other words, most of the energy consumed by a BS is independent of the traffic load. Therefore, cell sleeping can greatly enhance the energy efficiency of wireless networks.

While the above mentioned solutions have great potentials to address above mentioned challenges, the performance improvements using these solutions can be easily squandered if quality of service (QoS) requirements are not ensured for networks' UEs. In particular, different services transmitted over wireless networks have different QoS requirements. In order to maintain these QoS requirements, resource allocation mechanisms of radio resources such as power and bandwidth play an important role. More importantly, analytical models that enable the system designer to gauge and compare data link layer QoS performances of different resource allocation mechanisms are highly desirable. Moreover, these models will provide an excellent opportunity to tune various design parameters in order to meet QoS requirements.

Cross-layer design and performance analysis allow to measure and to improve performances of wireless networks while accounting for interactions among different layers of communication protocol stack. Data link layer is the second layer in the open systems interconnection (OSI) model, which consists of seven layers, and it is concerned with packet-level data delivery. The QoS parameters of the data link layer include delay constraint and packet loss probability (PLP). Of particular interest is the investigation of data link layer QoS parameters such as packet delay and PLP while jointly capturing various data link layer and physical layer parameters such as link error, time varying nature of the channels, channel scheduling mechanisms, channel quality feedback, and bursty packet arrivals.

1.2 Motivation, Objective and Contributions

When implementing a resource allocation mechanism, it is important to understand the relationships between different system parameters and the the resource allocation mechanism, and the resulting system performance. This can be realized by leveraging analytical models to derive these relationships in an accurate and readily verifiable way. Moreover, these analytical models are very useful to tune/select design parameters in order to maintain QoS requirements of UEs. For example, as long as QoS requirements are maintained, it is desired to maximize the number of served UEs in order to maximize revenue.

A common thread in this thesis is the development of innovative analytical models that take cross-layer interactions between physical layer and data link layer into consideration. These models can be used to evaluate QoS performances of UEs in the network and to tune various system and operating parameters to maintain QoS requirements. We consider following wireless networks: SCNs with non-line-of-sight wireless backhaul links, downlink (DL) dynamic cell selection (DCS) in wireless networks with cell sleeping, and DL multi-flow CA in HetNets. The resource allocation mechanisms include channel scheduling, packet scheduling, and cell selection.

The key contributions of this thesis are as follows.

1. In Chapter 2, we develop a queuing analytical model that considers the channel scheduling mechanisms in the backhaul and access links of SCNs, the time varying nature of the channels, bursty packet arrivals as well as the network topology e.g., the number and the coverage of the small cells.

2. In Chapter 3, we consider a DCS transmission scheme for serving sleeping cell UEs and develop a cross-layer analytical model that considers the time varying nature of the channels, channel scheduling mechanism, partial channel quality information (CQI) feedback, cell selection mechanism, bursty packet arrivals and packet scheduling mechanism.

3. In Chapter 4, we investigate the cross-layer performance of multi-flow CA in HetNets by developing a cross-layer queuing analytical model that takes into account the time varying channels, the channel scheduling algorithm, partial CQI feedback and the number of component carriers deployed at each tier of the HetNet. Our developed model also accounts for stochastic packet arrivals and the packet scheduling mechanism.

1.3 Background and Literature Review

In this section we provide the necessary background and literature review for various state-of-the-art wireless systems that are considered in this thesis.

1.3.1 Small cell networks with non-line-of-sight wireless backhaul links

SCNs[1] are considered as one of the potential solutions for cellular coverage and network capacity improvement. With small cells, traffic can be offloaded from the macrocells. Small cell base stations (SBSs) are easier and cheaper to manufacture and maintain. Moreover, they improve the energy efficiency of the networks and the networks' UEs due to a relatively shorter distance between the transmitter and the receiver [10]. In fact, small cells are an integral part of future wireless networks and have already been deployed.

Backhaul link is needed to connect the SBSs to the core/global network [11]. Many different wireless and wired technologies have been proposed as backhaul solutions for SBSs. A detailed portfolio of solutions available for backhauling small cells for various deployment scenarios has been provided in [11]. While fixed-line backhaul solutions provide better capacity, operators are generally limited by the lack of copper and fiber availability, as well as by the need to deploy SBSs on locations that have limited wireline access. Moreover, a line-of-sight microwave backhaul solution requires a direct line-of-sight, which is difficult to achieve in urban areas because of buildings and other structures. Also this solution cannot be applied for indoor SBSs. As such non-line-of-sight (NLOS) wireless link provides backhaul solution for cost-effective scalable small cell deployments [12].

Sub 6-GHz is of particular interest for NLOS backhaul solution due to its propagation characteristics [11]. Although this band can be area licensed or unlicensed, operators will often choose licensed spectrum to maintain QoS of the small cell UEs. Licensed backhaul spectrum is also preferred to avoid external interference and to allow a scalable high capacity backhaul network [11]. Licensed frequency bands in the sub-6 GHz range vary by geography. Although a number of spectrum allocations in this frequency range is fully occupied for mobile access services, there are many under-utilized allocations. These include small fragmented unpaired allocations, as well as frequency ranges above 3 GHz, which, due to higher propagation losses, are sub-optimal for providing mobile connectivity to handsets in the access link. These spectrum allocations are ideally suited to NLOS small cell backhaul [11]. A SBS, which is connected to the core/global network via a backhaul link, serves the UEs of that particular small cell. Throughout this thesis, we refer to the link between the SBS and the end UEs as the access link. While having

[1] In the literature, microcells, femtocells and picocells are referred to as small cells. Throughout this thesis, we use the term small cells in general.

separate frequencies for NLOS backhaul link and access link can be expensive, using same frequency for both links can lead to excessive interferences. If same frequency band is used for both links, the operators need to have some frequency reuse plan such as frequency/time division multiplexing to avoid interference between these links. In the literature, it has been suggested to use different frequencies for the access and backhaul links [11]. The spectrum allocated for access link can be shared by BSs from different tiers in two different methods, namely, dedicated and shared spectrum access [13], [14].

NLOS wireless link typically uses a mutlicarrier, i.e., orthogonal frequency division multiple access (OFDMA) transmission due to its high tolerance to multipath fading [11]. Also due to its inherent advantages, OFDMA based physical layer has been standardized as access technology for many contemporary wireless systems. Due to fading in wireless channels, channel qualities in both links can vary over time. In order to take advantage of the varying nature of wireless channels, rate adaptive transmission scheme is employed in practice. In such multi-carrier based dual hop systems, the channel scheduling mechanism employed in the backhaul link and the channel scheduling mechanism employed in the access link affect QoS parameters.

Recently research works have been done towards analyzing coverage and ideal capacity/spectral efficiency of SCNs that coexist with the traditional macrocells [15]-[18]. These works mainly focused on analyzing access link theoretical capacity, throughput and/or outage probability, and did not consider the impact of backhaul link in their studies [15]-[17]. In [18], authors have analyzed coverage and ideal capacity of the backhaul link without taking the access link of SCNs into consideration. The joint impact of both links on the data link layer performances of UEs in the small cells has been largely ignored in the literature.

1.3.2 DL DCS in wireless networks with cell sleeping

Inactivating under-utilized BSs, also referred to as cell sleeping, has been recently considered for improving the energy efficiency of emerging wireless networks. However, maintaining the QoS requirements of the UEs in a sleeping cell remains as a challenging issue. Various techniques such as cell zooming and coordinated multipoint (CoMP) transmission have been proposed to improve the performance of wireless networks with cell sleeping.

Recently, several works have been done towards analyzing cell sleeping performance and investigating various BS inactivation schemes/patterns [19]-[24]. In [19], the optimal density of sleeping cells to minimize the power consumption while maintaining certain coverage constraints has been studied for homogeneous cellular networks. The optimal density of sleeping cells to maximize the energy efficiency in heterogeneous cellular networks

has been investigated in [20], [21]. In [22], a BS inactivation strategy with guaranteed outage probability and call level QoS is proposed. Also, a distance-aware BS inactivation scheme, where a BS with maximum average distance from its UEs as well as neighbouring cell UEs is inactivated, is proposed in [23]. In [24], coverage and spectral efficiency of cellular systems with cell sleeping have been studied while taking UE association criteria and channel scheduling mechanisms into consideration. In previous works, user-centric approaches to evaluate and maintain the packet level QoS performances of sleeping cell UEs have been largely ignored.

DCS is a category of CoMP transmission that has been recently considered for improving coverage in LTE networks [25]-[28]. In CoMP DCS transmission, at a given time slot, a UE is served by a BS that is selected among a group of candidate BSs. The main limitation of the state-of-the-art DCS approaches is the over utilization of backhaul resources. In particular, as a rule of thumb, existing works assume that all data packets of a particular UE are available at all candidate BSs. Hence, a duplicate of each packet is sent to each candidate BS over the backhaul links. However, backhaul has been recently viewed as the bottleneck of the wireless industry's capacity crisis [3], [29]. It is estimated that the demand for mobile backhaul has increased 10 times from 2011 to 2016 [3]. As a result, the necessary backhaul infrastructure is increasing significantly, which leads to increased capital expenditure. Also, backhaul operational expenditure constitute 30% of the overall operational expenditure [3]. Therefore, packet duplication is cost inefficient for mobile network operators, especially with the flattening out revenue-per-UE and revenue-per-bit [3], [29]. In addition, the backhaul has a significant impact on the overall energy consumption [29], [26].

In OFDMA-based cellular networks, opportunistic resource allocation schemes are employed to take advantage of multiuser diversity and the time varying nature of the channels. For instance, opportunistic channel scheduling and adaptive transmission can be used to maximize the overall throughput of UEs. However, this requires the CQI of all UEs to be available at the BSs for DL transmission [30]. In order to avoid CQI feedback overhead, partial CQI reporting, e.g., best-m in LTE systems, has been proposed in the literature [31], [32]. Also, many current cellular systems are based on *fractional frequency reuse* to maintain high frequency reuse while reducing the interference at cell edge UEs [33].

1.3.3 DL multi-flow CA in HetNets

In HetNets, *cell range expansion* (CRE) has been considered for open access small cells to exploit traffic offloading from the macrocells to the small cells [34],[7],[35]. This enables small cells to serve not only small cell user equipments (SUEs) that are in the coverage area

of the small cells, but also macro user equipments (MUEs) that are in the expanded range (ER) of the small cells. This improves macrocell reliability, load balancing and overall system performance [34].

Moreover, multi-flow CA can be utilized to serve MUEs in the ER of the small cells. This can be achieved through dual connectivity, which was introduced in Release 12 of the 3GPP specifications. From a data plane prospective, two types of dual connectivity have been standardized as follows: the first one with split of data in the core network and the other one with the split of data at the macrocell [36]. While the former is useful when low-latency high-throughput backhaul is available, the latter can be used for median-latency backhaul and/or for supporting mobility [36].

Carrier deployment in HetNets can be done in a shared manner where the small cells utilize component carriers that are also used by the macrocells, or in a dedicated manner where the small cells utilize separate component carriers [5], [37]. While the former has the advantage of full spectrum reuse by all BSs from all tiers, the latter eliminates cross-tier interference. If the available bandwidth for network operators is large ($\geq$ 20 MHz), dedicated carrier deployment is the preferred option [7]. Moreover, multi-flow CA can provide efficient means of utilizing the divided spectrum under dedicated carrier deployment while still eliminating cross-tier interference. This can be achieved by allowing MUEs in the ER of the small cells to be served by all tiers over the entire spectrum [7].

Opportunistic resource allocation algorithms such as adaptive transmission and max-rate channel scheduling are utilized in most of the contemporary wireless networks with OFDMA. Such algorithms can significantly improve the overall network performance through exploiting the time varying channels and the multiuser diversity. For the DL transmission, this requires the UEs to feed back their CQI to the serving BSs. In practice, partial CQI feedback such as best-m in LTE systems is used to reduce CQI feedback overhead, especially in situations where UEs are served by multiple BSs [31], [32], [38]. Also, when a UE is served by multiple BSs in the DL transmission, random packet scheduling can be employed to randomly forward each arriving packet to one of the serving BSs. Then, each BS transmits the forwarded packets to the corresponding UE [38].

In previous works, CRE has been studied to balance the load among the macrocells and the small cells. In [34], [35], the performance of CRE and inter-cell interference coordination (ICIC) techniques has been investigated for shared carrier deployment with a single component carrier. In [5], a load aware model for single-flow CA has been studied for various carrier deployment scenarios. Multi-flow CA with dedicated carrier deployment for load balancing in HetNets has been proposed in [7]. Analytical models that assist to offload traffic from the macrocells to the small cells while maintaining packet-level QoS requirements of MUEs in the ER of the small cells under multi-flow CA have not been

investigated in the literature.

In the literature, queuing analytical models to investigate packet-level performance of traditional cellular networks (where UEs are served by a single BS) have been presented [39], [40]. Also, queuing analytical models have been developed to study packet-level performance of multi-hop cellular networks [41]-[43]. On the other hand, queuing analytical models to investigate packet-level performance of parallel transmission schemes such as multi-flow CA for MUEs in the ER of small cells and multi-RATs have been largely ignored in previous works. Developing such models is highly desirable to study the packet-level performance of emerging parallel transmission technologies [44].

1.4 Queuing Models

Markov processes account for the fundamental theory behind queuing systems. Let $\{X_0, X_1, \cdots, X_n\}$ denote the family of random variables defining a stochastic process. The stochastic process is referred to as a Markov process if the conditional cumulative distribution function (CDF) of its random variable at a given time X_n depends only on its value at the previous time X_{n-1} [45]. A discrete time and discrete state space Markov process is referred to as a discrete time Markov chain (DTMC). Also, a DTMC is characterized by its transition probability matrix $\mathbf{P}$ which describes the one-step transitions between different states (i.e., the transitions from time step n to time step $(n+1)$). If $\mathbf{P}$ is independent of the time step n, the DTMC is described as homogeneous.

For homogeneous DTMCs, a steady-state solution $\boldsymbol{\pi}$ can be obtained as follows:

$$\boldsymbol{\pi}\mathbf{P} = \boldsymbol{\pi}, \tag{1.1}$$

$$\boldsymbol{\pi}\mathbf{1} = 1, \tag{1.2}$$

where $\mathbf{1}$ is a column vector of proper size and all elements equal 1. The one-step transition probabilities given by the transition probability matrix $\mathbf{P}$ of the homogeneous DTMC have no effect on the steady-state solution $\boldsymbol{\pi}$.

For some cases, it is possible to represent a DTMC by a quasi birth and death (QBD)

process as follows:

$$\mathbf{P} = \begin{array}{c} 0 \\ 1 \\ 2 \\ 3 \\ \vdots \\ X-1 \\ X \end{array} \begin{bmatrix} \mathbf{C} & \mathbf{D} & & & & & \\ \mathbf{E} & \mathbf{F} & \mathbf{G} & & & & \\ & \mathbf{I_2} & \mathbf{I_1} & \mathbf{I_0} & & & \\ & & \mathbf{I_2} & \mathbf{I_1} & \mathbf{I_0} & & \\ & & & \ddots & \ddots & \ddots & \\ & & & & \mathbf{I_2} & \mathbf{I_1} & \mathbf{I_0}' \\ & & & & & \mathbf{I_2}' & \mathbf{I_1}' \end{bmatrix}, \tag{1.3}$$

where the elements of $\mathbf{P}$ are generally sub-matrices. It is highly desirable to represent DTMCs using QBD processes since one can apply the matrix-analytic procedure in [46] to efficiently calculate the steady-state probabilities $\boldsymbol{\pi}$.

Wireless networks often operate in a time-slotted manner. The system state space of such wireless networks can be defined as:

$$\boldsymbol{\Omega} = \{(q_1^{(n)}, q_2^{(n)}, \cdots, t_1^{(n)}, t_2^{(n)}, \cdots)\},$$

where $q_i^{(n)}$ is a state variable representing the state of the ith buffer at time slot n and $t_i^{(n)}$ is a state variable representing the state of the ith link at time slot n. All state variables of the systems under consideration are discrete and all these systems are time slotted. Therefore, each system can be represented as a DTMC with transition probability matrix $\mathbf{P}$. We develop analytical models to construct matrix $\mathbf{P}$ for each system under consideration. There are several factors that affect the development of the analytical models. For example, the arrangement of buffers in different systems has a significant impact on developing the analytical models. Also, the dynamics of these buffers in different systems greatly distinguish the analytical models for different systems. Moreover, links states and link selection, which depend on the specifications of each system, are important factors in the derivation of the analytical models. In each chapter, we show the detailed derivation of the analytical models for the system considered in that chapter.

Chapter 2

Cross-Layer Performance of Channel Scheduling Mechanisms in Small Cell Networks with Non-Line-of-Sight Wireless Backhaul Links

2.1 Synopsis

We summarize the main contributions and outcomes of this chapter as follows.

1. We investigate the performances of various channel scheduling mechanisms for the access link and the backhaul link in SCNs. For the access link we consider the so-called max rate/opportunistic channel scheduling mechanism in order to exploit multiuser diversity, while for the backhaul link we consider three different channel scheduling mechanisms, namely, fixed channel scheduling, round robin channel scheduling and access link dependent channel scheduling.

2. We develop an elaborate cross-layer analytical model to analyze various data link layer performances e.g., PLP and average queuing delay jointly capturing the time varying nature of the channels in both links, channel scheduling mechanisms in both links, stochastic packet arrivals, and network topology.

3. Using numerical examples, we demonstrate how the developed cross-layer analytical model can assist network designers to measure and compare beforehand various data link layer QoS performances e.g., end-to-end PLP and average queuing delay of packets for the considered channel scheduling mechanisms. We also show how the developed model can facilitate cross-layer design to select various design parameters such that the data link layer QoS requirements of the small cells' UEs are maintained.

For instance, the developed model can be used to determine whether it is feasible to deploy an additional SBS for given QoS requirements.

The rest of this chapter is organized as follows. In Section 2.2, we provide a detailed description of the system model and various channel scheduling mechanisms under consideration. While in Section 2.3 we develop the queuing analytical model and derive the data link layer performance measures, in Section 2.4 we present some selected numerical results.

2.2 System Model and Operating Assumptions

2.2.1 Overall system description

We consider a similar two-tier cellular network as considered in [15] with macrocells laid out in the traditional grid-based model, and with SBSs arbitrarily deployed within each macrocell as shown in Fig. 2.1. The SBSs are assumed to be of the same type with coverage radius R_{S} while the coverage radius of the macrocells is R_{M}. As considered in [15], we assume that the cell coverage in both tiers to be circular due to the analytical tractability yet with a high accuracy of this model [47]. The network consists of T-layer of neighbouring macrocells covering an area of radius $R_{\mathrm{T}} = R_{\mathrm{M}} + 2TR_{\mathrm{M}}, T = 0, 1, \cdots$.

We consider dedicated spectrum access between macrocell and small cells for simplicity. However, our work can readily be extended for shared spectrum access by using appropriate cross-tier interference model[2]. Since most practical systems today are multi-carrier systems, we consider multiple channels in both links. We consider that N_{A} channels are dedicated to small cells' UEs with full frequency reuse among SBSs.

As shown in Fig. 2.2, a typical SBS deployed within a macrocell serves a number of UEs through its access link. Each SBS is connected to the core/global network and a connector node (CN) (also referred to as a hub node) provides backhaul connection to the SBSs using a number of backhaul wireless channels [48]. The CN is typically situated at a fiber point-of-presence or where high-capacity LOS microwave link is available to connect the CN to the core network. An existing macrocell can be such a site. Each CN can serve a number of SBSs. A scheduler at the CN can allocate the backhaul channels among SBSs [12], [48]. Each group of SBSs (typically 2-10 SBSs) is served by a CN that can allocate the backhaul channels among these SBSs [48]. Also, the backhaul channels can be reused by other CNs to provide backhaul to other groups of SBSs. The interference in a particular backhaul channel due to the spatial reuse of that backhaul channel by another CN is expected to be

[2]In [15], a detailed model to obtain the statistics of the total cross-tier interference for the uplink (UL) transmission has been developed. Also, the authors have explained how that model can be extended to obtain the statistics of the cross-tier interference for DL transmission (see, **Remark 1** in [15]).

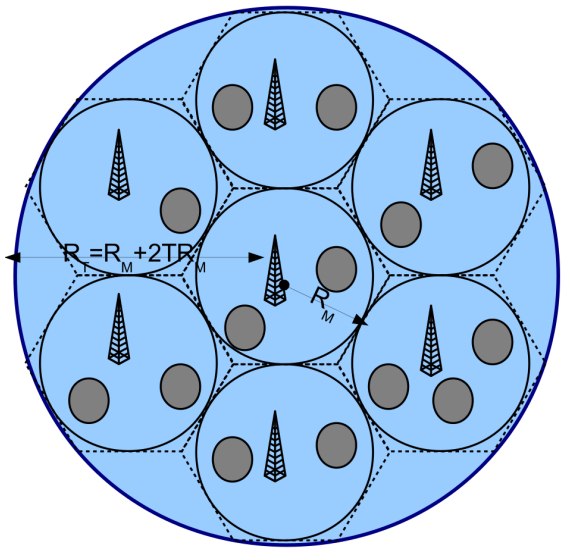

Figure 2.1: An example of a two-tier cellular network with macrocells and small cells (darker areas show the coverage of SBSs)

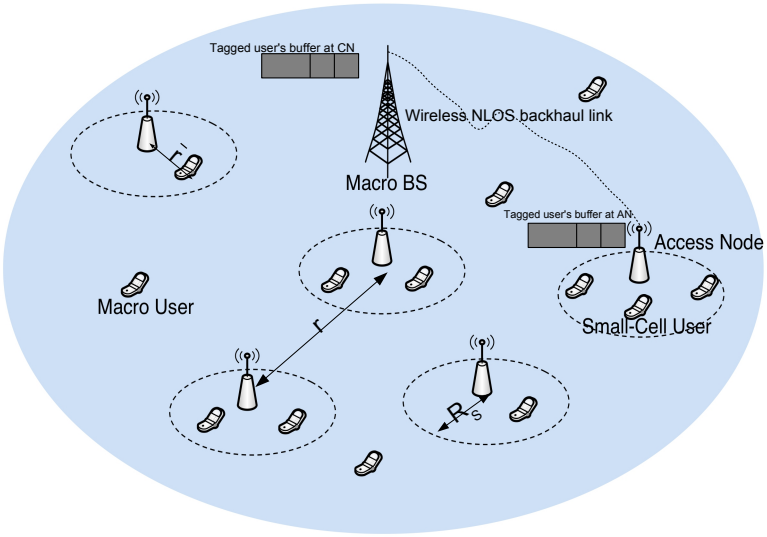

Figure 2.2: A typical SBS connected to the CN via NLOS wireless backhaul link. For clarity the CN buffer and the SBS buffer of a particular UE are shown in this figure.

limited if an appropriate backhaul resource allocation approach is used. For example, in [48], authors proposed a joint channel scheduling and power allocation mechanism in the backhaul network that enables efficient resource allocation while limiting the interference. Therefore, we do not consider interference in the backhaul channels due to the spatial reuse

of backhaul channels. However, our developed model can easily incorporate interference in backhaul channels using appropriate interference model. Let $N_{\mathrm{B},j}$ denote the number of backhaul channels assigned to SBS j.

We consider DL transmission scenario[3] and we analyze the performance of a typical UE in a reference small cell [15]. For notational convenience, we drop the index for the SBS and refer this typical UE as the tagged UE. Also, we assume that there are U UEs uniformly distributed within this reference small cell. There are two packet buffers corresponding to each UE served by the SBSs. The first buffer is referred to as the CN buffer and located at the CN. The second buffer is referred to as the SBS buffer and located at the SBS. Packets of a particular UE that arrive randomly from the core network are temporarily stored at that UE's CN buffer to be transmitted over the backhaul link to the corresponding SBS. These packets arriving at the SBS buffer from the CN buffer are temporarily stored before they are finally transmitted to the UE over the access link. We assume that all buffers have finite length and we consider a time slotted system.

2.2.2 Channel model and adaptive transmission

The Generalized-K composite fading distribution, which has been recently regarded for modelling shadowing and fading channels [49], can be approximated with the Gamma distribution using moment matching method [50]. So, we use the Gamma distribution to model channel fading gain in both backhaul and access links. For each channel in the access link of a particular UE, we assume that the received signal-to-interference-plus-noise-ratio (SINR) to be independent identically distributed (i.i.d) across time slots. Similarly, for each channel in the backhaul link we assume that the received signal-to-noise-ratio (SNR) across time slots to be i.i.d. We map the received SNR/SINR into a finite set of channel states $\mathcal{S} = \{0, 1, \cdots, K-1\}$. Therefore, the received SNR/SINR state of each channel in both links at any time slot can take a value from the set $\mathcal{S}$ randomly. Let us denote the channel state of the ith backhaul channel at time slot n by $s^{(n)}_{\mathrm{B},i}$ and similarly, $s^{(n)}_{\mathrm{A},j,m}$ is used to denote the channel state of the jth access channel of mth UE at time slot n. In order to take advantage of the time varying nature of the channels, transmission rate in each channel in both links is adjusted using adaptive modulation depending on the channel state. The number of packets that can be transmitted in a particular backhaul/access channel at any time slot is proportional to the channel state at that time slot and can be written as follows:

$$x = bk, \quad 0 \leq k \leq K-1, \tag{2.1}$$

[3]The queuing model developed here can easily be extended to analyze packet level performance for the UL transmission scenario.

where b is an integer parameter that depends on modulation order, coding rate and time slot duration.

The ith backhaul channel is said to be in state k at time slot n if $\gamma_k \leq \gamma_{\mathrm{B},i}^{(n)} < \gamma_{k+1}$, where $\gamma_{\mathrm{B},i}^{(n)}$ is the received SNR of the ith backhaul channel[4] at time slot n, and γ_k and γ_{k+1} are the lower boundary thresholds of channel states k and $k+1$, respectively [51], [52]. Similarly for the access link, the jth channel of the mth UE is said to be in state k at time slot n if $\gamma_k \leq \gamma_{\mathrm{A},j,m}^{(n)} < \gamma_{k+1}$, where $\gamma_{\mathrm{A},j,m}^{(n)}$ is the received SINR of the jth access channel of the mth UE at time slot n. The thresholds $\{\gamma_k\}_{k=0}^{K}$ are set to the values such that a target bit error rate (BER_0) is achieved for each transmission mode, i.e., transmission rate [53].

Since we consider the fading power gain in each channel to have Gamma distribution, the probabilities that the ith backhaul channel is in state k at time slot n, $\Pr\{s_{\mathrm{B},i}^{(n)} = k\}, k = 0, 1, \cdots, K-1$, can be calculated using the CDF of the Gamma distribution as follows:

$$\begin{aligned}\Pr\{s_{\mathrm{B},i}^{(n)} = k\} &= \Pr\{\gamma_k \leq \gamma_{\mathrm{B},i}^{(n)} < \gamma_{k+1}\} \\ &= \frac{\Gamma_{\mathrm{L}}(\kappa_{\mathrm{B}}, \gamma_{k+1}/(\bar{\gamma}\theta_{\mathrm{B}}))}{\Gamma(\kappa_{\mathrm{B}})} - \frac{\Gamma_{\mathrm{L}}(\kappa_{\mathrm{B}}, \gamma_k/(\bar{\gamma}\theta_{\mathrm{B}}))}{\Gamma(\kappa_{\mathrm{B}})},\end{aligned} \tag{2.2}$$

where $\Gamma_{\mathrm{L}}(m, x) = \int_0^x t^{m-1}\exp(-t)dt$ denotes the lower incomplete Gamma function, $\Gamma(m) = \int_0^\infty t^{m-1}\exp(-t)dt$ denotes the Gamma function, κ_{B} is the first parameter of the Gamma distribution, θ_{B} is the second parameter of the Gamma distribution, and $\bar{\gamma}$ is the average received SNR which depends on the distance between the SBS and the CN. Similarly, the probabilities that the jth access channel of the mth UE is in state k at time slot n, $\Pr\{s_{\mathrm{A},j,m}^{(n)} = k\}, k = 0, 1, \cdots, K-1$, can be calculated as follows:

$$\begin{aligned}\Pr\{s_{\mathrm{A},j,m}^{(n)} = k\} &= \Pr\{\gamma_k \leq \gamma_{\mathrm{A},j,m}^{(n)} < \gamma_{k+1}\} \\ &= \mathrm{P}_{\mathrm{th}}(\gamma_{k+1}) - \mathrm{P}_{\mathrm{th}}(\gamma_k), \quad k = 0, 1, \cdots, K-1,\end{aligned} \tag{2.3}$$

where $\mathrm{P}_{\mathrm{th}}(x)$ is the probability that the received SINR, $\gamma_{\mathrm{A},j,m}^{(n)}$, is less than the threshold x. This probability can be evaluated using the classical lemma presented in [54] as follows:

$$\mathrm{P}_{\mathrm{th}}(x) = \frac{1}{2} + \frac{1}{\pi}\int_0^\infty \mathrm{Im}\left(\frac{\Phi_D(-j\omega)\Phi_{I_{\mathrm{T}}}(jx\omega)\mathrm{e}^{jx\sigma\omega}}{\omega}\right)d\omega, \tag{2.4}$$

where σ is the thermal noise power, $\Phi_D(-j\omega)$ is the characteristics function (CF) of the received desired signal D, and $\Phi_{I_{\mathrm{T}}}(j\omega)$ is the CF of the total received interference. For Gamma distributed channel with parameters κ_{D} and θ_{D}, the CF of received desired signal

[4]For convenience we refer to the channels in the backhaul link as backhaul channels and channels in the access link as access channels.

$$\Phi_{I_{\mathrm{T}}}(j\omega) = \left[\frac{8\,{}_2F_1[1, \kappa_{\mathrm{I}}, \kappa_{\mathrm{I}}+1+\frac{2}{\eta}, \frac{1}{1-\frac{j\omega\theta_{\mathrm{I}}}{(2R_{\mathrm{T}})^{\eta}}}]}{(\eta\kappa_{\mathrm{I}}+2)(1-\frac{j\omega\theta_{\mathrm{I}}}{(2R_{\mathrm{T}})^{\eta}})^{\kappa_{\mathrm{I}}}} - \sum_{i=0}^{\infty} \frac{(2i-1)!\,{}_2F_1[1, \kappa_{\mathrm{I}}, \kappa_{\mathrm{I}}+1+\frac{3+2i}{\eta}, \frac{1}{1-\frac{j\omega\theta_{\mathrm{I}}}{(2R_{\mathrm{T}})^{\eta}}}]}{2^{i-5}\pi i!(1-4i^2)(\eta\kappa_{\mathrm{I}}+2i+3)(1-\frac{j\omega\theta_{\mathrm{I}}}{(2R_{\mathrm{T}})^{\eta}})^{\kappa_{\mathrm{I}}}} \right]^{\varphi}. \quad (2.6)$$

D can be written as [15]:

$$\Phi_D(j\omega) = {}_2F_1[\kappa_{\mathrm{D}}, \tfrac{-2}{\eta}, \tfrac{-2+\eta}{\eta}, \tfrac{j\omega\theta_{\mathrm{D}}}{R_{\mathrm{S}}^{\eta}}] - \frac{(-j\omega\theta_{\mathrm{D}})^{2/\eta}\Gamma(\kappa_{\mathrm{D}}+\frac{2}{\eta})\Gamma(\frac{-2+\eta}{\eta})}{R_{\mathrm{S}}^2\Gamma(\kappa_{\mathrm{D}})}, \quad (2.5)$$

where η is the path loss exponent and ${}_2F_1[.,.,.,.]$ denotes the Gauss hypergeometric function.

Since we consider dedicated spectrum access and full frequency reuse among the SBSs, in a particular access channel, there will be interferences from other SBSs while macrocells do not cause interference. The CF of the total interference, $\Phi_{I_{\mathrm{T}}}(j\omega)$ can be obtained using a similar approach as presented in [15]. In particular, assuming that all the interfering signals have i.i.d Gamma distribution with parameters κ_{I} and θ_{I}, the CF of I_{T} can be written as shown in eq. (2.6), where in this equation φ is the number of interfering SBSs and ! denotes factorial operation. For non-identically distributed interferers, the CF of I_{T} is the multiplication of the CFs of all interferers.

2.2.3 Channel scheduling mechanisms

For the access link, in order to exploit the multiuser diversity, we consider the so called max-rate/opportunistic channel scheduling which maximizes the overall throughput of the UEs [55]. According to the max-rate/opportunistic channel scheduling, the SBS assigns a particular channel in the access link to the UE which can support the highest transmission rate in that particular channel, i.e., the UE that has the highest channel state. If there are multiple UEs with the highest channel state in that particular channel, the channel is randomly assigned to one of these UEs. For the backhaul link multiuser diversity cannot be exploited since the communication between the CN and the reference SBS using a given set of channels is a one-to-one communication. However, since the CN has a certain number of backhaul channels, different backhaul channel scheduling mechanisms can be employed to transmit packets destined for different UEs over the backhaul link. For the backhaul link, we consider three different channel scheduling mechanisms as described below.

Fixed backhaul channel scheduling

According to the fixed channel scheduling, N_{B} backhaul channels are equally divided for transmitting packets of the U UEs from the CN to the reference SBS. For example, if $N_{\mathrm{B}} = 6$ and $U = 2$, channels 1, 2 and 3 are scheduled to transmit the packets of UE 1 whereas channels 4, 5 and 6 are scheduled to transmit the packets of UE 2.

Round robin backhaul channel scheduling

According to the round robin channel scheduling mechanism, at a particular time slot, all the N_{B} backhaul channels are scheduled to transmit the packets of a particular UE over the backhaul link. For example, if $N_{\mathrm{B}} = 6$ and $U = 2$, at time slot 1 all backhaul channels are scheduled to transmit the packets of UE 1 whereas at time slot 2 all backhaul channels are scheduled to transmit the packets of UE 2 over the backhaul link.

Access link dependent backhaul channel scheduling

According to this channel scheduling mechanism, the number of backhaul channels scheduled for transmitting packets, in a given time slot, for a particular UE is proportional to the number of channels assigned to that UE in the access link. For example, if the kth UE in the SBS is allocated with $N_{\mathrm{A},k}^{(n)}$ channels (using the max-rate scheduling) in the access link at time slot n, $N_{\mathrm{B},k}^{(n)} = \frac{N_{\mathrm{B}}}{N_{\mathrm{A}}} \times N_{\mathrm{A},k}^{(n)}$ backhaul channels are scheduled for transmitting the packets over the backhaul link for this UE at time slot n. For this channel scheduling mechanism, the number of channels in the backhaul link and the number of channels in the access link require to satisfy $\mod (N_{\mathrm{B}}, N_{\mathrm{A}}) = 0$ where $\mod$ is the modulus operator. Throughout this chapter, for simplicity we consider the number of channels in both links to be equal.

2.3 Development of the Queueing Model

2.3.1 Packet arrival and buffer dynamics

Random packet arrival process at the CN buffer of the tagged UE from the core network is assumed to follow a batch Bernoulli process with probability vector $\boldsymbol{\alpha} = \{\alpha_0, \alpha_1, \cdots ., \alpha_Z\}$, where α_i denotes the probability of i packets arrival at a given time slot and Z denotes the maximum number of packets that can arrive at a given time slot. The assumed batch Bernoulli arrival model is very general which can capture different level of burstiness in the traffic arrival process [39]. We assume that the waiting packets at a particular buffer are transmitted in a first-come first-served manner.

The number of packets arriving at the SBS buffer of the tagged UE at time slot n is equal to the number of packets transmitted from the CN buffer of the tagged UE over the backhaul link at time slot n, which can be written as:

$$\lambda^{(n)} = \min(r_{\mathrm{B}}^{(n)}, q_{\mathrm{C}}^{(n)}), \tag{2.7}$$

where $r_{\mathrm{B}}^{(n)}$ is the total number of packets that can be transmitted, at time slot n, over the backhaul channels scheduled for the tagged UE and $q_{\mathrm{C}}^{(n)}$ denotes the number of packets available at the CN buffer of the tagged UE at time slot n. It is obvious that the value of $r_{\mathrm{B}}^{(n)}$ depends on the employed channel scheduling mechanism in the backhaul link and the states of the backhaul channels scheduled for the tagged UE.

We assume that when a packet arrives to a given buffer at time slot n, it can be transmitted at time slot $n+1$ the earliest. So, the buffer dynamics can be written as follows:

$$\begin{aligned} q_{\mathrm{C}}^{(n+1)} &= q_{\mathrm{C}}^{(n)} + \alpha^{(n)} - \lambda^{(n)}, \\ q_{\mathrm{A}}^{(n+1)} &= q_{\mathrm{A}}^{(n)} + \lambda^{(n)} - \min(r_{\mathrm{A}}^{(n)}, q_{\mathrm{A}}^{(n)}), \end{aligned} \tag{2.8}$$

where $r_{\mathrm{A}}^{(n)}$ is the total number of packets that can be transmitted to the tagged UE, at time slot n, over the access channels assigned for the tagged UE. $\alpha^{(n)}$ denotes the number of packets arriving at the CN buffer at time slot n and $q_{\mathrm{A}}^{(n)}$ denotes SBS buffer state at time slot n. Obviously, the value of $r_{\mathrm{A}}^{(n)}$ depends on the number of channels assigned to the tagged UE in the access link and the states of these channels.

2.3.2 System's state space and transition probability

The system can be viewed as time slotted and all state variables are discrete. As such the system can be modelled as a DTMC with transition probability matrix $\mathbf{P}$ where the elements of $\mathbf{P}$ are the transition probabilities of the system's states. This transition probability depends on the channel scheduling mechanism employed at both links. Assuming buffers with finite sizes $Q_{\mathrm{C,max}}$ and and $Q_{\mathrm{A,max}}$ at the CN and at the SBS, respectively, in what follows, we develop the transition probability matrix for the system's state space for different channel scheduling mechanisms.

Fixed backhaul channel scheduling and opportunistic access channel scheduling

For U UEs in the reference SBS, $N_{\mathrm{P}} = \frac{N_{\mathrm{B}}}{U}$ backhaul channels will be scheduled for each UE at each time slot when the fixed backhaul channel scheduling is employed. Let us define a new state variable, $t_{\mathrm{B,FA}}^{(n)}(N_{\mathrm{P}}) = \sum_{i=1}^{N_{\mathrm{P}}} s_{\mathrm{B},i}^{(n)},\ 0 \leq t_{\mathrm{B,FA}}^{(n)}(N_{\mathrm{P}}) \leq (K-1)N_{\mathrm{P}}$. Next,

$$\Pr\{c_{\mathrm{A},i}^{(n)}=j\}=\begin{cases}\sum\limits_{k_2=0}^{j}\cdots\sum\limits_{k_U=0}^{j}\frac{1}{1+f_j(k_2)+\cdots+f_j(k_U)}\Pr\{s_{\mathrm{A},i}^{(n)}=j\}\\ \prod\limits_{l=2}^{U}\Pr\{s_{\mathrm{A},i}^{(n)}=k_l\},\quad 1\le j\le K-1,\\ 1-\sum\limits_{j=1}^{K-1}\Pr\{c_{\mathrm{A},i}^{(n)}=j\},\quad j=0.\end{cases}\tag{2.10}$$

we show the procedure to obtain vector $\grave{\mathbf{T}}_{\mathrm{FA}}(N_{\mathrm{P}})$, whose elements denote the probabilities $\Pr\{t_{\mathrm{B,FA}}^{(n)}(N_{\mathrm{P}})=j\}, j=0,1,\cdots,(K-1)N_{\mathrm{P}}$. We start by defining a function $f_x(y)$ which is equal to 1 if $x=y$ and 0 otherwise.

Then, the elements of $\grave{\mathbf{T}}_{\mathrm{FA}}(N_{\mathrm{P}})$ can be calculated as follows:

$$\begin{aligned}\Pr\{t_{\mathrm{B,FA}}^{(n)}(N_{\mathrm{P}})=j\}=&\sum_{k_1=0}^{K-1}\cdots\sum_{k_{N_{\mathrm{P}}}=0}^{K-1}f_j(k_1+\cdots+k_{N_{\mathrm{P}}})\\ &\prod_{l=1}^{N_{\mathrm{P}}}\Pr\{s_{\mathrm{B},l}^{(n)}=k_l\},\quad j=0,1,\cdots,(K-1)N_{\mathrm{P}}.\end{aligned}\tag{2.9}$$

Next, we define matrix $\mathbf{T}_{\mathrm{FA}}(N_{\mathrm{P}})$ of identical rows, with each row equals $\grave{\mathbf{T}}_{\mathrm{FA}}(N_{\mathrm{P}})$. For opportunistic scheduling in the access link, we define random variable $v_i^{(n)}\in\{0,1\}$ to indicate whether the ith access channel is assigned to the tagged UE at time slot n. If the ith access channel is assigned to the tagged UE, $v_i^{(n)}=1$, otherwise, $v_i^{(n)}=0$. Then, we define state variable for the ith access channel $c_{\mathrm{A},i}^{(n)}=v_i^{(n)}s_{\mathrm{A},i}^{(n)}, 0\le c_{\mathrm{A},i}^{(n)}\le K-1$. The probabilities $\Pr\{c_{\mathrm{A},i}^{(n)}=j\}, j=0,\cdots,K-1$ can be calculated using eq. (2.10).

Next, we define state variable $t_{\mathrm{A,OS}}^{(n)}(N_{\mathrm{A}})=\sum_{i=1}^{N_{\mathrm{A}}}c_{\mathrm{A},i}^{(n)},\ 0\le t_{\mathrm{A,OS}}^{(n)}(N_{\mathrm{A}})\le N_{\mathrm{A}}(K-1)$ with probability vector $\grave{\mathbf{T}}_{\mathrm{OS}}(N_{\mathrm{A}})$. Similar to the backhaul link, the elements of $\grave{\mathbf{T}}_{\mathrm{OS}}(N_{\mathrm{A}})$ can be calculated as follows:

$$\begin{aligned}\Pr\{t_{\mathrm{A,OS}}^{(n)}(N_{\mathrm{A}})=j\}=&\sum_{k_1=0}^{K-1}\cdots\sum_{k_{N_{\mathrm{A}}}=0}^{K-1}f_j(k_1+\cdots+k_{N_{\mathrm{A}}})\\ &\prod_{l=1}^{N_{\mathrm{A}}}\Pr\{c_{\mathrm{A},l}^{(n)}=k_l\},\quad j=0,1,\cdots,(K-1)N_{\mathrm{A}}.\end{aligned}\tag{2.11}$$

We also define matrix $\mathbf{T}_{\mathrm{OS}}(N_{\mathrm{A}})$ of identical rows, with each row equals $\grave{\mathbf{T}}_{\mathrm{OS}}(N_{\mathrm{A}})$. Note that the transition probabilities of the state variables $t_{\mathrm{B,FA}}^{(n)}(N_{\mathrm{P}})$ and $t_{\mathrm{A,OS}}^{(n)}(N_{\mathrm{A}})$ depend on the number of channels. Moreover, we can write the transition probability matrix for the joint state $(t_{\mathrm{B,FA}}^{(n)}(N_{\mathrm{P}}), t_{\mathrm{A,OS}}^{(n)}(N_{\mathrm{A}}))$ of the tagged UE with the fixed backhaul channel scheduling

and opportunistic access channel scheduling as:

$$\mathbf{W}(N_{\mathrm{A}}+N_{\mathrm{P}}) = \mathbf{T}_{\mathrm{FA}}(N_{\mathrm{P}}) \otimes \mathbf{T}_{\mathrm{OS}}(N_{\mathrm{A}}), \tag{2.12}$$

where $\otimes$ denotes the Kronecker product.

Now the transition probability matrix of the system $\mathbf{P}$, whose elements are the transition probabilities of the system's states $\Pr\{q_{\mathrm{C}}^{(n+1)}, q_{\mathrm{A}}^{(n+1)}, t_{\mathrm{B,FA}}^{(n+1)}, t_{\mathrm{A,OS}}^{(n+1)} \mid q_{\mathrm{C}}^{(n)}, q_{\mathrm{A}}^{(n)}, t_{\mathrm{B,FA}}^{(n)}, t_{\mathrm{A,OS}}^{(n)}\}$, can be represented by its block sub-matrices in eq. (2.13), whereas eq. (2.14) further defines the components of each block sub-matrix $\mathbf{A}_{\delta_1}^{(q_{\mathrm{C}})}$. Also, as eq. (2.13) suggests, $\mathbf{P}$ can be represented by a QBD process of the form shown in eq. (2.15). In eqs. (2.13)-(2.15), $Y_1 = bN_{\mathrm{P}}(K-1)$, $Y_2 = bN_{\mathrm{A}}(K-1)$, $X = \lfloor Q_{\mathrm{C,max}}/Y_1 \rfloor$, and $Z_2 = \min(q_{\mathrm{C}}, Y_1)$. Also, a block sub-matrix $\mathbf{A}_{\delta_1,\delta_2}^{(q_{\mathrm{C}},q_{\mathrm{A}})}$ in eq. (2.14) represents the transition of the tagged UE's buffers from state $(q_{\mathrm{C}}, q_{\mathrm{A}})$ to state $(q_{\mathrm{C}} \pm \delta_1, q_{\mathrm{A}} \pm \delta_2)$.

$$\mathbf{P} = \begin{array}{c} \\ 0 \\ 1 \\ 2 \\ 3 \\ \vdots \\ X-1 \\ X \end{array} \begin{bmatrix} \mathbf{C} & \mathbf{D} & & & & & & \\ \mathbf{E} & \mathbf{F} & \mathbf{G} & & & & & \\ & \mathbf{I_2} & \mathbf{I_1} & \mathbf{I_0} & & & & \\ & & \mathbf{I_2} & \mathbf{I_1} & \mathbf{I_0} & & & \\ & & & \ddots & \ddots & \ddots & & \\ & & & & \mathbf{I_2} & \mathbf{I_1} & \mathbf{I_0}' & \\ & & & & & \mathbf{I_2}' & \mathbf{I_1}' \end{bmatrix}. \tag{2.15}$$

In order to construct $\mathbf{P}$, we need to obtain expressions to build block sub-matrices $\mathbf{A}_{\delta_1,\delta_2}^{(q_{\mathrm{C}},q_{\mathrm{A}})}$ in eq. (2.14). In order to obtain these expressions, we define matrices $\mathbf{J}_1$ of size $(\frac{Y_1}{b}+1)\times(\frac{Y_1}{b}+1)$ and $\mathbf{J}_2$ of size $(\frac{Y_2}{b}+1)\times(\frac{Y_2}{b}+1)$ whose elements are one. We also define matrices $\mathbf{O}_1^{(l)}$ of size $(\frac{Y_1}{b}+1)\times(\frac{Y_1}{b}+1)$ with all elements are zero except the elements of lth $(l=0,\cdots,\frac{Y_1}{b})$ row are one. Similarly we define matrices $\mathbf{O}_2^{(m)}$ of size $(\frac{Y_2}{b}+1)\times(\frac{Y_2}{b}+1)$ with all elements are zero except the elements of the mth $(m=0,1,\cdots,\frac{Y_2}{b})$ row are one. Then, we proceed to derive block sub-matrices of $\mathbf{P}$ as shown in eq. (A.1)-(A.9) in Appendix A. In these equations $\circ$ denotes the Hadamard product, and $\mathbf{B2}_{\delta 2}^{(q2)}(\lambda)$ represents the change of the SBS buffer from state, q_2 to state $(q_2 \pm \delta_2)$ with λ packets transmitted from the CN buffer, which is shown in eqs. (B.1)-(B.10) in Appendix B.

Access link dependent backhaul channel scheduling and opportunistic access channel scheduling

For this mechanism, the number of channels scheduled for the tagged UE in the backhaul link is proportional to the number of channels scheduled for this UE in the access

$$
\mathbf{P} = \left[\begin{array}{c|ccccc|c}
\mathbf{A}_0^{(0)} & \mathbf{A}_{1+}^{(0)} & \cdots & \mathbf{A}_{Z+}^{(0)} & & & \\
\hline
\mathbf{A}_{1-}^{(1)} & \mathbf{A}_0^{(1)} & \mathbf{A}_{1+}^{(1)} & \cdots & \mathbf{A}_{Z+}^{(1)} & & \\
\vdots & \vdots & & & \ddots & & \\
\mathbf{A}_{(Y_1-Z+1)-}^{(Y_1-Z+1)} & \mathbf{A}_{(Y_1-Z)-}^{(Y_1-Z+1)} & \cdots & \mathbf{A}_0^{(Y_1-Z+1)} & \cdots & \mathbf{A}_{(Z-1)+}^{(Y_1-Z+1)} & \\
\vdots & \vdots & & & & \vdots & \\
\mathbf{A}_{Y_1-} & \mathbf{A}_{(Y_1-1)-} & \cdots & \cdots & \mathbf{A}_{1-} & \mathbf{A}_0 & \\
\hline
 & \mathbf{A}_{Y_1-} & \cdots & \cdots & \cdots & \mathbf{A}_{1-} & \\
 & & \ddots & & & \vdots & \\
 & & & \mathbf{A}_{Y_1-} & & \mathbf{A}_{(Y_1-Z+1)-} & \\
 & & & & \ddots & \vdots & \\
 & & & & & \mathbf{A}_{Y_1-} & \\
\hline
 & & & & \ddots & &
\end{array}\right.
$$

$$
\left.\begin{array}{ccccccc}
 & & & & & & \\
\hline
 & & & & & & \\
 & & & & & & \\
 & & & & & & \\
\mathbf{A}_{Z+}^{(Y_1-Z+1)} & & & & & & \\
\vdots & \ddots & & & & & \\
\mathbf{A}_{1+} & \cdots & \mathbf{A}_{Z+} & & & & \\
\hline
\mathbf{A}_0 & \cdots & \cdots & \mathbf{A}_{Z+} & & & \\
\vdots & & & \ddots & & & \\
\mathbf{A}_{(Y_1-Z)-} & \cdots & \cdots & \cdots & \mathbf{A}_{(Z-1)+} & \mathbf{A}_{Z+} & \\
\vdots & & & \ddots & \vdots & \vdots & \ddots \\
\mathbf{A}_{(Y_1-1)-} & \cdots & \cdots & \mathbf{A}_{1-} & \mathbf{A}_0 & \mathbf{A}_{1+} & \cdots \\
\hline
 & & & \ddots & & &
\end{array}\right] . \qquad (2.13)
$$

$$
\mathbf{A}_{\delta_1}^{(q_{\mathrm{C}})} = \left[\begin{array}{c|ccccc|cc}
\mathbf{A}_{\delta_1,0}^{(q_{\mathrm{C}},0)} & \mathbf{A}_{\delta_1,1^+}^{(q_{\mathrm{C}},0)} & \cdots & \mathbf{A}_{\delta_1,Z_2^+}^{(q_{\mathrm{C}},0)} & & & \\
\hline
\mathbf{A}_{\delta_1,1^-}^{(q_{\mathrm{C}},1)} & \mathbf{A}_{\delta_1,0}^{(q_{\mathrm{C}},1)} & \mathbf{A}_{\delta_1,1^+}^{(q_{\mathrm{C}},1)} & \cdots & \mathbf{A}_{\delta_1,Z_2^+}^{(q_{\mathrm{C}},1)} & & \\
\vdots & \vdots & & & \ddots & & \\
\mathbf{A}_{\delta_1,(Y_2-Z_2+1)^-}^{q_{\mathrm{C}},(Y_2-Z_2+1)} & \mathbf{A}_{\delta_1,(Y_2-Z_2)^-}^{q_{\mathrm{C}},(Y_2-Z_2+1)} & \cdots & \mathbf{A}_{\delta_1,0}^{(q_{\mathrm{C}})} & \cdots & \mathbf{A}_{\delta_1,(Z_2-1)^+}^{q_{\mathrm{C}},(Y_2-Z_2+1)} & \\
\vdots & \vdots & & & & \vdots & \\
\mathbf{A}_{\delta_1,Y_2^-}^{(q_{\mathrm{C}})} & \mathbf{A}_{\delta_1,(Y_2-1)^-}^{(q_{\mathrm{C}})} & \cdots & \cdots & \mathbf{A}_{\delta_1,1^-}^{(q_{\mathrm{C}})} & \mathbf{A}_{\delta_1,0}^{(q_{\mathrm{C}})} & \\
\hline
 & \mathbf{A}_{\delta_1,Y_2^-}^{(q_{\mathrm{C}})} & \cdots & \cdots & \cdots & \mathbf{A}_{\delta_1,1^-}^{(q_{\mathrm{C}})} & \\
 & & \ddots & & & \vdots & \\
 & & & \mathbf{A}_{\delta_1,Y_2^-}^{(q_{\mathrm{C}})} & & \mathbf{A}_{\delta_1,(Y_2-Z_2+1)^-}^{(q_{\mathrm{C}})} & \\
 & & & & \ddots & \vdots & \\
 & & & & & \mathbf{A}_{\delta_1,Y_2^-}^{(q_{\mathrm{C}})} & \\
\hline
 & & & & \ddots & & \\
\end{array}\right.
$$

$$
\left.\begin{array}{ccccccc|cc}
 & & & & & & & & \\
\hline
 & & & & & & & & \\
 & & & & & & & & \\
\mathbf{A}_{\delta_1,Z_2^+}^{(q_{\mathrm{C}})} & & & & & & & & \\
\vdots & \ddots & & & & & & & \\
\mathbf{A}_{\delta_1,1^+}^{(q_{\mathrm{C}})} & \cdots & \mathbf{A}_{\delta_1,Z_2^+}^{(q_{\mathrm{C}})} & & & & & & \\
\hline
\mathbf{A}_{\delta_1,0}^{(q_{\mathrm{C}})} & \cdots & \cdots & \mathbf{A}_{\delta_1,Z_2^+}^{(q_{\mathrm{C}})} & & & & & \\
\vdots & & & \ddots & & & & & \\
\mathbf{A}_{\delta_1,(Y_2-Z_2)^-}^{(q_{\mathrm{C}})} & \cdots & \cdots & \cdots & \mathbf{A}_{\delta_1,(Z_2-1)^+}^{(q_{\mathrm{C}})} & & \mathbf{A}_{\delta_1,Z_2^+}^{(q_{\mathrm{C}})} & & \\
\vdots & & & \ddots & \vdots & & \vdots & \ddots & \\
\mathbf{A}_{\delta_1,(Y_2-1)^-}^{(q_{\mathrm{C}})} & \cdots & \cdots & \mathbf{A}_{\delta_1,1^-}^{(q_{\mathrm{C}})} & \mathbf{A}_{\delta_1,0}^{(q_{\mathrm{C}})} & & \mathbf{A}_{\delta_1,1^+}^{(q_{\mathrm{C}})} & \cdots & \mathbf{A}_{\delta_1,Z_2^+}^{(q_{\mathrm{C}})} \\
\hline
 & & & \ddots & & & & & \ddots \\
\end{array}\right]
\tag{2.14}
$$

$$\Pr\{v_i^{(n)}=h, s_{\mathrm{A},i}^{(n)}=j\}=\begin{cases}\sum\limits_{k_2=0}^{j}\cdots\sum\limits_{k_U=0}^{j}\frac{1}{1+f_j(k_2)+\cdots+f_j(k_U)}\Pr\{s_{\mathrm{A},i}^{(n)}=j\}\\ \prod\limits_{l=2}^{U}\Pr\{s_{\mathrm{A},i}^{(n)}=k_l\},\ \text{if } v=1,\\ \Pr\{s_{\mathrm{A},i}^{(n)}=j\}(1-\frac{\Pr\{s_{\mathrm{A},i}^{(n)}=j,v_i^{(n)}=1\}}{\Pr\{s_{\mathrm{A},i}^{(n)}=j\}}),\quad \text{if } v=0.\end{cases} \tag{2.16}$$

$$\begin{aligned}\Pr\{t_{\mathrm{B,AD}}^{(n)}(N)=l, t_{\mathrm{A,OS}}^{(n)}(N)=j\}=\sum_{k_1=0}^{K^2-1}\cdots\sum_{k_N=0}^{K^2-1}f_j(\lfloor k1/K\rfloor+\cdots+\lfloor k_N/K\rfloor)\\ f_l((k_1 \mod K)+\cdots+(k_N \mod K))\prod_{i=1}^{N}h_{k_i+1}.\end{aligned} \tag{2.18}$$

link. From the previous subsection, we define state variable $t_{\mathrm{A,OS}}^{(n)}(N_{\mathrm{A}})=\sum_{i=1}^{N_{\mathrm{A}}}c_{\mathrm{A},i}^{(n)},\ 0\le t_{\mathrm{A,OS}}^{(n)}(N_{\mathrm{A}})\le N_{\mathrm{A}}(K-1)$ for the access link. Similarly, here we define state variable, $t_{\mathrm{B,AD}}^{(n)}(N_{\mathrm{B}})=\sum_{i=1}^{N_{\mathrm{B}}}c_{\mathrm{B},i}^{(n)},\ 0\le t_{\mathrm{B,AD}}^{(n)}(N_{\mathrm{B}})\le N_{\mathrm{B}}(K-1)$, where $c_{\mathrm{B},i}^{(n)}=v_i^{(n)}s_{\mathrm{B},i}^{(n)}$ for the backhaul link. Our objective is to find the joint state probabilities $\Pr\{t_{\mathrm{B,AD}}^{(n)}(N_{\mathrm{B}})=l, t_{\mathrm{A,OS}}^{(n)}(N_{\mathrm{A}})=j\}$. We start by considering the joint probabilities $\Pr\{v_i^{(n)}=h, s_{\mathrm{A},i}^{(n)}=j\}$, which can be calculated as shown in eq. (2.16).

Furthermore, the joint probabilities $\Pr\{v_i^{(n)}=h, s_{\mathrm{A},i}^{(n)}=j, s_{\mathrm{B},i}^{(n)}=l\}$ are given by:

$$\begin{aligned}\Pr\{v_i^{(n)}=h, s_{\mathrm{A},i}^{(n)}=j, s_{\mathrm{B},i}^{(n)}=l\}=\\ \Pr\{v_i^{(n)}=h, s_{\mathrm{A},i}^{(n)}=j\}\Pr\{s_{\mathrm{B}}^{(n)}=l\}.\end{aligned} \tag{2.17}$$

Next, we define vector $\mathbf{H}$ whose elements are the probabilities $\Pr\{c_{\mathrm{A},i}^{(n)}=j, c_{\mathrm{B},i}^{(n)}=l\}$ that can be calculated by adding all corresponding probabilities from eq. (2.17). Then, we define vector $\grave{\mathbf{W}}_{\mathrm{OS}}(N_{\mathrm{A}}+N_{\mathrm{B}})$ whose elements are the joint probabilities $\Pr\{t_{\mathrm{B,AD}}^{(n)}(N_{\mathrm{B}})=l, t_{\mathrm{A,OS}}^{(n)}(N_{\mathrm{A}})=j\}$. Assuming $N_{\mathrm{A}}=N_{\mathrm{B}}=N$, these elements can be calculated as shown in eq. (2.18), where in this equation h_i is the ith element of vector $\mathbf{H}$.

Finally, the transition probability matrix for the joint state $(t_{\mathrm{B,AD}}^{(n)}(N), t_{\mathrm{A,OS}}^{(n)}(N))$ of the tagged UE with access link dependent backhaul channel scheduling and opportunistic access channel scheduling is $\mathbf{W}(2N)$ with identical rows, and with each row equals $\grave{\mathbf{W}}_{\mathrm{OS}}(2N)$. Now the QBD process of the system, $\mathbf{P}$, can be obtained using eqs. (A.1)-(B.10). For the access link dependent backhaul channel scheduling mechanism, $Y_1=Y_2=b(K-1)N$.

Round robin backhaul channel scheduling and opportunistic access channel scheduling

For this scheduling mechanism, for simplicity, we start by developing the transition probability matrix of the joint system space for two UEs in the reference small cell, and then the discussion is extended for any number of UEs. According to the round robin backhaul channel scheduling mechanism, the packets of the tagged UE will be transmitted from the CN to the reference SBS in alternate time slots with two UEs in the reference SBS. Without loss of generality, let us assume that UE 1 is the tagged UE and its packets are transmitted over all the backhaul channels at time slots $n \in \{1, 3, 5, \cdots .\}$, while the other UE's packets are transmitted over the backhaul link at time slots $n \in \{2, 4, 6, \cdots .\}$. Based on the time slot index, there are two different cases as follows.

Case I-All backhaul channels are scheduled for the tagged UE: At odd time slots, i.e., at $n \in \{1, 3, 5, \cdots .\}$, all N_{B} backhaul channels are scheduled for the tagged UE. So, in these time slots the packets of the tagged UE are transmitted over the N_{B} backhaul channels from the CN buffer to the SBS buffer. We define the state variable $t^{(n)}_{\mathrm{B,RR}}(N_{\mathrm{B}}) = \sum_{i=1}^{N_{\mathrm{B}}} s^{(n)}_{\mathrm{B},i}$. It is obvious that in this case, the system's dynamic is similar to that of fixed backhaul channel scheduling and opportunistic access channel scheduling with all the N_{B} backhaul channels are scheduled for the tagged UE. As such the transition probability matrix of the state variables for this case corresponds to the transition probability matrix of fixed backhaul channel scheduling and opportunistic access channel scheduling developed in Section 2.3.2 with $N_{\mathrm{P}} = N_{\mathrm{B}}$ backhaul channels, i.e., $\mathbf{T}_{\mathrm{RR}}(N_{\mathrm{B}}) = \mathbf{T}_{\mathrm{FA}}(N_{\mathrm{B}})$. The corresponding transition probability matrix for the joint state of $(t^{(n)}_{\mathrm{B,RR}}(N_{\mathrm{B}}), t^{(n)}_{\mathrm{A,OS}}(N_{\mathrm{A}}))$ of the tagged UE with round robin backhaul channel scheduling and opportunistic access channel scheduling can be expressed as $\mathbf{W}(N_{\mathrm{B}} + N_{\mathrm{A}}) = \mathbf{T}_{\mathrm{RR}}(N_{\mathrm{B}}) \otimes \mathbf{T}_{\mathrm{OS}}(N_{\mathrm{A}})$. Now, we define $\mathbf{P}_{\mathrm{I}}$ to describe the transition of the system from an odd time slot to an even time slot. $\mathbf{P}_{\mathrm{I}}$ can be obtained using eqs. (A.1)-(B.10), where $Y_1 = b(K-1)N_{\mathrm{B}}$ and $Y_2 = b(K-1)N_{\mathrm{A}}$.

Case II-All backhaul channels are scheduled for the other UE: At even time slots, no backhaul channel is scheduled for the tagged UE. Therefore, no packets are transmitted from the CN buffer to the SBS buffer of the tagged UE, however, packets can be transmitted from the SBS buffer to the tagged UE. Therefore, the dynamics of the CN buffer and the SBS buffer are independent for this particular case. Let us use $\tilde{\mathbf{P}}_1$ and $\tilde{\mathbf{P}}_2$ to denote the transition probability matrices of the tagged UE's CN and SBS buffers, respectively. The block sub-matrices of $\tilde{\mathbf{P}}_1$ can be derived as follows:

$$\mathbf{B1}_{\delta_1^-} = \mathbf{0}, \tag{2.19}$$

$$\mathbf{B1}_{\delta_1^+} = \alpha_{\delta_1} \mathbf{T}_{\mathrm{OS}}, 0 \leq \delta_1 \leq Z, \tag{2.20}$$

$$\mathbf{B1}_{\delta_1^+}^{(Q_{\mathrm{C,max}}-\delta_1)} = \sum_{\delta_1 \le i \le Z} \alpha_i \mathbf{T}_{\mathrm{OS}}, 0 \le \delta_1 \le Z. \tag{2.21}$$

Block sub-matrices of $\tilde{\mathbf{P}_2}$ can be calculated using eqs. (B.1)-(B.10) by assuming no arrival to the SBS buffer of the tagged UE, i.e., $\lambda = 0$, and by multiplying these equations by $\mathbf{T}_{\mathrm{OS}}$ using the Hadamard product. Then, we define the transition probability matrix $\mathbf{P'}_{\mathrm{II}} = \tilde{\mathbf{P}_1} \otimes \tilde{\mathbf{P}_2}$, which describes the transition of the system from an even time slot to an odd time slot. Finally, we obtain the transition probability matrix for case II, $\mathbf{P}_{\mathrm{II}}$, by rearranging the rows of $\mathbf{P'}_{\mathrm{II}}$ so that the desired order of state variables is achieved.

The transition of the system over a single time slot n is described by $\mathbf{P}_{\mathrm{I}}$ for $n \in \{1, 3, 5, \cdots .\}$, and by $\mathbf{P}_{\mathrm{II}}$ for $n \in \{2, 4, 6, \cdots .\}$. However, if we consider the transition of the system over any arbitrary two consecutive time slots n and $n+1$, the resulting DTMC is time-homogenous and describes the system partially. In order to fully describe the system, we need to consider all possible transitions that can occur over two consecutive time slots. Obviously, there are two possibilities, namely, the transition from an odd time slot to the next odd time slot and the transition from an even time slot to the next even time slot. Now we define the corresponding two-step transition probability matrices $\mathbf{P}^{(1)}_{n\to(n+2)}$ and $\mathbf{P}^{(2)}_{n\to(n+2)}$ which can be obtained using $\mathbf{P}_{\mathrm{I}}$ and $\mathbf{P}_{\mathrm{II}}$ as follows:

$$\begin{array}{l} \mathbf{P}^{(1)}_{n\to(n+2)} = \mathbf{P}_{\mathrm{I}}\mathbf{P}_{\mathrm{II}}, \quad n = 1, 3, 5, \cdots, \\ \mathbf{P}^{(2)}_{n\to(n+2)} = \mathbf{P}_{\mathrm{II}}\mathbf{P}_{\mathrm{I}}, \quad n = 2, 4, 6, \cdots \end{array} . \tag{2.22}$$

In general, for U UEs in the reference small cell, U consecutive time slots should be considered in order to completely describe the system's joint transition probability. Let us consider n, $(n+1)$, $\cdots$, $(n+U-1)$ as the U consecutive time slots. There can be U possible scenarios and the corresponding U-step transition probability matrices can be expressed in terms of $\mathbf{P}_{\mathrm{I}}$ and $\mathbf{P}_{\mathrm{II}}$ as follows:

$$\begin{array}{lll} \mathbf{P}^{(1)}_{n\to(n+U)} = & \mathbf{P}_{\mathrm{I}}\mathbf{P}_{\mathrm{II}}^{U-1}, & n = 1, U+1, 2U+1, \cdots, \\ \mathbf{P}^{(2)}_{n\to(n+U)} = & \mathbf{P}_{\mathrm{II}}\mathbf{P}_{\mathrm{I}}\mathbf{P}_{\mathrm{II}}^{U-2}, & n = U, 2U, 3U, , \cdots, \\ \vdots & & \\ \mathbf{P}^{(U)}_{n\to(n+U)} = & \mathbf{P}_{\mathrm{II}}^{U-1}\mathbf{P}_{\mathrm{I}}, & n = 2, U+2, 2U+2, \cdots \end{array} . \tag{2.23}$$

Using these U-step transition probability matrices, the steady-state probabilities of the system for round robin backhaul channel scheduling and opportunistic access channel scheduling are obtained as discussed in the next subsection.

2.3.3 Derivation of performance measures

We define $\boldsymbol{\pi}_{\mathrm{FA}}$, $\boldsymbol{\pi}_{\mathrm{OS}}$ and $\boldsymbol{\pi}_{\mathrm{RR}}$ as steady-state solutions of the DTMCs developed earlier for the different channel scheduling mechanisms. For fixed backhaul channel scheduling and access link dependent backhaul channel scheduling, the transition probability matrices are developed in Sections 2.3.2 and 2.3.2 and represented as a QBD process. Therefore, we can apply the matrix-analytic procedure in [46] to calculate the steady-state probabilities $\boldsymbol{\pi}_{\mathrm{FA}}$ and $\boldsymbol{\pi}_{\mathrm{OS}}$. On the other hand, the average steady-state probabilities corresponding to round robin backhaul channel scheduling $\boldsymbol{\pi}_{\mathrm{RR}}$ are given by:

$$\boldsymbol{\pi}_{\mathrm{RR}} = \frac{\boldsymbol{\pi}^{(1)} + \boldsymbol{\pi}^{(2)} + \cdots + \boldsymbol{\pi}^{(U)}}{U}, \tag{2.24}$$

where $\boldsymbol{\pi}^{(i)}$ is the steady-state solution of the ith U-step transition probability matrix $\mathbf{P}^{(i)}_{n\rightarrow(n+U)}$ and can be calculated by solving: $\boldsymbol{\pi}^{(i)}\mathbf{P}^{(i)}_{n\rightarrow(n+U)} = \boldsymbol{\pi}^{(i)}$, and $\boldsymbol{\pi}^{(i)}\mathbf{1} = 1$ where $\mathbf{1}$ is a column vector of appropriate size with all elements equal 1.

Using the steady-state probabilities, one can measure different data link layer performance parameters, i.e., PLP and average queuing delay of packets for the channel scheduling mechanisms under consideration as follows. A steady-state solution $\boldsymbol{\pi}$ can be organized as follows: $\boldsymbol{\pi} = [\boldsymbol{\pi}_0,\ \boldsymbol{\pi}_1, \cdots,]\ \boldsymbol{\pi}_{Q_{\mathrm{C,max}}}]$, where $\boldsymbol{\pi}_j = [\boldsymbol{\pi}_{j,0},\ \boldsymbol{\pi}_{j,1}, \cdots, \boldsymbol{\pi}_{j,Q_{\mathrm{A,max}}}]$. The steady-state probability of finding i packets in the CN buffer of the tagged UE, $\xi_1(i) = \boldsymbol{\pi}_i\mathbf{1}$, and the steady-state probability of finding j packets in the SBS buffer of the tagged UE, $\xi_2(j) = \sum_{i=0}^{Q_{\mathrm{C,max}}} \boldsymbol{\pi}_{i,j}\mathbf{1}$.

Packet loss probability

Packets are lost due to buffer overflow if they find the buffer full upon their arrival. PLP due to buffer overflow can be measured from the steady-state probabilities of the states leading to buffer overflow upon arrival of packets and the corresponding arrival probabilities.

The average packet drop rate due to buffer overflow at the CN buffer is given by eq. (2.25), where in this equation $\pi(i)$ is the ith element of a particular steady-state solution, and $x_{j,h,m}$ depends on the buffer dynamics corresponding to that particular steady-state solution. In particular, $x_{j,h,m} = \max(0, j - \min(j, bh) + m - Q_{\mathrm{C,max}})$ for $\boldsymbol{\pi}_{\mathrm{FA}}$, $\boldsymbol{\pi}_{\mathrm{OS}}$, and $\boldsymbol{\pi}^{(1)}$, and $x_{j,h,m} = \max(0, j + m - Q_{\mathrm{C,max}})$ for $\boldsymbol{\pi}^{(i)}, i \neq 1$. The overall average packet drop rate for round robin backhaul channel scheduling can be obtained by averaging the packet dropping rate corresponding to different steady-state solutions. The PLP due to buffer

$$\bar{\rho}_{\mathrm{C}} = \sum_{j=0}^{Q_{\mathrm{C,max}}} \sum_{i=0}^{Q_{\mathrm{A,max}}} \sum_{h=0}^{\frac{Y_1}{b}} \sum_{l=0}^{\frac{Y_2}{b}} \sum_{m=0}^{Z} \alpha_m \pi(j(Q_{\mathrm{A,max}}+1)(\tfrac{Y_1}{b}+1)(\tfrac{Y_2}{b}+1) + i(\tfrac{Y_1}{b}+1)(\tfrac{Y_2}{b}+1) + h(\tfrac{Y_2}{b}+1) + l) x_{j,h,m}. \tag{2.25}$$

$$\bar{\rho}_{\mathrm{A}} = \sum_{j=0}^{Q_{\mathrm{C,max}}} \sum_{i=0}^{Q_{\mathrm{A,max}}} \sum_{h=0}^{\frac{Y_1}{b}} \sum_{l=0}^{\frac{Y_2}{b}} \pi(j(Q_{\mathrm{A,max}}+1)(\tfrac{Y_1}{b}+1)(\tfrac{Y_2}{b}+1) + i(\tfrac{Y_1}{b}+1)(\tfrac{Y_2}{b}+1) + h(\tfrac{Y_2}{b}+1) + l) \max(0, \min(j, bh) + i - \min(i, bl - Q_{\mathrm{A,max}})). \tag{2.30}$$

overflow at the CN buffer can be calculated as:

$$\mathcal{P}_{\mathrm{C}} = \frac{\bar{\rho}_{\mathrm{C}}}{\bar{\mu}_{\mathrm{C}}}, \tag{2.26}$$

where $\bar{\mu}_{\mathrm{C}}$ is the average packet arrival rate at CN buffer of the tagged UE and can be obtained as:

$$\bar{\mu}_{\mathrm{C}} = \sum_{i=0}^{Z} i\alpha_i. \tag{2.27}$$

The steady-state probabilities of packet arrivals to the SBS buffer correspond to the probability vector $\boldsymbol{\lambda} = \{\lambda_0, \lambda_1, \lambda_2, \cdots, \lambda_{Y_2}\}$. These probabilities are given by:

$$\lambda_h = \sum_{i=0}^{Q_{\mathrm{C,max}}} \sum_{j=0}^{\frac{Y_1}{b}} f_h(\min(i, bj)) \sum_{u=0}^{Q_{\mathrm{A,max}}} \sum_{h=l}^{m} \pi(h), \tag{2.28}$$

where $l = i(Q_{\mathrm{A,max}}+1)(\frac{Y_1}{b}+1)(\frac{Y_2}{b}+1) + u(\frac{Y_1}{b}+1)(\frac{Y_2}{b}+1) + j(\frac{Y_2}{b}+1) + 1$, and $m = i(Q_{\mathrm{A,max}}+1)(\frac{Y_1}{b}+1)(\frac{Y_2}{b}+1) + u(\frac{Y_1}{b}+1)(\frac{Y_2}{b}+1) + j(\frac{Y_2}{b}+1) + (\frac{Y_2}{b}+1)$. Now the average packet arrival rate to the SBS buffer of the tagged UE can be obtained as:

$$\bar{\mu}_{\mathrm{A}} = \sum_{i=0}^{Y_1} i\lambda_i. \tag{2.29}$$

The average packet drop rate due to buffer overflow of SBS buffer of the tagged UE is given by eq. (2.30).

Finally, the PLP due to buffer overflow at the SBS buffer of the tagged UE is calculated as follows:

$$\mathcal{P}_{\mathrm{A}} = \frac{\bar{\rho}_{\mathrm{A}}}{\bar{\mu}_{\mathrm{A}}}. \tag{2.31}$$

Finally, the end-to-end PLP can be calculated using the PLP at both buffers of the tagged UE and the PLP due to error in both links as follows [42]:

$$\mathcal{P} = 1 - (1 - \mathcal{P}_{\mathrm{C}})(1 - \mathcal{P}_{\mathrm{A}})(1 - \mathrm{PER}_0)^2, \tag{2.32}$$

where PER_0 is the average packet error rate corresponding to the target average bit error rate, BER_0. In particular, $\mathrm{PER}_0 = 1 - (1 - \mathrm{BER}_0)^{\epsilon}$, where ϵ is the packet size in bits.

Average packet queuing delay

The average queuing delay of a packet corresponds to the sum of the average queuing delay at the CN buffer and the average queuing delay at the SBS buffer. This delay can be calculated using the Little's law as follows [42]:

$$\bar{\mathcal{D}} = \frac{\sum_{i=1}^{Q_{\mathrm{C,max}}} i\xi_1(i)}{\bar{\mu}_{\mathrm{C}}(1 - \mathcal{P}_{\mathrm{C}})} + \frac{\sum_{j=1}^{Q_{\mathrm{A,max}}} j\xi_2(j)}{\bar{\mu}_{\mathrm{A}}(1 - \mathcal{P}_{\mathrm{A}})}. \tag{2.33}$$

2.4 Numerical Results and Discussions

The main objective of the analytical model developed here is to facilitate cross-layer system analysis and design jointly considering the time varying nature of channels, bursty packet arrival at the CN buffer, the channel scheduling mechanisms in both links and the effect of network topology. In this section, we present selected numerical results. To derive the numerical results, we coded, in MATLAB, the steps involved in the queuing model developed in Section 2.3. We also validate the results via computer simulation using MATLAB. We consider a two-tier network with the parameters in Table I unless other values are specified. We assumed a target average bit error rate $\mathrm{BER}_0 = 10^{-6}$ and $b = 1$.

2.4.1 Effect of number of interfering small cells

First, we investigate the performance of the considered scheduling mechanisms when varying the number of interfering SBSs in the network. The PLP and the average queuing delay versus the number of interfering SBSs are plotted in Fig. 2.3 and Fig. 2.4, respectively. From Fig. 2.3 we can observe that the fixed backhaul channel scheduling mechanism outperforms the round robin backhaul channel scheduling mechanism under any number of interfering SBSs. On the other hand, it is obvious from this figure that the access link dependent backhaul channel scheduling mechanism outperforms other backhaul channel scheduling mechanisms as the the number of interfering SBSs increases. However this comes at a certain expense of queuing delay as shown in Fig. 2.4. From Fig. 2.4, it is also

Table 2.1: Summary of parameter values.

Parameter description	**Symbol**	**Value**
Number of layers of macrocells	T	1
Macrocell radius	R_{M}	500 m
Small cell radius	R_{S}	50 m
Number of UEs in the reference small cell	U	3
Number of channels in the access link	N_{A}	3
Number of channels in the backhaul link	N_{B}	3
Number of channel states	K	3
Transmit power	p	25 dBm
Thermal noise power	σ	-121 dBm
Average SNR in the backhaul link	$\bar{\gamma}$	22 dB
Path loss exponent	η	3.2
Shadowing and fading parameters in the backhaul link	$\kappa_{\mathrm{B}}, \theta_{\mathrm{B}}$	$2, 2$
Shadowing and fading parameters of interference in the access link	$\kappa_{\mathrm{I}}, \theta_{\mathrm{I}}$	$1.5, 3.5$
Shadowing and fading parameters of desired signal	$\kappa_{\mathrm{D}}, \theta_{\mathrm{D}}$	$1.5, 3.5$
Packet size	ϵ	1024 bits
Probability vector of packet arrival at the CN buffer	$\boldsymbol{\alpha}$	{0.1 0.2 0.7}
Frequency reuse factor		1
Distribution of UEs in small cell		uniform

obvious that the fixed channel scheduling outperforms other backhaul channel scheduling mechanisms. The access link dependent channel scheduling has a higher average queuing delay than the other scheduling mechanisms for a large number of interfering SBSs. From the PLP and queuing delay performance plotted in Figs. 2.3 and 2.4, respectively, we observe that the choice of a backhaul channel scheduling mechanism is not unique and depends on the number of interfering SBSs as well as the QoS requirements of the UEs. The developed model can assist the system designer to make such a decision.

2.4.2 Effect of the size of the small cells

Here, we investigate the performance of the considered channel scheduling mechanisms when varying the coverage radius of the SBSs. Fig. 2.5 and Fig. 2.6 show the effect of varying the radius of the small cells on the PLP and the average queuing delay, respectively, in presence of 50 interfering small cells. To obtain the results presented in Figs. 5 and 6, we do not consider fixed UE locations within the cell. Rather, we consider that fixed number of UEs are uniformly distributed within the cell irrespective of the cell size. These figures show that the cell radius has a similar effect as the effect of the number of small cells on the PLP and the average queuing delay. In particular, the fixed channel scheduling mechanism outperforms other channel scheduling mechanisms in terms of queuing delay performance for any value of R_{S}. Also, the fixed channel scheduling outperforms other channel scheduling mechanisms in terms of PLP performance for small values of R_{S}. As

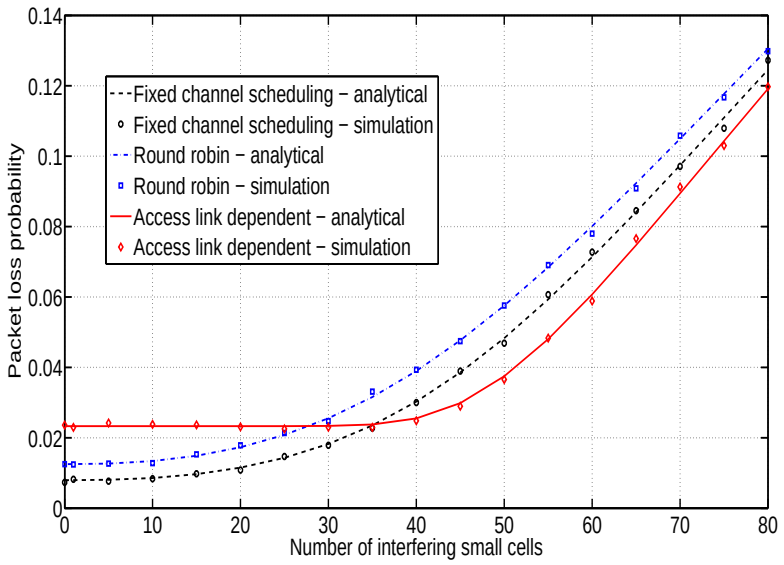

Figure 2.3: Packet loss rate vs. number of interfering SBSs.

the value of R_{S} increases, the access link dependent channel scheduling mechanism offers a superior PLP performance at the expense of higher average queuing delay with respect to other channel scheduling mechanisms.

2.4.3 Effect of average SNR in the backhaul link

Next, we show the performance of the considered channel scheduling mechanisms for different values of the average SNR in the backhaul link with 60 interfering small cells. In Fig. 2.7 and Fig. 2.8, we plot the PLP and the average queuing delay, respectively. From these figures, we observe that at lower values of the average SNR, all backhaul channel scheduling mechanisms have almost similar PLP performance, however, the access link dependent channel scheduling mechanism has a better average queuing delay performance compared to the other mechanisms. From these figures, it is also obvious that as the average SNR increases, the access link dependent channel scheduling offers a lower PLP while the fixed channel scheduling provides a better average queuing delay performance. So again the choice of a backhaul channel scheduling is not unique and depends on the average SNR and the required QoS parameters. Our developed model can assist to readily evaluate the QoS parameters for given system parameters and to make a decision for using a particular backhaul channel scheduling mechanism depending on the QoS requirements.

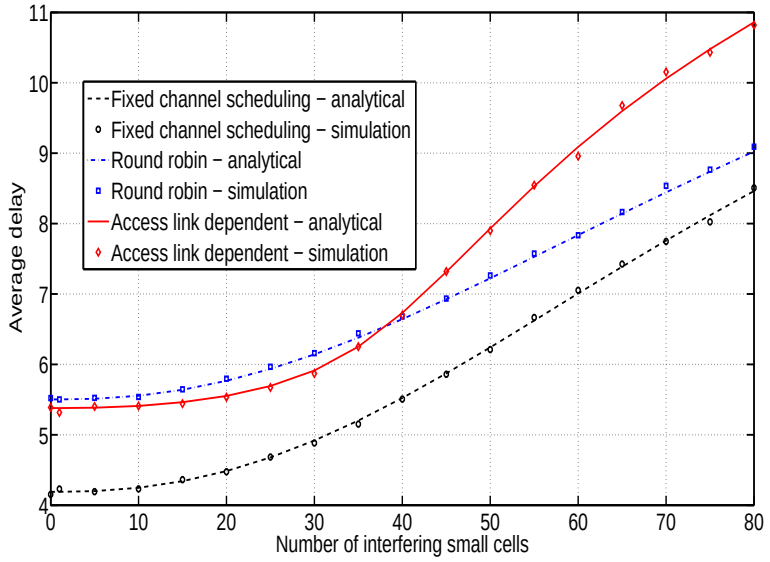

Figure 2.4: Average delay vs. number of interfering SBSs.

2.4.4 Effect of target bit error rate

Here, we investigate the performance of the channel scheduling mechanisms under consideration for various values of BER_0. As the value of BER_0 decreases, PER_0 and consequently PLP due to the link error decrease. However, decreasing the value of BER_0 increases the SINR thresholds. This decreases the probability of transmitting at relatively higher rates from both buffers and eventually, packet loss due to the overflow increases. As such there exists a trade-off and there is an optimal target bit error rate that minimizes the end-to-end PLP. Considering different number of interfering small cells in the network, in Fig. 2.9, we plot the PLP versus BER_0. In Fig. 2.10, we plot the average queuing delay for different values of BER_0 and this figure shows that as the value of BER_0 increases, delay decreases for all the channel scheduling mechanisms. From this figure we also observe that, depending on the range of BER_0 as well as QoS requirements, a particular channel scheduling mechanism can be preferable.

2.4.5 Effect of varying the number of UEs

Figs. 2.11 and 2.12, respectively, plot the PLP and average queuing delay of the channel scheduling mechanisms under consideration when varying the number of UEs in the reference small cell. We consider 6 channels in each link, average SNR in the backhaul link $\bar{\gamma} = 18$ dB, and 65 interfering small cells. For small number of UEs, all channel scheduling

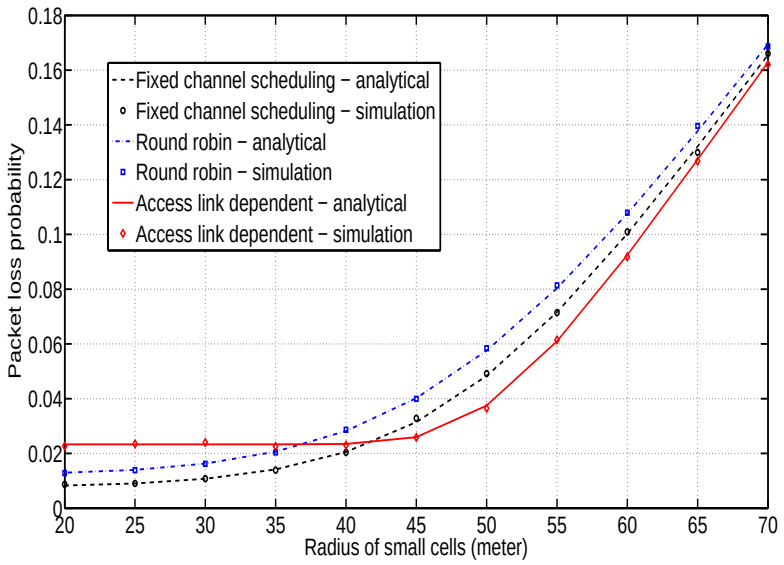

Figure 2.5: Packet loss probability vs. the radius of the small cells.

mechanisms provide similar PLP performance as observed from Fig. 2.11. Fixed backhaul channel scheduling provides slightly better average delay performance compared to other mechanisms as observed from Fig. 2.12. These figures also show that as the number of UEs increases, the access link dependent channel scheduling offers better PLP and average delay performances than other channel scheduling mechanisms.

2.4.6 Example applications of the developed queuing model

In this section we provide some example applications of the developed queuing model for the channel scheduling mechanisms under consideration. One application is that the system designer can leverage our developed model to measure and compare beforehand various data link layer QoS parameters of the small cell UEs for various system and operating parameters. In particular, the system designer can implement the steps for the queuing model developed in Section 2.3 that takes system parameters (e.g., packet arrival statistics, number of channels, fading parameters, and number of interfering SBSs) as inputs and provides QoS parameters (e.g., PLP and average queuing delay) as outputs for a given channel scheduling mechanism. Eventually based on the QoS requirements and for given system parameters, the system designer can decide to use a particular backhaul channel scheduling mechanism. Another application is that the developed model can facilitate cross-layer design to select some system parameters e.g., number of SBSs for given other parameters and QoS requirements. For example, let us consider that the target average

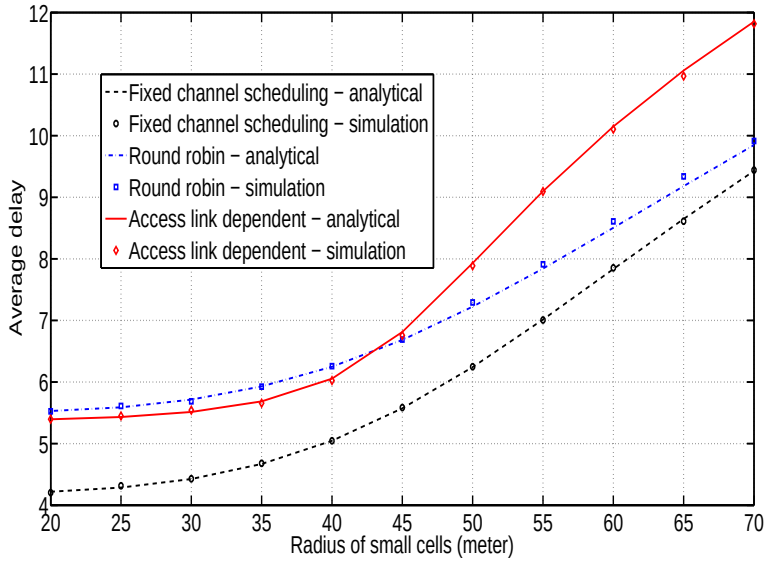

Figure 2.6: Average queuing delay vs. the radius of the small cells.

queueing delay and PLP are 5 time slots and 0.2, respectively. For given value of other system parameters, these QoS parameters can be maintained if there are 32 SBSs in the network in a given time as determined from Figs. 2.3 and 2.4. If more SBSs are added to the system, the QoS will not be guaranteed.

The developed queuing model can be used to search for optimal values of some parameters such as the optimal value of BER_0 for given other system and operating parameters. The developed queueing model can also be utilized by the call admission controller (CAC) module at the SCNs. In particular when a UE requests a connection, the CAC module at the SCNs can use the queueing model to make the call admission decision. The model outputs can determine whether the required QoS of the new and existing UEs can be maintained if a new UE is admitted. If the QoS of the requested and existing UEs cannot be maintained, the connection request may be refused. Otherwise it can be accepted.

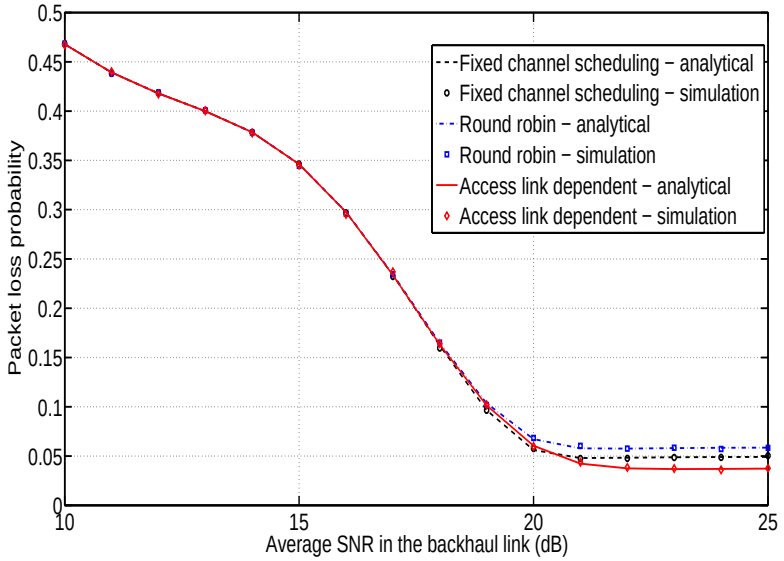

Figure 2.7: Packet loss probability for different values of the average received SNR in the backhaul link.

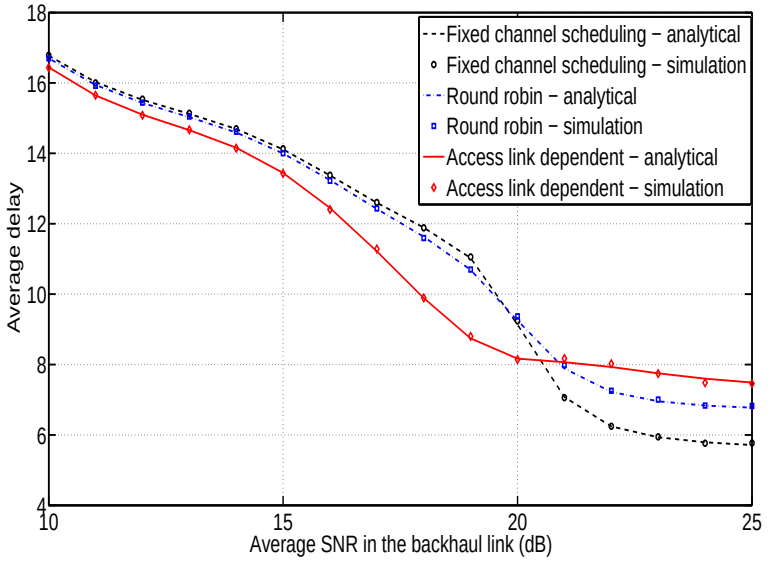

Figure 2.8: Average delay for different values of the average received SNR in the backhaul link.

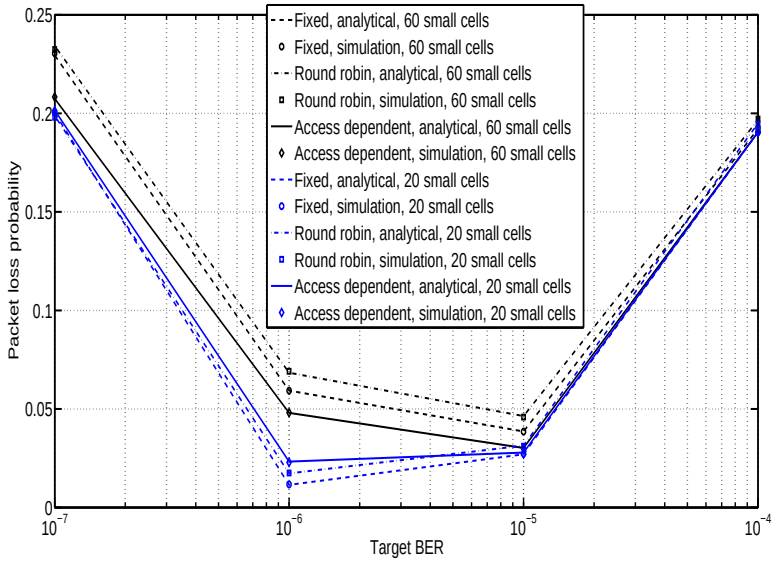

Figure 2.9: Packet loss probability for different values of target bit error rate, BER_0.

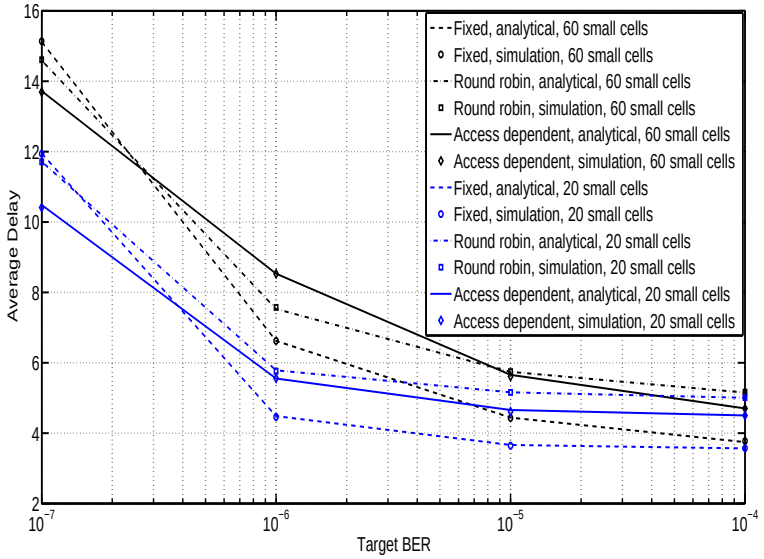

Figure 2.10: Average queuing delay for different values of target bit error rate, BER_0.

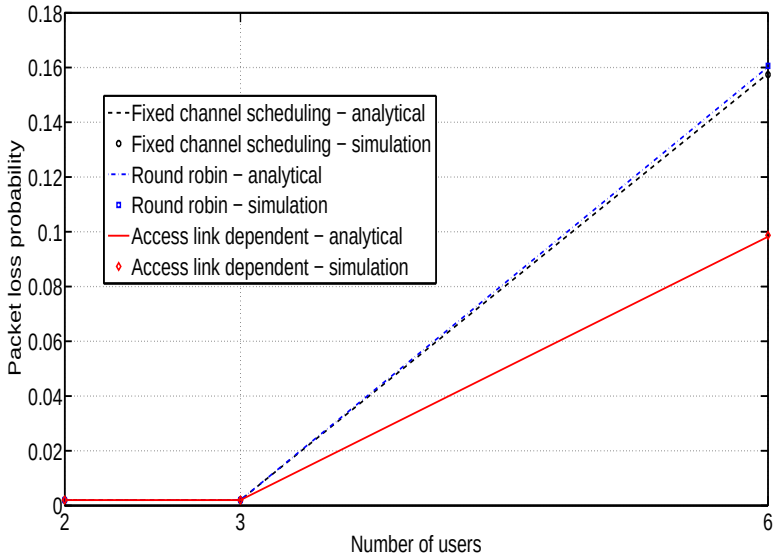

Figure 2.11: Packet loss probability vs. number of UEs in the reference small cell.

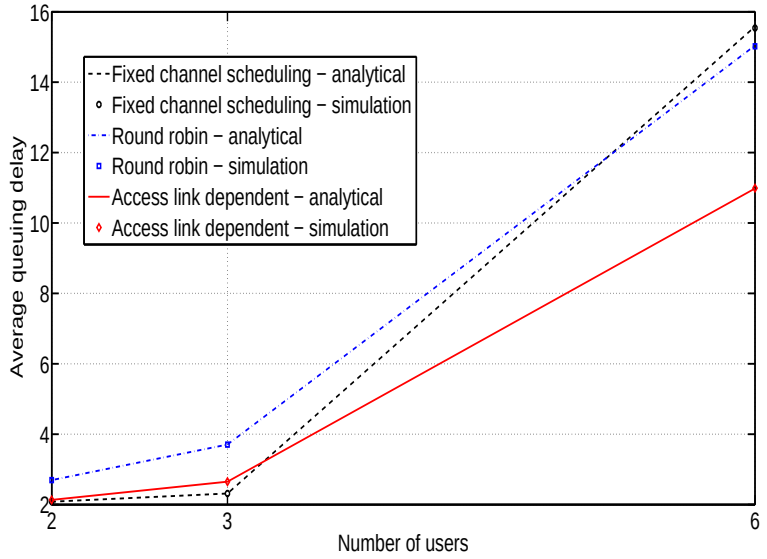

Figure 2.12: Average queuing delay vs. number of UEs in the reference small cell.

Chapter 3

DL Dynamic Cell Selection in Wireless Networks with Cell Sleeping

3.1 Synopsis

The contributions and main outcomes of this chapter are summarized below.

1. For a given BS inactivation scheme/pattern, we consider a CoMP DCS scheme for serving sleeping cell UEs. According to this DCS scheme, each packet of a particular UE in a sleeping cell arriving from the core network to the packet serving gateway (PSG) is randomly forwarded to one of the potential active BSs and the UE in the sleeping cell dynamically selects its serving BS from these active BSs. Unlike the conventional DCS scheme, the considered packet scheduling/forwarding mechanism does not require additional backhaul resources since a particular packet is forwarded only to one particular active BS.

2. For the CoMP DCS scheme under consideration, we model the system as a fork/join (F/J) queuing system and develop a cross-layer analytical model that considers the time varying nature of the channels, channel scheduling mechanism, partial CQI feedback, cell selection mechanism, bursty packet arrivals and packet scheduling mechanism.

3. The developed analytical model can be used to measure various packet level performance parameters such as PLP and queuing delay while accounting for out-of-sequence packet delivery. The model is also useful to tune the amount of CQI feedback and to find the optimal packet scheduling by the PSG such that the packet level QoS requirements of the UEs in the sleeping cell are maintained. We validate the accuracy of the developed analytical model via simulations. We compare the performance of the DCS scheme under consideration with the conventional fixed cell selection and with the state-of-the-art DCS. Presented numerical results show that

the DCS scheme under consideration significantly improves the PLP performance. Queuing delay performance, on the other hand, depends on the system and operating parameters.

The rest of this chapter is organized as follows. In Section 3.2, we present a detailed description of the system model and the considered CoMP DCS scheme. In Section 3.3, we develop the queuing analytical model and derive packet level performances. In Section 3.4 we present some selected numerical results and example applications of our developed model.

3.2 System Model and Operating Assumptions

3.2.1 Overall system description

We consider a cellular network with traditional grid-based macrocell layout as shown in Fig. 3.1. There are two different states that a macrocell can be, namely, a macrocell is either active or sleeping. In this figure, a single tier of macrocells is shown with the sleeping cell arbitrarily located in the centre[5]. Although we consider a single tier of macrocells, our model can be readily extended for any number of tiers of macrocells by accounting for interference from other tiers. We assume the coverage area of the macrocells to be circular with radius R_{M}. We are interested in the DL transmission scenario and we consider a time slotted system. We consider fractional frequency reuse in the active cells where each cell is divided into an inner part with radius R_{I} and an outer part with different frequency sub-bands dedicated for UEs in each part. Moreover, the frequency sub-band of the outer part is different for different cells within the same cluster, and the frequency sub-band of the inner part is same throughout the network. Without loss of generality we consider that the frequency sub-band used for the outer part of each cell is divided into N channels. Furthermore, we assume that the UEs within a sleeping cell can only be served by the frequency sub-bands of the outer parts of neighbouring active BSs. In contrast to [27], [28], since UEs in the sleeping cell are served by different BSs using orthogonal channels, coordination between BSs for channel scheduling is not needed in our considered DCS scheme.

UEs in the sleeping cell are assumed to be uniformly distributed within the cell. Also, UEs in the outer parts of active cells are assumed to be uniformly distributed within a

[5]The location of the sleeping cell does not affect the cell selection mechanism. However, the performances of UEs in the sleeping cell are affected by the sleeping cell location. Our developed analytical model is applicable for any location of the sleeping cell.

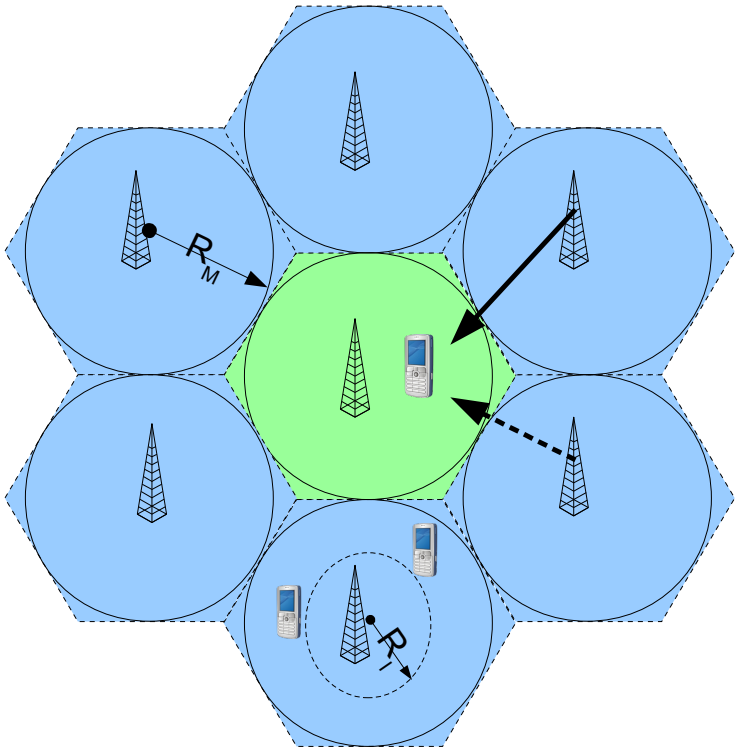

Figure 3.1: An example of first tier of a cellular network with a sleeping cell (green cell corresponds to the sleeping cell).

circular ring with inner and outer radii R_{I} and R_{M}, respectively[6]. The number of UEs in the outer part of active cell h is denoted as U_h and the number of UEs in the sleeping cell who are served by the BS of cell h is denoted as U_{sh}. In this chapter, we are interested in analyzing the packet level QoS performances of sleeping cell UEs.

3.2.2 Channel model and adaptive transmission

Composite shadowing and fading channels can be well approximated with the Gamma distribution [49], [50]. So we use the Gamma distribution to model the received SNR of all channels of all UEs in the network. Also, for each channel of a particular UE, we assume the received SNR to be independent identically distributed (i.i.d) across time slots. Furthermore, we map the received SNR into a finite set of channel states $\mathcal{S} = \{0, 1, \cdots, K-1\}$. Adaptive transmission is employed to exploit the time varying nature of the channels, and the number of packets transmitted over a particular channel at a given

[6]This assumption is to restrict UEs locations to the outer parts of active cells when generating these locations in simulations.

time slot is proportional to the channel state at that time slot. Let x denote the number of packets that can be transmitted over a particular channel at a given time slot. x can be written as:

$$x = bk, \quad 0 \leq k \leq K-1, \tag{3.1}$$

where b is an integer parameter that depends on the system resource allocation and k is the channel state [51].

Channel i between BS h and UE j is considered to be in state k at time slot n if $\gamma_k \leq \gamma_{i,h,j}^{(n)} < \gamma_{k+1}$, where $\gamma_{i,h,j}^{(n)}$ is the received SNR of ith channel between the hth BS and the jth UE at time slot n and γ_k is the lower boundary threshold of channel state k [51], [52]. The values of the thresholds $\{\gamma_k\}_{k=0}^{K}$ are chosen such that a target average bit error rate (BER_0) is satisfied for each transmission mode (see for example [53]).

Let us denote the channel state of the ith channel between the hth BS and the jth UE at time slot n by $s_{i,h,j}^{(n)}$. Then, probabilities $\Pr\{s_{i,h,j}^{(n)} = k\}, k = 0, 1, \cdots, K-1$, can be calculated as:

$$\Pr\{s_{i,h,j}^{(n)} = k\} = \Pr\{\gamma_k \leq \gamma_{i,h,j}^{(n)} < \gamma_{k+1}\} = \mathrm{P}_{\mathrm{th}}(\gamma_{k+1}) - \mathrm{P}_{\mathrm{th}}(\gamma_k), \quad k = 0, 1, \cdots, K-1, \tag{3.2}$$

where $\mathrm{P}_{\mathrm{th}}(x)$ is essentially the outage probability. When there is no interference, $\mathrm{P}_{\mathrm{th}}(\gamma_k)$ can be calculated as follows:

$$\mathrm{P}_{\mathrm{th}}(\gamma_k) = \frac{\Gamma_{\mathrm{L}}(\kappa_{jh}, \gamma_k/(\bar{\gamma}_{jh}\theta_{jh}))}{\Gamma(\kappa_{jh})}, \quad k = 0, 1, \cdots, K-1, \tag{3.3}$$

where $\Gamma_{\mathrm{L}}(m, x) = \int_0^x t^{m-1}\exp(-t)dt$ and denotes the lower incomplete Gamma function. Also, $\Gamma(m) = \int_0^\infty t^{m-1}\exp(-t)dt$ and denotes the Gamma function. κ_{jh} and θ_{jh} respectively denote the first and the second parameter of the Gamma distribution of the received SNR between BS h and UE j. $\bar{\gamma}_{jh}$ is the average received SNR which depends on the value of transmit power p, thermal noise σ, the distance between BS h and UE j and path loss exponent η.

In the presence of I interferers, $\mathrm{P}_{\mathrm{th}}(\gamma_k)$ can be calculated using the classical lemma presented in [54] as follows:

$$\mathrm{P}_{\mathrm{th}}(\gamma_k) = \frac{1}{\pi}\int_0^\infty \mathrm{Im}\left(\frac{\mathrm{e}^{j\gamma_k\sigma\omega}\Phi_D(-j\omega)\prod_{i=1}^{I}\Phi_i(j\gamma_k\omega)}{\omega}\right)d\omega + \frac{1}{2}, \tag{3.4}$$

where $\Phi_D(-j\omega)$ is the CF of the received desired signal D, and $\Phi_i(j\omega)$ is the CF of the received interference from interferer i.

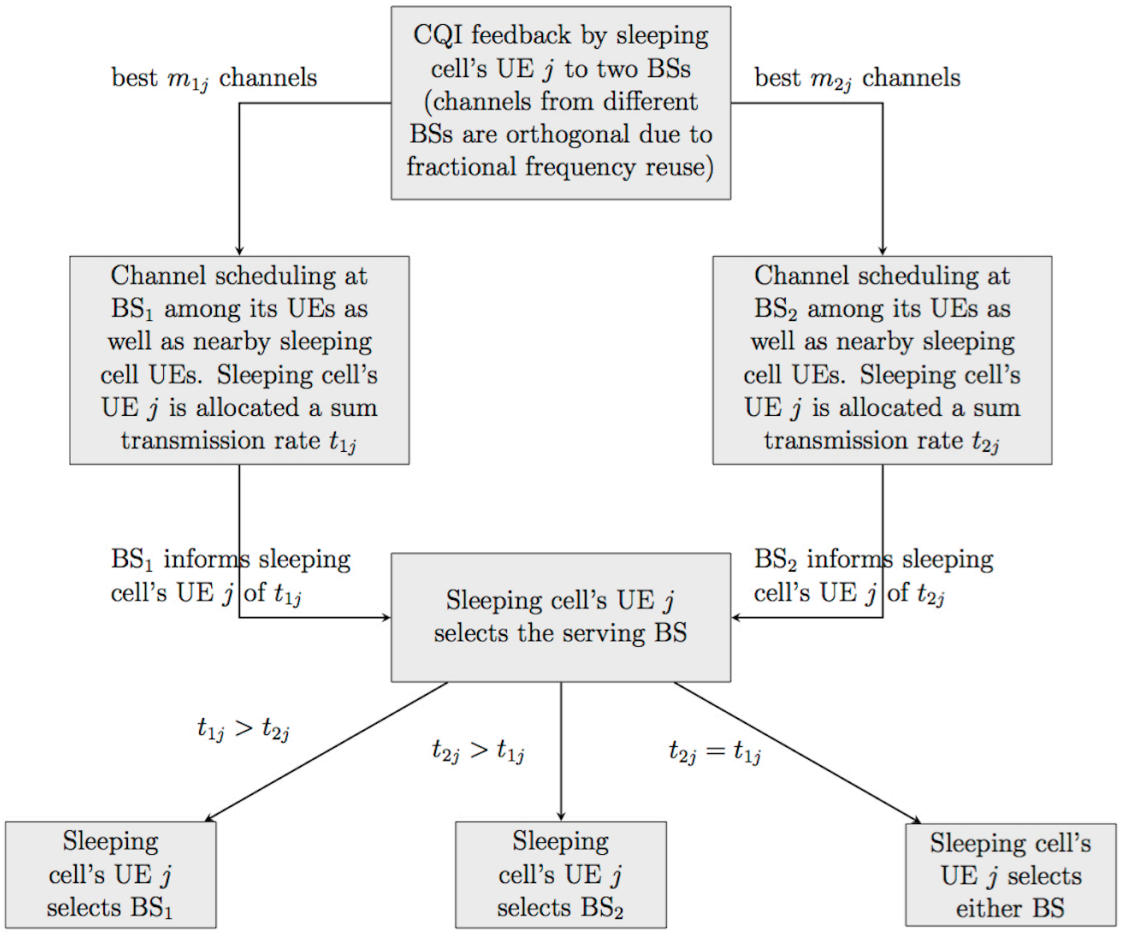

Figure 3.2: A flow chart of the considered DCS scheme.

3.2.3 Channel scheduling and cell selection

We assume that all active BSs employ the so called max-rate/opportunistic channel scheduling to take advantage of the multiuser diversity. According to this channel scheduling mechanism, at every time slot, each channel is allocated to the UE having the highest state at that particular channel. If there are multiple UEs with the highest channel state, the channel is randomly allocated to one of these UEs.

We consider that, at a given time slot, a UE in a sleeping cell can select one of the two closest active BSs, which we refer to as BS_1 and BS_2. Both BSs consider the UE in their channel scheduling and offer a sum transmission rate according to the employed opportunistic channel scheduling. The sum transmission rate offered by a BS depends on the number of channels allocated to the UE as well as the states of these channels. Then the UE selects the BS offering the highest sum transmission rate. If both BSs offer equal

sum transmission rate at a particular time slot, the UE selects either BS randomly as the serving BS[7].

Since two active BSs consider each sleeping cell's UE in their channel scheduling, a UE in the sleeping cell needs to feed back the CQI to both BSs. As the number of sleeping cells in the network increases, the CQI feedback overhead becomes unbearable. However, since a UE in a sleeping cell is relatively far from the two closest active BSs, many of its channels will be at low states and thus the UE will have low probability to be allocated with those channels. Therefore, to reduce CQI feedback overhead, we consider the so-called best-m CQI feedback mechanism. According to this mechanism, the jth UE in the sleeping cell can feed back its best m_{j1} channels to BS_1 and its best m_{j2} channels to BS_2, where $m_{ji} \in \{1, \cdots, N\}$. The amount of CQI feedback to each BS that is needed for maintaining the QoS requirements of a particular UE depends on its distance from the serving BSs as well as the traffic loads of these BSs. We perform the analysis for a tagged UE in the sleeping cell, and we investigate the effect of the amount of CQI feedback on the performance of the tagged UE. The DCS considered in this chapter is explained in the detailed flow chart in Fig. 3.2.

For the considered DCS scheme, the information exchange between the jth UE in the sleeping cell and the ith serving BS is explained as follows. First, the BS broadcasts a pilot signal. Then, the UE measures its channel states and feeds back the states of the best m_{ji} channels to the BS. The minimum number of bits needed to feed back the states of the best m_{ji} channels is $m_{ji}\lfloor \log_2(K) \rfloor$. Next, the BS performs channel scheduling and offers channels (and consequently a sum transmission rate) to the UE. The value of the offered sum transmission rate is between 0 and $m_{ji}(K-1)$, and the minimum number of bits needed by the BS to notify the UE of the offered sum transmission rate is $\lfloor \log_2(m_{ji}(K-1)) \rfloor$. Finally, the UE notifies the BS of the cell selection decision using a minimum of 1 bit.

3.2.4 Packet arrival and scheduling

Packets of the tagged UE arriving from the core network to the PSG are assumed to follow a batch Bernoulli process, which is a general model that captures different levels of burstiness in the packet arrival process [39], [41]. The batch Bernoulli process is described by probability vector $\boldsymbol{\alpha} = \{\alpha_0, \alpha_1, \cdots ., \alpha_Z\}$, where α_i is the probability of i packets arriving at a given time slot and Z is the maximum possible packet arrival at a given time slot. Then, each packet is forwarded to one of the two closest active BSs (but not both). In particular, a packet arriving from the core network to the PSG is forwarded either to BS_1

[7]The DCS considered in this chapter can be employed using more BSs. This will increase the sum transmission rates available for UEs in the sleeping cell at the expense of severe out-of-sequence packet delivery, which can affect the delay performance.

with probability β or to BS_2 with probability $1-\beta$. The developed analytical model can be used to find the optimal value of β for a given performance measure as demonstrated later. Let $\psi_{i,j}$ denote the joint probabilities of i packet arrivals to BS_1 and j packet arrivals to BS_2. These probabilities can be expressed as:

$$\psi_{i,j} = \begin{cases} \frac{(i+j)!}{i!j!}\alpha_{i+j}\beta^i(1-\beta)^j, i,j \geq 0, i+j \leq Z, \\ 0, \quad \text{otherwise}, \end{cases} \tag{3.5}$$

where ! denotes the factorial operator and factor $(i+j)!/(i!j!)$ is to account for all possible packet forwarding scenarios with i packets forwarded to BS_1 and j packets forwarded to BS_2.

A particular BS is considered to have a packet buffer dedicated for each UE served by this BS. The arriving packets are temporarily stored in the packet buffer until they are transmitted to the UE. Since the tagged UE is dynamically served by two BSs, there are two packet buffers at the two BSs, respectively, for the tagged UE as shown in Fig. 3.3. Since packets of the tagged UE are randomly forwarded to one of the BSs and dynamically served according to the considered DCS scheme, packets can arrive at the tagged UE out-of-sequence. Also, we assume that packets at a given buffer are served in the same order they arrive to that buffer. Moreover, we consider that packets arriving to a given buffer at time slot n cannot be served until time slot $n+1$ at the earliest. The queuing system of the tagged UE shown in Fig. 3.3 can be modelled as a discrete time F/J queuing system. In particular, F/J queueing systems are used to model parallel and distributed systems where *"jobs"* are split upon arrival to multiple *"servers"* and then rejoined when they leave the system. In our system, data packets of a particular UE are forwarded to two BSs upon arrival according to the packet scheduling mechanism. Then, these packets are served by the BSs according to the considered DCS scheme and rejoined at the UE. Therefore, the overall system can be viewed as a F/J queuing system.

3.3 Formulation of the Queueing Model

3.3.1 Tagged UE's joint cell selection and sum transmission rate

In this subsection, we develop an analytic procedure to account for the cell selection mechanism and the sum transmission rate of the tagged UE while considering partial CQI feedback and max rate/opportunistic channel scheduling. In particular, state variables to jointly account for cell selection and sum transmission rate at a given time slot are obtained. Let us denote the state of the ith channel between BS_h and its jth UE at time slot n as $s_{i,j}^{(n)}$. Then, the probabilities $\Pr\{s_{i,j}^{(n)} = k\}, k = 0, 1, \cdots, K-1$, can be calculated using

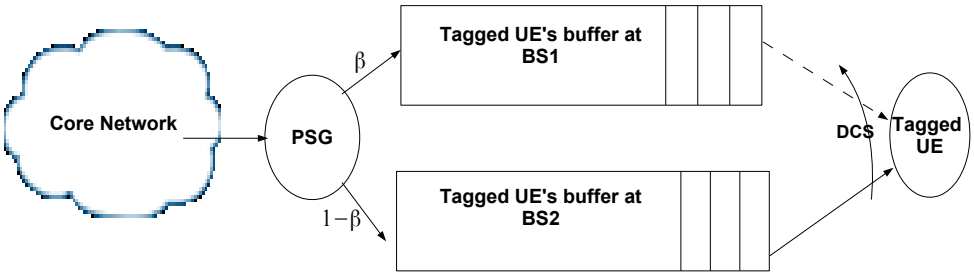

Figure 3.3: The resulting F/J queuing system.

$$\Pr\{c_{1,h,j}^{(n)}=k\}=\begin{cases}\sum_{k_2=0}^{K-1}\cdots\sum_{k_N=0}^{K-1}\min(1,\max(0,\frac{m_{jh}-(g_k(k_2)+\cdots+g_k(k_N))}{1+f_k(k_2)+\cdots+f_k(k_N)}))\Pr\{s_{1,h,j}^{(n)}=k\}\\ \prod_{i=2}^{N}\Pr\{s_{i,h,j}^{(n)}=k_i\}, \qquad 1\le k\le K-1,\\ 1-\sum_{k=1}^{K-1}\Pr\{c_{1,h,j}^{(n)}=k\}, \qquad k=0.\end{cases} \tag{3.6}$$

eq. (3.2). Note that we drop the index of BS_h from the channel state since the channel is between BS_h and its own UE.

We denote the state of the ith channel between BS_h and the jth sleeping cell UE which is served by BS_h at time slot n as $s_{i,h,j}^{(n)}$. The probabilities $\Pr\{s_{i,h,j}^{(n)}=k\}, k=0,1,\cdots,K-1$, can be calculated using eq. (3.2). Then, we define random variable $v_{i,h,j}^{(n)}\in\{0,1\}$ where $v_{i,h,j}^{(n)}=1$ if the CQI of the ith channel between BS_h and its jth UE in the sleeping cell is fed back at time slot n, and $v_{i,h,j}^{(n)}=0$ otherwise. We also define state variable $c_{i,h,j}^{(n)}=v_{i,h,j}^{(n)}s_{i,h,j}^{(n)}$, $0\le c_{i,h,j}^{(n)}\le K-1$. Without loss of generality, for the first channel between BS_h and its jth sleeping cell UE, the probabilities $\Pr\{c_{1,h,j}^{(n)}=k\}, k=0,1,\cdots,K-1$, can be calculated using eq. (3.6), which is proven in Appendix D. where we define function $f_x(y)$ which is equal to 1 if $x=y$ and 0 otherwise, and function $g_x(y)$ which is equal to 1 if $x<y$ and 0 otherwise.

Without loss of generality, we choose UE 1 in the sleeping cell as the tagged UE. Given the channel state of ith fed back channel between the tagged UE and BS_h (i.e., the ith channel from the set of best m_{1h} channels), we define random variable $u_{i,h,1}^{(n)}\in\{0,1\}$ where $u_{i,h,1}^{(n)}=1$ if the ith fed back channel between the tagged UE and BS_h is allocated to the tagged UE at time slot n, and $u_{i,h,1}^{(n)}=0$ otherwise. Then, conditional probabilities $\Pr\{u_{i,h,1}^{(n)}=a\mid c_{i,h,1}^{(n)}=k\}, a=0,1$, can be calculated using eq. (3.7). The proof of eq.

$$\Pr\{u_{i,h,1}^{(n)}=a \mid c_{i,h,1}^{(n)}=k\}=\begin{cases}\sum\limits_{k_1=0}^{k}\cdots\sum\limits_{k_{U_h}=0}^{k}\sum\limits_{l_2=0}^{k}\cdots\sum\limits_{l_{U_{sh}}=0}^{k}\frac{1}{1+f_k(k_1)+\cdots+f_k(k_{U_h})+f_k(l_2)+\cdots+f_k(l_{U_{sh}})} \\ \prod\limits_{j=1}^{U_h}\Pr\{s_{i,j}^{(n)}=k_j\}\prod\limits_{j=2}^{U_{sh}}\Pr\{c_{i,h,j}^{(n)}=l_j\}, \quad a=1, \\ 1-\Pr\{u_{i,h,1}^{(n)}=1 \mid c_{i,h,1}^{(n)}=k\}, \quad a=0.\end{cases} \tag{3.7}$$

(3.7) can be found in Appendix E. It is noteworthy that eq. (3.7) is based on max-rate channel scheduling. Our work can be extended to other channel scheduling mechanisms by modifying eq. (3.7) according to the considered channel scheduling mechanism. For example, the conditional probabilities $\Pr\{u_{i,h,1}^{(n)}=a \mid c_{i,h,1}^{(n)}=k\}, a=0,1$, for proportional fair channel scheduling can be calculated as shown in.

Next, the joint state space of the joint channel states of the best m_{1h} channels of the tagged UE with BS_h is denoted as: $\mathbf{\Lambda}_{h,1}=\{(s_{1,h,1}^{(n)},\cdots,s_{m_{1h},h,1}^{(n)}) \mid 0\leq s_{i,h,1}^{(n)}\leq K-1\}$. The number of unique states in state space $\Lambda_{h,1}$ is simply the number of combinations (with repetition) of the states of the best m_{1h} channels of the tagged UE with BS_h, which is denoted as M and can be calculated as follows:

$$M=\frac{(K+m_{1h}-1)!}{m_{1h}!(K-1)!}. \tag{3.8}$$

The probability of a particular state in state space $\mathbf{\Lambda}_{h,1}$, $\Pr\{s_{1,h,1}^{(n)}=k_1,\cdots,s_{m_{1h},h,1}^{(n)}=k_{m_{1h}}\}$, can be calculated as follows:

$$\Pr\{s_{1,h,1}^{(n)}=k_1,\cdots,s_{m_{1h},h,1}^{(n)}=k_{m_{1h}}\}=\sum_{k_{m_{1h}+1}=0}^{k_l}\sum_{k_{m_{1h}+2}=k_{m_{1h}+1}}^{k_l}\cdots\sum_{k_N=k_{N-1}}^{k_l}\frac{N!}{c_1!\times\cdots\times c_{K-1}!}\prod_{i=1}^{N}\Pr\{s_{i,h,1}^{(n)}=k_i\}, \tag{3.9}$$

where $k_l=\min(k_1,\cdots,k_{m_{1h}})$ and c_i's are to indicate the number of repetitions of a particular channel state across different channels.

Then, the joint state space of the channels allocation and the channels states of the best m_{1h} channels of the tagged UE with BS_h can be denoted as: $\mathbf{\Upsilon}_{h,1}=\{(s_{1,h,1}^{(n)},\cdots,s_{m_{1h},h,1}^{(n)}, u_{1,h,1}^{(n)},\cdots,u_{m_{1h},h,1}^{(n)}) \mid 0\leq s_{i,h,1}^{(n)}\leq K-1, 0\leq u_{i,h,1}^{(n)}\leq 1\}$. The joint probabilities of elements in state space $\mathbf{\Upsilon}_{h,1}$ can be calculated using the conditional probabilities in eq. (3.7) and the corresponding joint probabilities in eq. (3.9). Moreover, we define state variable $t_h^{(n)}=\sum\limits_{i=1}^{m_{1h}}u_{i,h,1}^{(n)}s_{i,h,1}^{(n)}, 0\leq t_h^{(n)}\leq(K-1)m_{1h}$, to indicate the sum of the channel states of all channels offered to the tagged UE from the serving BS_h. Let y_t ($y_t\subset\mathbf{\Upsilon}_{h,1}$) denote the

set of states that result in $t_h^{(n)} = t$. The probabilities $\Pr\{t_h^{(n)} = t\}, 0 \leq t \leq (K-1)m_{1h}$, can be calculated as: $\Pr\{t_h^{(n)} = t\} \sum_{w \in y_t} \Pr\{w\}$. The sum transmission rate offered by BS_h to the tagged UE at time slot n can readily be obtained using eq. (3.1).

Following the procedure described above, one can obtain the probabilities of state variables $t_1^{(n)}$ and $t_2^{(n)}$, which respectively represent the sum of channel states of the channels offered by BS_1 and BS_2 to the tagged UE at time slot n. Now, we define state variables $h^{(n)}, 1 \leq h^{(n)} \leq 2$, and $t^{(n)}, 0 \leq t^{(n)} \leq (K-1)m_{1h^{(n)}}$, to jointly represent the selected BS and the sum channel states of the channels offered to the tagged UE from the selected BS at time slot n. The joint probabilities $\Pr\{h^{(n)} = i, t^{(n)} = j\}, 1 \leq i \leq 2, 0 \leq j \leq (K-1)m_{1i}$, are given by:

$$\Pr\{h^{(n)} = i, t^{(n)} = j\} = \Pr\{t_i^{(n)} = j\} \sum_{k=0}^{j} \frac{1}{1 + f_j(k)} \Pr\{t_{\bar{i}}^{(n)} = k\}, \tag{3.10}$$

where $\bar{i}$ indicates the BS that is not selected at a given time slot i.e., $\bar{i} = 2$ if $i = 1$ and $\bar{i} = 1$ if $i = 2$. The proof of eq. (3.10) can be found in Appendix F.

3.3.2 System's overall state space and transition probability

We assume that all buffers have finite sizes. The joint system's state space can be defined as: $\mathbf{\Omega} = \{(h^{(n)}, q_1^{(n)}, q_2^{(n)}, t^{(n)}) \mid 1 \leq h^{(n)} \leq 2, 0 \leq q_1^{(n)} \leq Q_1, 0 \leq q_2^{(n)} \leq Q_2, 0 \leq t^{(n)} \leq (K-1)m_{1h^{(n)}}\}$, where $q_1^{(n)}$ and $q_2^{(n)}$ represent the number of packets at time slot n in the tagged UE's buffers at BS_1 and BS_2 respectively, and Q_1 and Q_2 are the sizes of the tagged UE's buffers at BS_1 and BS_2 respectively. Since the system under consideration is time discrete with discrete state variables, the system can be modelled as a DTMC. The transition probability matrix of the DTMC is denoted as $\mathbf{P}$ and its elements represent the joint transition probability $\Pr\{h^{(n+1)}, q_1^{(n+1)}, q_2^{(n+1)}, t^{(n+1)} \mid h^{(n)}, q_1^{(n)}, q_2^{(n)}, t^{(n)}\}$. $\mathbf{P}$ can be represented by its block sub-matrices as follows:

$$\mathbf{P} = \begin{bmatrix} \mathbf{P}_{1\to1} & \mathbf{P}_{1\to2} \\ \mathbf{P}_{2\to1} & \mathbf{P}_{2\to2} \end{bmatrix}, \tag{3.11}$$

where block sub-matrix $\mathbf{P}_{i\to j}$ represents the transition from all states with $h^{(n)} = i$ to all states with $h^{(n+1)} = j$. Furthermore, the components of each block sub-matrix $\mathbf{P}_{i\to j}$ are defined in eq. (3.12), where $Y_i = b(K-1)m_{1i}$. Moreover, the components of each block sub-matrix $\mathbf{A}_{\delta_1}^{(q_1)}(i,j)$ are defined in eq (3.13), where block sub-matrices $\mathbf{A}_{\delta_1,\delta_2}^{(q_1,q_2)}(i,j)$ represent the transition of the system from states (i, q_1, q_2) at time slot n to states $(j, q_1+\delta_1, q_2+\delta_2)$ at time slot $n+1$.

$$
\mathbf{P}_{i\to j} = \left[\begin{array}{c|c|ccc|cc}
\mathbf{A}_0^{(0)}(i,j) & \mathbf{A}_{1^+}^{(0)}(i,j) & \cdots & \mathbf{A}_{Z^+}^{(0)}(i,j) & & & \\
\hline
\mathbf{A}_{1^-}^{(1)}(i,j) & \mathbf{A}_0^{(1)}(i,j) & \mathbf{A}_{1^+}^{(1)}(i,j) & \cdots & \mathbf{A}_{Z^+}^{(1)}(i,j) & & \\
\vdots & \vdots & & & \ddots & & \\
\mathbf{A}_{(Y_i-Z+1)^-}^{(Y_i-Z+1)}(i,j) & \mathbf{A}_{(Y_i-Z)^-}^{(Y_i-Z+1)}(i,j) & \cdots & \mathbf{A}_0^{(Y_i-Z+1)}(i,j) & \cdots & \mathbf{A}_{(Z-1)^+}^{(Y_i-Z+1)}(i,j) & \\
\vdots & \vdots & & & & \vdots & \\
\mathbf{A}_{Y_i^-}(i,j) & \mathbf{A}_{(Y_i-1)^-}(i,j) & \cdots & \cdots & \mathbf{A}_{1^-}(i,j) & \mathbf{A}_0(i,j) & \\
\hline
 & \mathbf{A}_{Y_i^-}(i,j) & \cdots & \cdots & \cdots & \mathbf{A}_{1^-}(i,j) & \\
 & & \ddots & & & \vdots & \\
 & & & \mathbf{A}_{Y_i^-}(i,j) & & \mathbf{A}_{(Y_i-Z+1)^-}(i,j) & \\
 & & & & \ddots & \vdots & \\
 & & & & & \mathbf{A}_{Y_i^-}(i,j) & \\
\hline
 & & & & \ddots & &
\end{array}\right.
$$

$$
\left.\begin{array}{ccccc|ccc}
 & & & & & & & \\
\hline
\mathbf{A}_{Z^+}^{(Y_i-Z+1)}(i,j) & & & & & & & \\
\vdots & \ddots & & & & & & \\
\mathbf{A}_{1^+}(i,j) & \cdots & \mathbf{A}_{Z^+}(i,j) & & & & & \\
\hline
\mathbf{A}_0(i,j) & \cdots & \cdots & \mathbf{A}_{Z^+}(i,j) & & & & \\
\vdots & & & \ddots & & & & \\
\mathbf{A}_{(Y_i-Z)^-}(i,j) & \cdots & \cdots & \cdots & \mathbf{A}_{(Z-1)^+}(i,j) & \mathbf{A}_{Z^+}(i,j) & & \\
\vdots & & & \ddots & \vdots & \vdots & \ddots & \\
\mathbf{A}_{(Y_i-1)^-}(i,j) & \cdots & \cdots & \mathbf{A}_{1^-}(i,j) & \mathbf{A}_0(i,j) & \mathbf{A}_{1^+}(i,j) & \cdots & \mathbf{A}_{Z^+}(i,j) \\
\hline
 & & & \ddots & & & & \ddots
\end{array}\right] . \tag{3.12}
$$

$$
\mathbf{A}_{\delta_1}^{(q_1)}(i,j) = \left[\begin{array}{c|cccc|cc}
\mathbf{A}_{\delta_1,0}^{(q_1,0)}(i,j) & \mathbf{A}_{\delta_1,1^+}^{(q_1,0)}(i,j) & \cdots & \mathbf{A}_{\delta_1,Z^+}^{(q_1,0)}(i,j) & & & \\
\hline
\mathbf{A}_{\delta_1,1^-}^{(q_1,1)}(i,j) & \mathbf{A}_{\delta_1,0}^{(q_1,1)}(i,j) & \mathbf{A}_{\delta_1,1^+}^{(q_1,1)}(i,j) & \cdots & \mathbf{A}_{\delta_1,Z^+}^{(q_1,1)}(i,j) & & \\
\vdots & \vdots & & & \ddots & & \\
\mathbf{A}_{\delta_1,(Y_i-Z+1)^-}^{(q_1,Y_i-Z+1)}(i,j) & \mathbf{A}_{\delta_1,(Y_i-Z)^-}^{(q_1,Y_i-Z+1)}(i,j) & \cdots & \mathbf{A}_{\delta_1,0}^{(q_1)}(i,j) & \cdots & \mathbf{A}_{\delta_1,(Z-1)^+}^{(q_1,Y_i-Z+1)}(i,j) & \\
\vdots & \vdots & & & & \vdots & \\
\mathbf{A}_{\delta_1,Y_i^-}^{(q_1)}(i,j) & \mathbf{A}_{\delta_1,(Y_i-1)^-}^{(q_1)}(i,j) & \cdots & \cdots & \mathbf{A}_{\delta_1,1^-}^{(q_1)}(i,j) & \mathbf{A}_{\delta_1,0}^{(q_1)}(i,j) & \\
\hline
 & \mathbf{A}_{\delta_1,Y_i^-}^{(q_1)}(i,j) & \cdots & \cdots & \cdots & \mathbf{A}_{\delta_1,1^-}^{(q_1)}(i,j) & \\
 & & \ddots & & & \vdots & \\
 & & & \mathbf{A}_{\delta_1,Y_i^-}^{(q_1)}(i,j) & & \mathbf{A}_{\delta_1,(Y_i-Z+1)^-}^{(q_1)}(i,j) & \\
 & & & & \ddots & \vdots & \\
 & & & & & \mathbf{A}_{\delta_1,Y_i^-}^{(q_1)}(i,j) & \\
\hline
 & & & & \ddots & &
\end{array}\right.
$$

$$
\left.\begin{array}{c|ccc|cc|ccc}
 & & & & & & & & \\
\hline
\mathbf{A}_{\delta_1,Z^+}^{(q_1,Y_i-Z+1)}(i,j) & & & & & & & & \\
\vdots & \ddots & & & & & & & \\
\mathbf{A}_{\delta_1,1^+}^{(q_1)}(i,j) & \cdots & \mathbf{A}_{\delta_1,Z^+}^{(q_1)}(i,j) & & & & & & \\
\hline
\mathbf{A}_{\delta_1,0}^{(q_1)} & \cdots & \cdots & \mathbf{A}_{\delta_1,Z^+}^{(q_1)}(i,j) & & & & & \\
\vdots & & & \ddots & & & & & \\
\mathbf{A}_{\delta_1,(Y_i-Z)^-}^{(q_1)}(i,j) & \cdots & \cdots & \cdots & \mathbf{A}_{\delta_1,(Z-1)^+}^{(q_1)}(i,j) & \mathbf{A}_{\delta_1,Z^+}^{(q_1)}(i,j) & & & \\
\vdots & & & \ddots & \vdots & \vdots & \ddots & & \\
\mathbf{A}_{\delta_1,(Y_i-1)^-}^{(q_1)}(i,j) & \cdots & \cdots & \mathbf{A}_{\delta_1,1^-}^{(q_1)}(i,j) & \mathbf{A}_{\delta_1,0}^{(q_1)}(i,j) & \mathbf{A}_{\delta_1,1^+}^{(q_1)}(i,j) & \cdots & \mathbf{A}_{\delta_1,Z^+}^{(q_1)}(i,j) & \\
\hline
 & & & \ddots & & & & \ddots &
\end{array}\right] . \tag{3.13}
$$

$$\mathbf{P} = \begin{array}{c} 0 \\ 1 \\ 2 \\ 3 \\ \vdots \\ X-1 \\ X \end{array} \begin{bmatrix} \mathbf{C} & \mathbf{D} & & & & & \\ \mathbf{E} & \mathbf{F} & \mathbf{G} & & & & \\ & \mathbf{I_2} & \mathbf{I_1} & \mathbf{I_0} & & & \\ & & \mathbf{I_2} & \mathbf{I_1} & \mathbf{I_0} & & \\ & & & \ddots & \ddots & \ddots & \\ & & & & \mathbf{I_2} & \mathbf{I_1} & \mathbf{I_0}' \\ & & & & & \mathbf{I_2}' & \mathbf{I_1}' \end{bmatrix}. \tag{3.15}$$

Next, we define matrix $\mathbf{T}$, which is expressed in terms of its block sub-matrices as follows:

$$\mathbf{T} = \begin{bmatrix} \mathbf{T}_{11} & \mathbf{T}_{12} \\ \mathbf{T}_{21} & \mathbf{T}_{22} \end{bmatrix}, \tag{3.14}$$

where the elements of block sub-matrix $\mathbf{T}_{ij}$ are the joint probabilities $\Pr\{h^{(n)} = j, t^{(n)} = k\}, 1 \leq j \leq 2, 0 \leq k \leq (K-1)m_{1j}$, which can be calculated using eq. (3.10), and its size is $(\frac{Y_i}{b}+1) \times (\frac{Y_j}{b}+1)$. Also, we define set of matrices $\mathbf{O}_{ij}^{(l)}$ of size $(\frac{Y_i}{b}+1) \times (\frac{Y_j}{b}+1)$ as follows:

$$\mathbf{O}_{ij}^{(l)}(k,e) = \begin{cases} \mathbf{T}_{ij}(k,e) & \text{if} \quad k = l \\ 0 & \text{if} \quad k \neq l \end{cases}, \quad 0 \leq l \leq Y_i/b.$$

The detailed derivation of block sub-matrices $\mathbf{A}_{\delta_i,\delta_{\bar{i}}}^{(q_i,q_{\bar{i}})}(i,j)$ of each block sub-matrix $\mathbf{P}_{i \to j}$ is shown in Appendix C and $\mathbf{P}$ can be constructed accordingly.

By changing the order of state variables in the system's state space from $\mathbf{\Omega} = \{(h^{(n)}, q_1^{(n)}, q_2^{(n)}, t^{(n)}) \mid 1 \leq h^{(n)} \leq 2, 0 \leq q_1^{(n)} \leq Q_1, 0 \leq q_2^{(n)} \leq Q_2, 0 \leq t^{(n)} \leq (K-1)m_{1h^{(n)}}\}$ to $\mathbf{\Omega} = \{(q_1^{(n)}, q_2^{(n)}, h^{(n)}, t^{(n)}) \mid 0 \leq q_1^{(n)} \leq Q_1, 0 \leq q_2^{(n)} \leq Q_2, 1 \leq h^{(n)} \leq 2, 0 \leq t^{(n)} \leq (K-1)m_{1h^{(n)}}\}$, $\mathbf{P}$ can be represented as a QBD process as shown in eq. (3.15) where $X = \lfloor Q_1/Y_1 \rfloor$. In the rest of this chapter we drop the tagged UE's index from the number of channels that are fed back by the tagged UE to one of the serving BSs, and hence the number of channels that are fed back by the tagged UE to BS_h is m_h.

3.3.3 Steady state solution and derivation of performance measures

The steady state solution of the DTMC developed in Section 3.3.2 is denoted as $\boldsymbol{\pi}$ and can be calculated by solving: $\boldsymbol{\pi}\mathbf{P} = \boldsymbol{\pi}$ and $\boldsymbol{\pi}\mathbf{1} = 1$, where $\mathbf{1}$ is a column vector with all elements equal 1. Alternatively, since $\mathbf{P}$ can be represented as a QBD process, steady state solution $\boldsymbol{\pi}$ can be obtained using the matrix-analytic procedure in [46]. Steady state solution $\boldsymbol{\pi}$ can be written as: $\boldsymbol{\pi} = [\boldsymbol{\pi}^{(1)}\ \boldsymbol{\pi}^{(2)}]$, where $\boldsymbol{\pi}^{(h)}$ corresponds to states in which the tagged UE is served by BS_h and can further be expanded as $\boldsymbol{\pi}^{(h)} = [\boldsymbol{\pi}_{(0,0)}^{(h)} \ \cdots \ \boldsymbol{\pi}_{(Q_1,Q_2)}^{(h)}]$.

Buffers' length distribution

The buffers length distribution of the tagged UE's buffers at BS_1 and BS_2 can be easily obtained from steady state solution $\boldsymbol{\pi}$. In particular, the marginal probability $\Pr\{q_1 = i, q_2 = j\}, 0 \leq i \leq Q_1, 0 \leq j \leq Q_2$, is given by:

$$\Pr\{q_1 = i, q_2 = j\} = \sum_{h=1}^{2} \boldsymbol{\pi}_{(i,j)}^{(h)} \mathbf{1}, 0 \leq i \leq Q_1, 0 \leq j \leq Q_2. \tag{3.16}$$

Delay distribution

Since packets are randomly forwarded to two BSs which in turn dynamically transmit these packets to the tagged UE, it is obvious that packets can arrive at the tagged UE out-of-sequence. For example, if the first arriving packet is forwarded to BS_1 and the second arriving packet is forwarded to BS_2, the second arriving packet can be transmitted to the tagged UE before the first arriving packet depending on which BS is selected first. In this chapter, we define the delay as the number of time slots that takes for a packet to arrive at the tagged UE along with all packets ahead of it. Clearly, this definition accounts for out-of-sequence packet delivery since a packet arriving at the tagged UE is considered to be delayed until all packets ahead of it arrive at the tagged UE. Developing analytical models to account for this out-of-sequence packet delivery is highly desirable and has many applications in measuring delay for parallel transmission schemes such as the DCS scheme considered in this chapter, the soft load balancing scheme proposed in [56] and the parallel transmission scheme considered in [44].

In order to proceed to deriving the delay and other performance measures, we define absorbing Markov chain $\mathbf{P}_{\text{abs}}$, which can be derived by following the same procedure to derive $\mathbf{P}$ while setting $\alpha_0 = 1$ and $\alpha_i = 0, 1 \leq i \leq Z$. Then, we define $\boldsymbol{\pi}_0$ as follows: $\boldsymbol{\pi}_0 = \boldsymbol{\pi}\mathbf{P}_{\text{abs}}$, which can be expanded as $\boldsymbol{\pi}_0 = [\boldsymbol{\pi}_0^{(1)}\ \boldsymbol{\pi}_0^{(2)}]$. Also, $\boldsymbol{\pi}_0^{(h)}$ can further be expanded as $\boldsymbol{\pi}_0^{(h)} = [\boldsymbol{\pi}_{0(0,0)}^{(h)}\ \cdots\ \boldsymbol{\pi}_{0(Q_1,Q_2)}^{(h)}]$.

Next, we define $\boldsymbol{\omega}$ as the probability vector of the joint probabilities of the tagged UE's buffers states as seen by an arriving packet. $\boldsymbol{\omega}$ can be written as $\boldsymbol{\omega} = [\boldsymbol{\omega}^{(1)}\ \boldsymbol{\omega}^{(2)}]$, where $\boldsymbol{\omega}^{(h)}$ can further be expanded as: $\boldsymbol{\omega}^{(h)} = [\boldsymbol{\omega}_{(0,0)}^{(h)}\ \cdots\ \boldsymbol{\omega}_{(Q_1+Z,Q_2+Z)}^{(h)}]$. Then, probability vector $\boldsymbol{\omega}_{(q_1,q_2)}^{(h)}$ can be calculated as shown in eq. (3.17), where in this equation ξ_{ij} can be calculated as: $\xi_{ij} = \sum_{k=1}^{j} f_i(e_k)$ and function $\tilde{g}_x(y)$ is equal to 1 if $x \leq y$ and 0 otherwise. The proof of eq. (3.17) can be found in Appendix G.

A packet arriving to one of the tagged UE's buffers at BS_1 and BS_2 will be dropped if that buffer is full. Note that the probability that an arriving packet will see overflow in

$$\boldsymbol{\omega}^{(h)}_{(q_1,q_2)} = \frac{1}{1-\alpha_0}\sum_{z=1}^{Z}\sum_{e_1=1}^{2}\cdots\sum_{e_z=1}^{2}\sum_{k=1}^{z}\frac{\psi_{\xi_{1z},\xi_{2z}}(\xi_{1z}!\xi_{2z}!)}{z(\xi_{1z}+\xi_{2z})!}\tilde{g}_{\xi_{1k}}(q_1)\tilde{g}_{\xi_{2k}}(q_2)(\tilde{g}_{q_1}(Q_1+f_1(e_k)\xi_{1k})$$
$$\tilde{g}_{q_2}(Q_2+f_2(e_k)\xi_{2k})\boldsymbol{\pi}^{(h)}_{0(q_1-\xi_{1k},q_2-\xi_{2k})} + f_{q_1}(Q_1)f_2(e_k)\sum_{i=Q_1-\xi_{1k}+1}^{Q_1}\boldsymbol{\pi}^{(h)}_{0(i,q_2-\xi_{2k})} \tag{3.17}$$
$$+f_{q_2}(Q_2)f_1(e_k)\sum_{j=Q_2-\xi_{2k}+1}^{Q_2}\boldsymbol{\pi}^{(h)}_{0(q_1-\xi_{1k},j)}).$$

both buffers is 0. Therefore, all probabilities corresponding to overflow in both buffers are discarded and the probability that an arriving packet is dropped due to buffer overflow is denoted as $\mathcal{P}_{\mathrm{O}}$ and can be calculated as follows:

$$\mathcal{P}_{\mathrm{O}} = \sum_{h=1}^{2}\sum_{i=Q_1+1}^{Q_1+Z}\sum_{j=0}^{Q_2}\boldsymbol{\omega}^{(h)}_{(i,j)}\mathbf{1} + \sum_{h=1}^{2}\sum_{i=0}^{Q_1}\sum_{j=Q_2+1}^{Q_2+Z}\boldsymbol{\omega}^{(h)}_{(i,j)}\mathbf{1}. \tag{3.18}$$

Since queuing delay is only experienced by packets admitted to one of the tagged UE's buffers, we define probability vector $\boldsymbol{\Delta}$ of the joint probabilities of the tagged UE's buffers' states as seen by an admitted packet. $\boldsymbol{\Delta}$ can be written as $\boldsymbol{\Delta} = [\boldsymbol{\Delta}^{(1)}\ \boldsymbol{\Delta}^{(2)}]$, where $\boldsymbol{\Delta}^{(h)}$ can further be expanded as $\boldsymbol{\Delta}^{(h)} = [\boldsymbol{\Delta}^{(h)}_{(0,0)}\ \cdots\ \boldsymbol{\Delta}^{(h)}_{(Q_1,Q_2)}]$. Then, probability vector $\boldsymbol{\Delta}^{(h)}_{(q_1,q_2)}$ can be calculated by dividing the probabilities of the tagged UE's buffers states as seen by an arriving packet over the probability that an arriving packet is dropped due to buffer overflow as follows:

$$\boldsymbol{\Delta}^{(h)}_{(q_1,q_2)} = \frac{\boldsymbol{\omega}^{(h)}_{(q_1,q_2)}}{1-\mathcal{P}_{\mathrm{O}}}. \tag{3.19}$$

For an admitted packet, the states of the tagged UE's buffers after d time slots is denoted as $\boldsymbol{\chi}(d)$ and can be obtained as: $\boldsymbol{\chi}(d) = \boldsymbol{\Delta}\mathbf{P}^{d}_{\mathrm{abs}}$. $\boldsymbol{\chi}(d)$ can be written as $\boldsymbol{\chi}(d) = [\boldsymbol{\chi}^{(1)}(d)\,\boldsymbol{\chi}^{(2)}(d)]$, where $\boldsymbol{\chi}^{(h)}(d)$ can further be expanded as $\boldsymbol{\chi}^{(h)}(d) = [\boldsymbol{\chi}^{(h)}_{(0,0)}(d)\ \cdots\ \boldsymbol{\chi}^{(h)}_{(Q_1,Q_2)}(d)]$. Let D denote the queuing delay experienced by packets admitted to one of the tagged UE's buffers, The CDF of D can be calculated as:

$$F_D(d) = \sum_{h=1}^{2}\boldsymbol{\chi}^{(h)}_{(0,0)}(d)\mathbf{1}. \tag{3.20}$$

Note that eq. (3.20) accounts for out-of-sequence packet delivery since it considers not only the arrival of a particular packet, but also the arrival of all packets ahead in both buffers of the tagged UE. Moreover, the average queuing delay $\bar{\mathcal{D}}$ can be calculated as follows:

$$\bar{\mathcal{D}} = \sum_{d=1}^{d_m} d(F_D(d) - F_D(d-1)), \tag{3.21}$$

Table 3.1: Summary of parameter symbols and values.

Parameter Description	**Symbol**	**Value**
Macrocell radius	R_{M}	600 m
Inner cell radius	R_{I}	450 m
Target average bit error rate	BER_0	10^{-5}
Tagged UE's buffers sizes	Q_1, Q_2	$30, 30$
Packet size	ϵ	1024 bits
Packet arrival probability vector for first scenario	$\boldsymbol{\alpha_1}$	{0.2 0.3 0.3 0.2}
Packet arrival probability vector for second scenario	$\boldsymbol{\alpha_2}$	{0.2 0.1 0.4 0.3}
Number of outer band channels	N	20
Path loss exponent	η	2.8
Transmit power	p	43 dBm
Thermal noise power	σ	-121 dBm
Shadowing-fading parameters between BS_h and its UEs	κ_{hh}, θ_{hh}	1.6, 2.3
Shadowing-fading parameters between BS_h and sleeping cell UEs	κ_{sh}, θ_{sh}	1.2, 1.8
Adaptive transmission parameter	b	1
Number of channel states	K	3

where $F_D(d_m) = 1$.

The delay CDF offers a more elaborate measure of the delay performance of the tagged UE in the sleeping cell and is useful to guarantee statistical delay constraint. In particular, rather than having only average queuing delay requirements, the delay requirements of the tagged UE can be in the form $F_D(d_i) \geq \zeta$, where d_i is a specific number of time slots and ζ is the required delay guarantee probability.

Packet loss probability

Packets can be lost either due to buffer overflow or due to link error. The overall PLP can be calculated as follows:

$$\mathcal{P} = 1 - (1 - \mathcal{P}_{\mathrm{O}})(1 - \mathrm{PER}_0), \tag{3.22}$$

where PER_0 is the average packet error rate. In particular, for given target average bit error rate BER_0 and packet size ϵ, PER_0 is given by: $\mathrm{PER}_0 = 1 - (1 - \mathrm{BER}_0)^{\epsilon}$.

3.4 Numerical Results and Example Applications

In this section, we provide some selected numerical results using the analytical model developed in Section 3.3. We validate all numerical results via Monte Carlo using MATLAB. We compare the performance of the considered DCS scheme with the conventional

fixed cell selection where the tagged UE is served by a single BS. The results for fixed cell selection are obtained using the traditional queuing models developed in [39], [57]. We consider full CQI feedback in the case of fixed cell selection with $m_1 = N$ and $m_2 = 0$ if the tagged UE is served by BS_1, and $m_1 = 0$ and $m_2 = N$ if the tagged UE is served by BS_2.

We consider the first tier of a cellular network with the sleeping cell arbitrarily located in the centre as shown in Fig. 3.1. Locations of all UEs in the system are generated randomly. We randomly select UE 1 in the sleeping cell as the tagged UE and we label the two closest active BSs to the tagged UE as BS_1 and BS_2 respectively. The numbers of UEs who are served by BS_1, BS_2 (or both) are: $U_1 = 9$, $U_2 = 10$, $U_{s1} = 8$ and $U_{s2} = 10$. Other system parameters are shown in Table I unless other values are specified. We consider two different packet arrival scenarios with probability vectors $\boldsymbol{\alpha_1}$ and $\boldsymbol{\alpha_2}$ as shown in Table I.

3.4.1 Effect of the packet forwarding probability

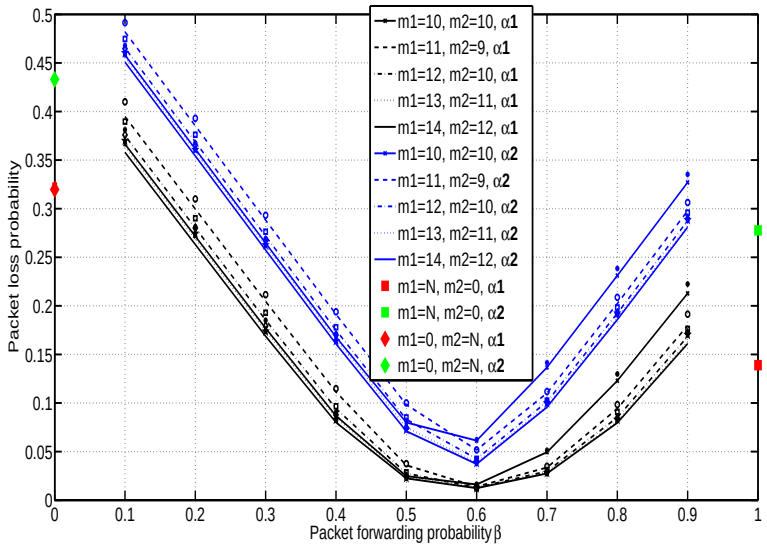

Figure 3.4: Packet loss probability vs. packet forwarding probability (markers correspond to Monte Carlo simulation results. $m_2 = 0$ corresponds to fixed cell selection with BS_1 and $m_1 = 0$ corresponds to fixed cell selection with BS_2).

First, we investigate the performance of the considered DCS scheme when varying the packet forwarding probability (β) for various CQI feedback and packet arrival scenarios. The PLP and average queuing delay performances versus β are shown in Fig. 3.4 and Fig. 3.5 respectively. From these figures, we can see that the values of β that result in optimal

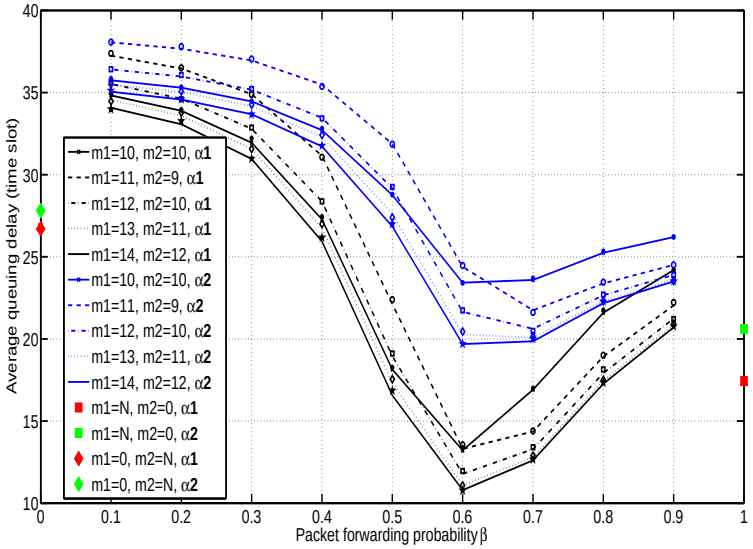

Figure 3.5: Average queuing delay vs. packet forwarding probability (markers correspond to Monte Carlo simulation results. $m_2 = 0$ corresponds to fixed cell selection with BS_1 and $m_1 = 0$ corresponds to fixed cell selection with BS_2).

PLP and optimal average queuing delay are not necessarily the same and β can be set to a value based on the QoS requirements as shown later through example applications. Also, it is obvious from Fig. 3.4 that the DCS scheme under consideration significantly improves the PLP performance in comparison with fixed cell selection for any packet arrival scenario. On the other hand, for the first packet arrival scenario with corresponding probability vector $\boldsymbol{\alpha_1}$, the average queuing delay of the considered DCS scheme is less than the average queuing delay when fixed cell selection with either BS is considered. For the second packet arrival scenario with probability vector $\boldsymbol{\alpha_2}$, which corresponds to a higher packet arrival rate, fixed cell selection with BS_1 outperforms the considered DCS scheme for the same amount of CQI feedback. As the amount of CQI feedback increases, the DCS scheme slightly improves the average queuing delay compared to fixed cell selection with BS_1.

Next, we investigate the CDF of delay for various packet scheduling, CQI feedback and packet arrival scenarios as shown in Fig. 3.6. In this figure, for a given CQI feedback and packet arrival scenario, we plot the delay CDF using the value of β that minimizes the average queuing delay. As expected, for a given packet scheduling and packet arrival scenario, increasing the amount of CQI feedback improves the delay performance of the tagged UE.

The value of β affects the inputs to the two buffers and the impacting factors of the

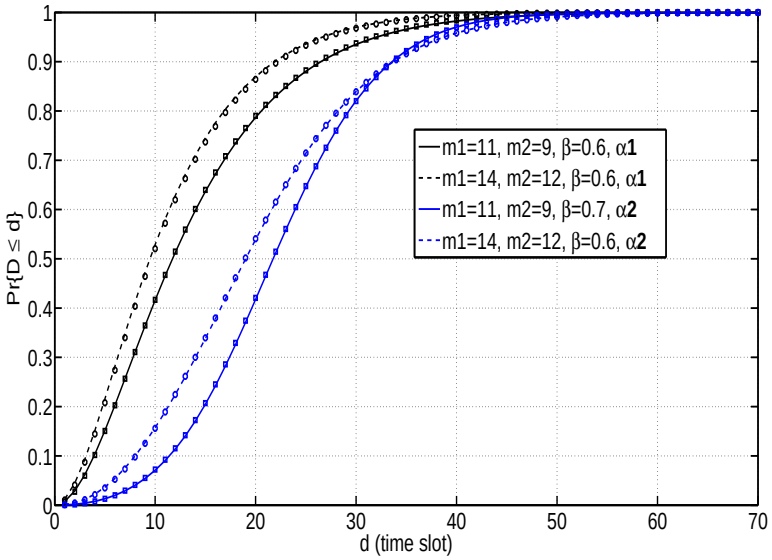

Figure 3.6: Delay CDF of various packet scheduling, CQI feedback and packet arrival scenarios (markers correspond to Monte Carlo simulation results).

optimal value of β are all parameters affecting the inputs or the outputs of the two buffers. These include the packet arrival scenario, the distance of the UE from the serving BSs, the number of UEs served by each BS and their locations, the number of outer band channels and the amount of CQI feedback to each BS.

3.4.2 Effect of varying the number of channels

Next, we show the performance of the tagged UE in the sleeping cell when varying the number of channels, N for various packet arrival and CQI feedback scenarios. The PLP and average queuing delay performances versus N are shown in Fig. 3.7 and Fig. 3.8 respectively. In Fig 3.7, for given value of N, packet arrival and CQI feedback scenario, we plot the PLP using the value of β that minimizes the PLP. Similarly, for given value of N, packet arrival and CQI feedback scenario, we plot the average queuing delay using the value of β that minimizes the average queuing delay in Fig 3.8. In the rest of this chapter, we use the optimal value of β with respect to the PLP when showing PLP performance. Also, we use the optimal value of β with respect to the average queuing delay when we show the average delay performance or the delay CDF.

Fig. 3.7 and Fig. 3.8 also show the PLP and the average queuing delay performances of the tagged UE under fixed cell selection with BS_1 and BS_2 for various packet arrival scenarios. For the PLP shown in Fig. 3.7, it is obvious that the considered DCS scheme

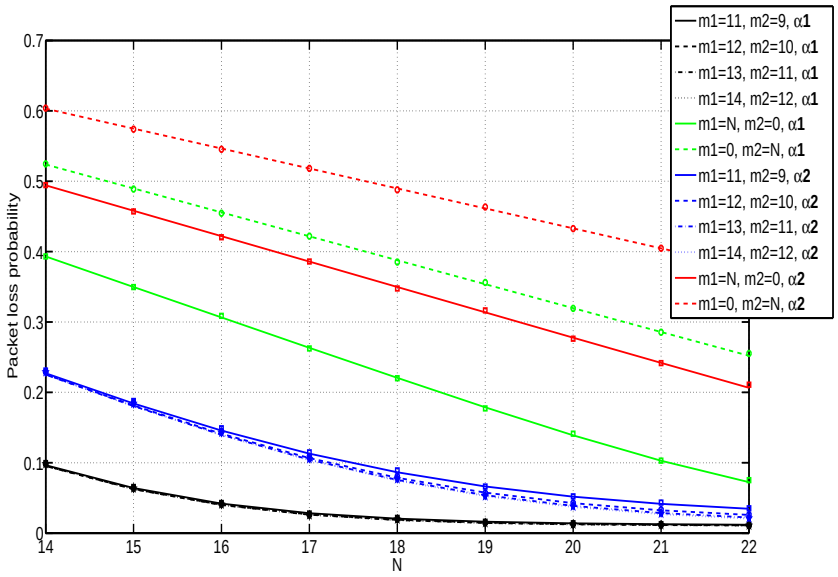

Figure 3.7: Packet loss probability vs. the number of outer band channels (markers correspond to Monte Carlo simulation results. $m_2 = 0$ corresponds to fixed cell selection with BS_1 and $m_1 = 0$ corresponds to fixed cell selection with BS_2).

outperforms fixed cell selection for any number of channels and for all packet arrival scenarios. In contrast, the average queuing delay performance of the DCS scheme with respect to fixed cell selection with BS_1 depends on the number of channels, N as well as the packet arrival scenario. In particular, for the first packet arrival scenario, it can be observed from Fig. 3.8 that fixed cell selection with BS_1 outperforms the considered DCS scheme for $N < 16$. As N increases, the DCS scheme outperforms fixed cell selection for the same amount of CQI feedback. Also, for the second packet arrival scenario, fixed cell selection with BS_1 outperforms the DCS scheme for $N < 20$ for the same amount of CQI feedback. For $N \geq 20$, the average queuing delay performance of the DCS scheme is improved by increasing the amount of CQI feedback.

Delay CDF for various packet scheduling, packet arrival, number of channels, N and CQI feedback scenarios is shown in Fig. 3.9. In this figure we observe that, for $N = 16$, only slight improvement in the delay is achieved when increasing the amount of CQI feedback for both packet arrival scenarios. On the other hand, for $N = 21$, increasing the amount of CQI feedback significantly improves the delay performance for both packet arrival scenarios. This is expected since the states of the best-m_h channels that are fed back by the tagged UE to BS_h is improved as N increases.

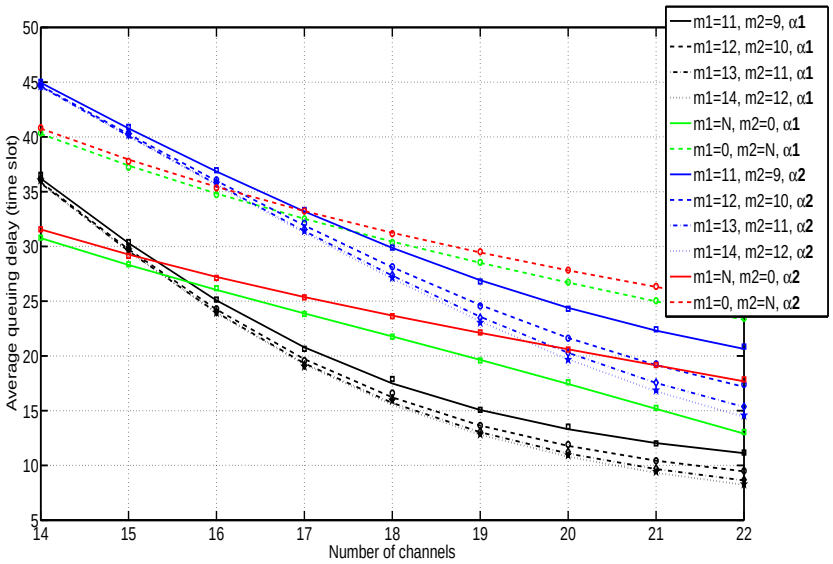

Figure 3.8: Average queuing delay vs. the number of outer band channels (markers correspond to Monte Carlo simulation results. $m_2 = 0$ corresponds to fixed cell selection with BS_1 and $m_1 = 0$ corresponds to fixed cell selection with BS_2).

3.4.3 Effect of varying the location of the tagged UE

Here, we investigate the performance of the tagged UE in the sleeping cell when varying its location. In particular, we consider locations of the tagged UE at various distances from the centre of the sleeping cell along a fixed direction. We refer to the distance between the centre of the sleeping cell and the tagged UE as r. Also, the locations of all other UEs in the sleeping cell as well as the locations of UEs in the active neighbouring cells are kept the same as the previous subsections. Fig. 3.10 and Fig. 3.11 respectively show the PLP and the average queuing delay performances of the DCS scheme under consideration for various packet scheduling, packet arrival and CQI feedback scenarios.

Fig. 3.10 and Fig. 3.11 also show the PLP and the average queuing delay performances of the tagged UE under fixed cell selection with BS_1 and BS_2 for various packet arrival scenarios. For the PLP shown in Fig. 3.10, it is obvious that the considered DCS scheme outperforms fixed cell selection at all locations and for all the considered packet arrival scenarios. On the other hand, the average queuing delay performance of the considered DCS scheme with respect to the average queuing delay performance of fixed cell selection with BS_1 varies significantly with distance. For example, it is observed in Fig. 3.11, for the first packet arrival scenario, that fixed cell selection with BS_1 outperforms the DCS scheme when $0 \leq r \leq 200$ and $400 \leq r \leq 500$ for the same amount of CQI feedback. The

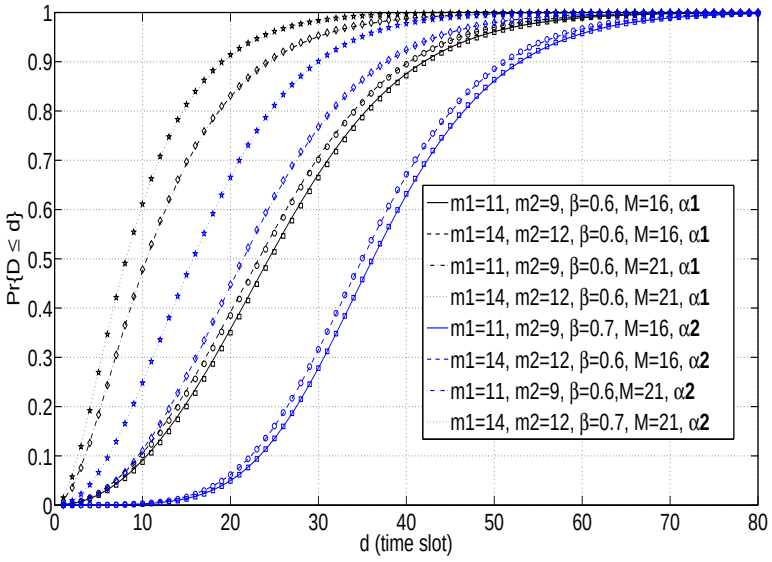

Figure 3.9: Delay CDF for various number of outer band channels, packet scheduling, CQI feedback and packet arrival scenarios (markers correspond to Monte Carlo simulation results).

DCS scheme under consideration outperforms fixed cell selection with BS_1 for the same amount of CQI feedback when $200 \leq r \leq 400$. Also, for the second packet arrival scenario, fixed cell selection with BS_1 outperforms the DCS scheme under consideration for the same amount of CQI feedback. As distance r increases, the average queuing delay of the DCS scheme is improved when increasing the amount of CQI feedback.

Finally, Fig. 3.12 shows the delay CDF for various tagged UE's locations, packet scheduling, packet arrival and CQI feedback scenarios. It is obvious from this figure that increasing the amount of CQI feedback does not improve the delay performance when the tagged UE is close to the centre of the sleeping cell. However, some improvement in the delay performance can be obtained by increasing the amount of CQI feedback at locations that are further away from the centre of the sleeping cell.

3.4.4 Effect of varying the number of UEs in the sleeping cell

Next, we show the performance of the DCS scheme under consideration versus the number of UEs in the sleeping cell. Here, locations of UEs in the sleeping cell are independent from the locations obtained in previous subsections. The PLP and the average queuing delay performances of the tagged UE under the considered DCS scheme for various packet scheduling, packet arrival, and CQI feedback scenarios are plotted in Fig. 3.13 and Fig.

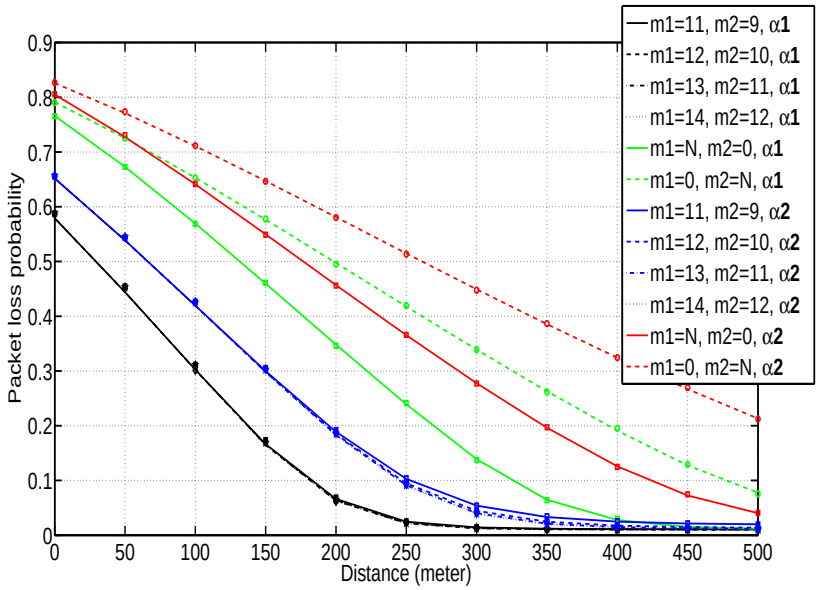

Figure 3.10: Packet loss probability vs. tagged UE's location (markers correspond to Monte Carlo simulation results. $m_2 = 0$ corresponds to fixed cell selection with BS_1 and $m_1 = 0$ corresponds to fixed cell selection with BS_2).

3.14 respectively.

Fig. 3.13 and Fig. 3.14 also show the PLP and the average queuing delay performances of the tagged UE under fixed cell selection with BS_1 and BS_2 for various packet arrival scenarios. For the PLP shown in Fig. 3.13, it is obvious that the considered DCS scheme outperforms fixed cell selection for any number of UEs in the sleeping cell and for all packet arrival scenarios. In contrast, the average delay performance of the DCS scheme with respect to fixed cell selection with BS_1 depends on the number of UEs in the sleeping cell as well as the packet arrival scenario. As shown in Fig. 3.14, for the first packet arrival scenario, the DCS scheme under consideration outperforms fixed cell selection with BS_1 for small number of UEs in the sleeping cell. As the number of UEs in the sleeping cell exceeds 12 UEs, the DCS scheme and fixed cell selection with BS_1 have similar performances. For the second packet arrival scenario, the DCS scheme under consideration outperforms fixed cell selection with BS_1 when the number of UEs in the sleeping cell is less than 4. Otherwise, fixed cell selection with BS_1 outperforms the DCS scheme.

Delay CDF for various packet scheduling, packet arrival, number of UEs in the sleeping cell and CQI feedback scenarios is shown in Fig. 3.15. In this figure, only slight improvement in the delay performance is achieved when increasing the amount of CQI feedback.

The numerical results in this chapter show that the considered DCS scheme provides

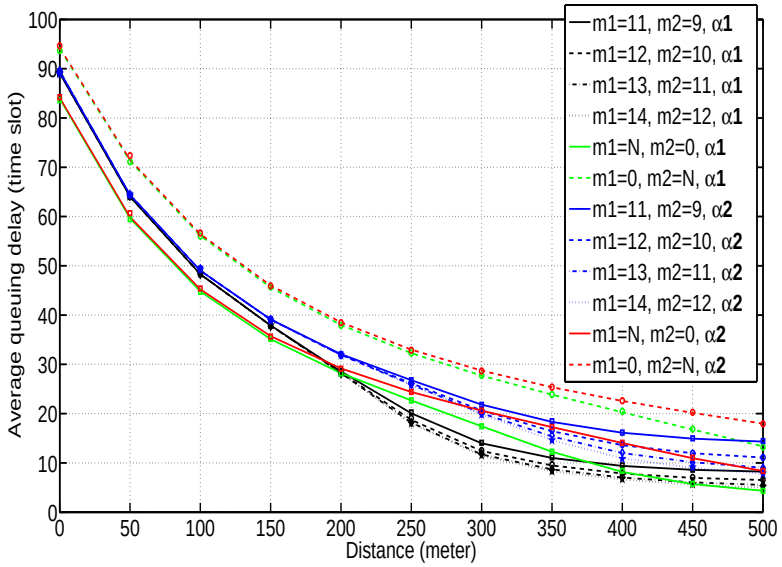

Figure 3.11: Average queuing delay vs. tagged UE's location (markers correspond to Monte Carlo simulation results. $m_2 = 0$ corresponds to fixed cell selection with BS_1 and $m_1 = 0$ corresponds to fixed cell selection with BS_2).

better PLP performance compared to fixed cell selection. There are two reasons, which are explained as follows. First, two BSs are used in the DCS scheme while one BS is used in fixed cell selection to store the same number of packets. Second, packets are transmitted at a higher rate in the DCS scheme since UEs are served using the BS with higher sum transmission rate. As a result, the probability of packet loss due to buffer overflow is less for the DCS scheme.

On the other hand, queuing delay performance of the DCS scheme varies significantly depending on the system and operating parameters. The reason is that, while packets are transmitted at a higher rate in the DCS scheme, out-of-sequence packet delivery results in extra delay. The tradeoff between these two factors depends on the system and operating parameters.

3.4.5 Comparison with state-of-the-art DCS

State-of-the-art DCS schemes consider that all data packets of the tagged UE are available at all candidate BSs and then one of the BSs is selected for transmission. On the other hand, our considered DCS only forwards a particular packet to a particular BS in order to avoid packet duplication. As such the bandwidth requirement and energy consumption for backhaul transmission are reduced. Unlike the considered DCS scheme,

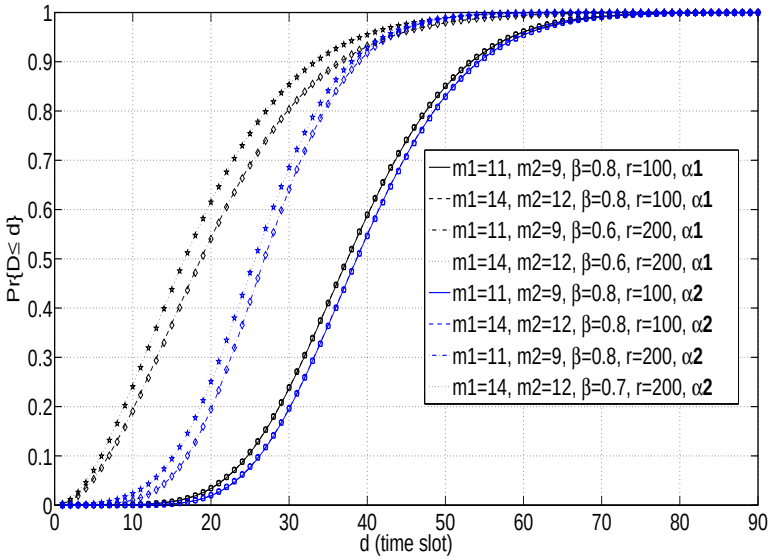

Figure 3.12: Delay CDF of various locations, packet scheduling, CQI feedback and packet arrival scenarios (markers correspond to Monte Carlo simulation results).

when a BS is selected at a given time slot with the state-of-the-art scheme, the selected BS needs to notify the other BS with the number of packets that are transmitted at that time slot. Then, these packets are discarded from the tagged UE's queue at the other BS. In LTE, the signalling between active neighbouring BSs is done using X2 interface. The effectiveness of the state-of-the-art DCS scheme depends on the delay of the X2 interface. Here, we compare the performance of our considered DCS scheme with the state-of-the-art DCS scheme for various values of X2 interface delay.

First, we show the performance of the considered DCS scheme compared to the state-of-the-art DCS scheme when varying the number of channels N for various cases of packet arrival and amount of CQI feedback. The PLP and average queuing delay performances versus N are shown in Fig. 3.16 and Fig. 3.17, respectively. From Fig. 3.16, we can see that the considered DCS scheme significantly improves the PLP performance compared to the state-of-the-art DCS scheme. On the other hand, average queuing delay performance of the state-of-the-art DCS scheme compared to the considered DCS scheme depends on the X2 interface delay and the various system and operating parameters as shown in Fig 3.17. For X2 interface delay of 2 time slots, the state-of-the-art DCS scheme outperforms the considered DCS scheme. However, for X2 interface delay of 5 time slots, the average queuing delay of the state-of-the-art DCS scheme compared to the considered DCS scheme depends on the number of channels and the packet arrival scenario. The average queuing

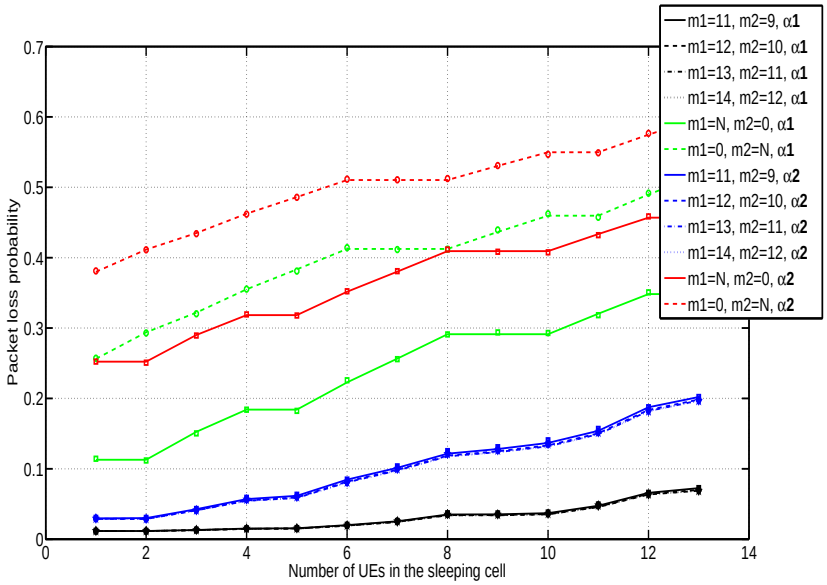

Figure 3.13: Packet loss probability vs. number of UEs in the sleeping cell (markers correspond to Monte Carlo simulation results. $m_2 = 0$ corresponds to fixed cell selection with BS_1 and $m_1 = 0$ corresponds to fixed cell selection with BS_2).

delay performance of the considered DCS scheme is significantly improved as N increases, especially for the first packet arrival scenario, which has a lower packet arrival rate. This indicates that the effect of out-of-sequence packet delivery is reduced in the considered DCS scheme when the packet arrival rate decreases or when the sum transmission rate increases due to increasing N.

The delay CDF of various packet arrival and CQI feedback scenarios are shown in Fig. 3.18 for $N = 21$. Clearly, the queuing delay performance of the state-of-the-art DCS scheme is significantly affected by X2 interface delay. Also, the queuing delay performance of the state-of-the-art DCS scheme compared to the considered DCS scheme depends on the value of X2 interface delay, the amount of CQI feedback and the packet arrival scenario.

Next, we investigate the performance of the state-of-the-art DCS scheme compared to the considered DCS scheme when varying the value of X2 interface delay. The PLP and average queuing delay performances versus X2 interface delay are shown in Fig. 3.19 and Fig. 3.20, respectively. The considered DCS scheme provides better PLP performance compared to the state-of-the-art DCS scheme except for very low values of X2 interface delay as shown in Fig. 3.19. On the other hand, average queuing delay performance of the state-of-the-art DCS scheme compared to the considered DCS scheme depends on the X2 interface delay as well as the packet arrival scenario as shown in Fig. 3.20. From Fig. 3.19

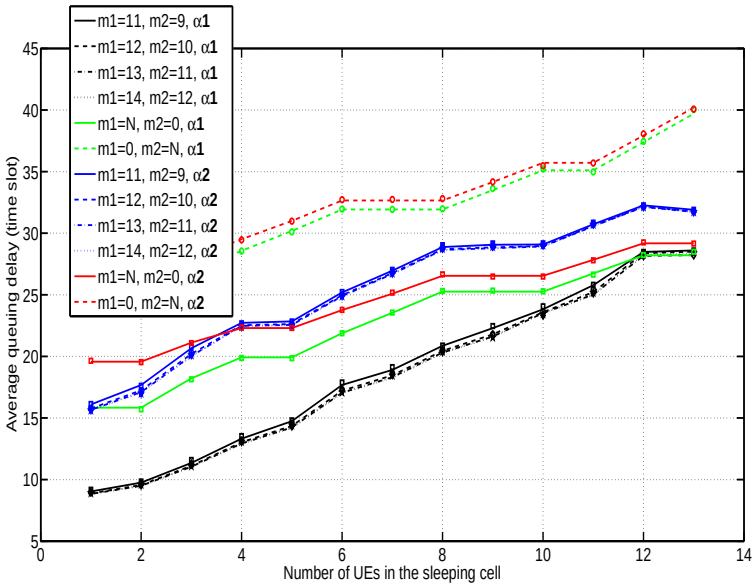

Figure 3.14: Average queuing delay vs. number of UEs in the sleeping cell (markers correspond to Monte Carlo simulation results. $m_2 = 0$ corresponds to fixed cell selection with BS_1 and $m_1 = 0$ corresponds to fixed cell selection with BS_2).

and Fig. 3.20, it is obvious that the performance of the state-of-the-art DCS scheme is significantly impacted by X2 interface delay. This is expected since the delay in discarding packets from a BS that is not selected at a given time slot is equal to the delay of the X2 interface. This delay in packet discarding results in increasing packet loss due to queue overflow and increasing queuing delay.

Next, we show the performance of the considered DCS scheme compared to the state-of-the-art DCS scheme when varying the distance of the tagged UE for various cases of packet arrival and amount of CQI feedback. The PLP and average queuing delay performances versus r are shown in Fig. 3.21 and Fig. 3.22, respectively. From Fig. 3.21, we can see that the considered DCS scheme provides better PLP performance compared to the state-of-the-art DCS scheme. On the other hand, average queuing delay performance of the state-of-the-art DCS scheme compared to the considered DCS scheme depends on the X2 interface delay and the various system and operating parameters as shown in Fig 3.22. For X2 interface delay of 2 time slots, the state-of-the-art DCS scheme outperforms the considered DCS scheme. However, for X2 interface delay of 5 time slots, the average queuing delay of the state-of-the-art DCS scheme compared to the considered DCS scheme depends on the distance r. As the sum transmission rate increases due to increasing r, the considered DCS scheme provides better average queuing delay performance.

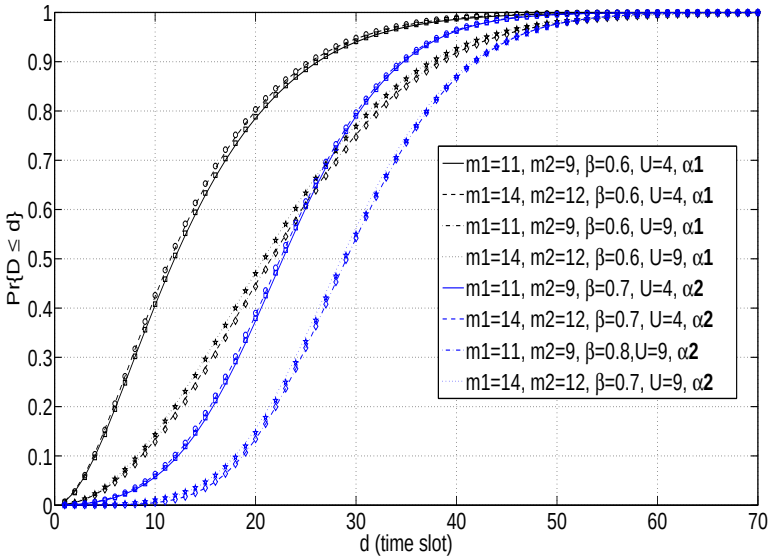

Figure 3.15: Delay CDF of various packet scheduling, number of UEs in the sleeping cell, CQI feedback and packet arrival scenarios (markers correspond to Monte Carlo simulation results).

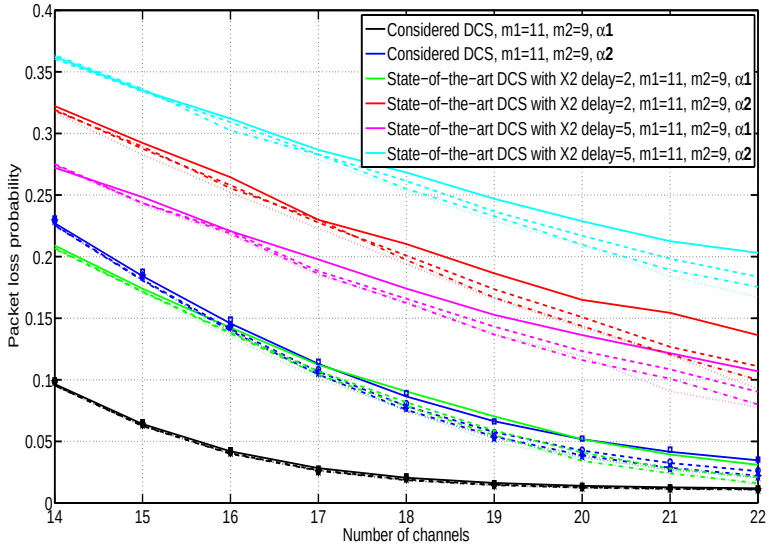

Figure 3.16: Packet loss probability vs. the number of outer band channels (Non-solid lines correspond to various CQI feedback scenarios and markers correspond to simulation results of the considered DCS scheme)

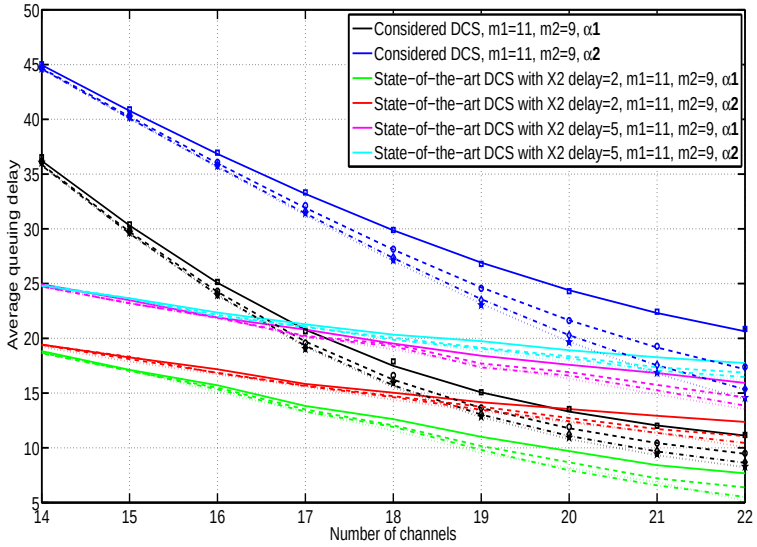

Figure 3.17: Average queuing delay vs. the number of outer band channels (Non-solid lines correspond to various CQI feedback scenarios and markers correspond to simulation results of the considered DCS scheme).

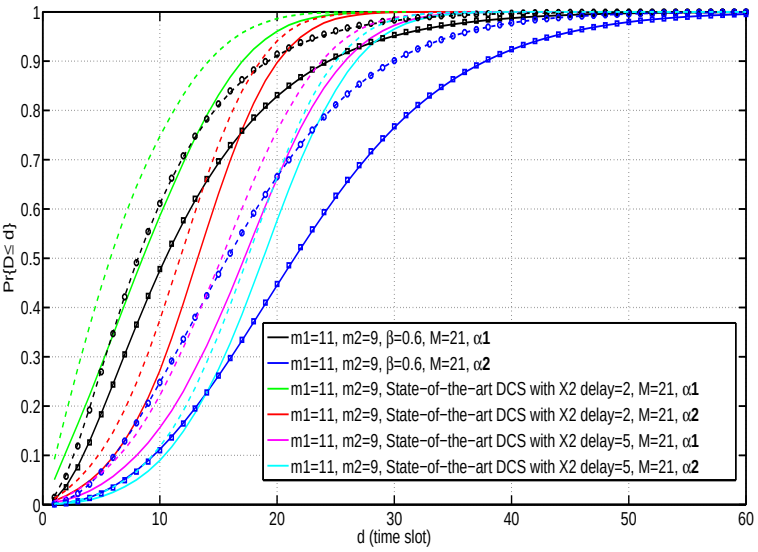

Figure 3.18: Delay CDF for various number of outer band channels, packet scheduling, CQI feedback and packet arrival scenarios (Non-solid lines correspond to various CQI feedback scenarios and markers correspond to simulation results of the considered DCS scheme).

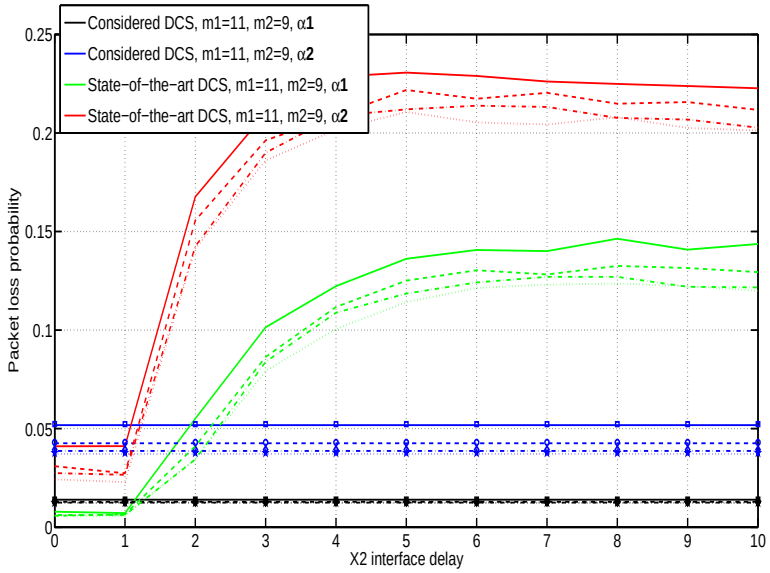

Figure 3.19: Packet loss probability vs. X2 interface delay (Non-solid lines correspond to various CQI feedback scenarios and markers correspond to simulation results of the considered DCS scheme)

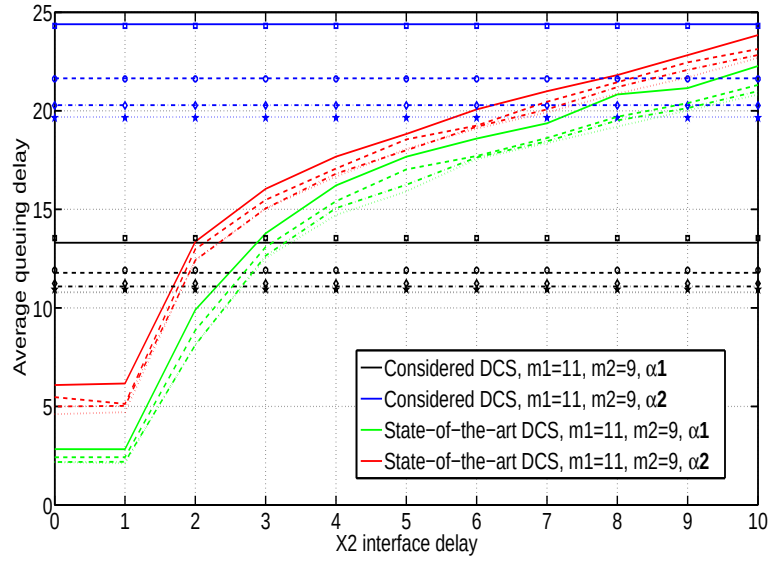

Figure 3.20: Average queuing delay vs. X2 interface delay (Non-solid lines correspond to various CQI feedback scenarios and markers correspond to simulation results of the considered DCS scheme).

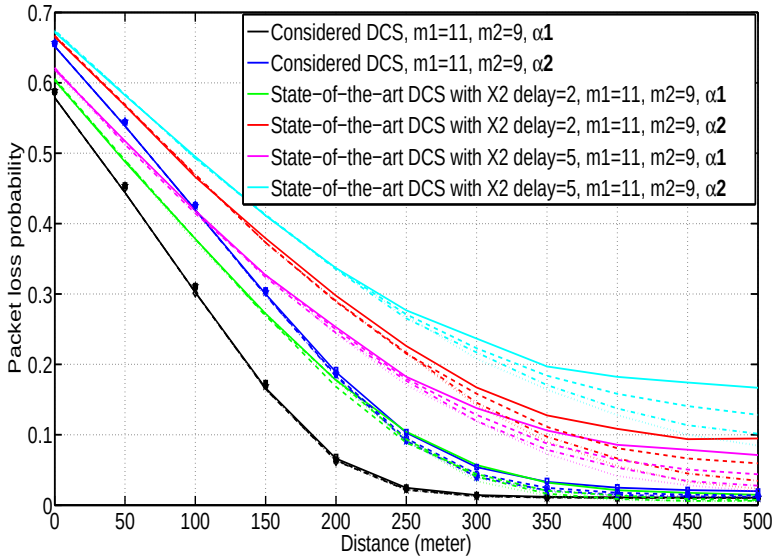

Figure 3.21: Packet loss probability vs. tagged UE's location (Non-solid lines correspond to various CQI feedback scenarios and markers correspond to simulation results of the considered DCS scheme)

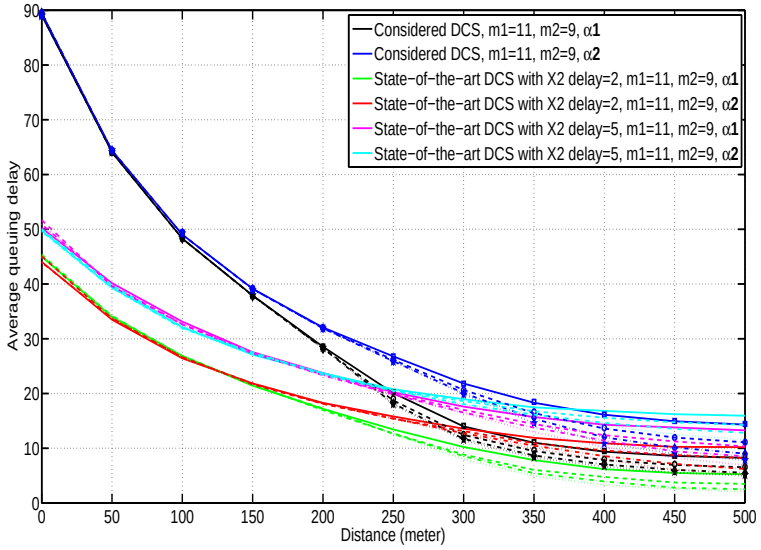

Figure 3.22: Average queuing delay vs. tagged UE's location (Non-solid lines correspond to various CQI feedback scenarios and markers correspond to simulation results of the considered DCS scheme).

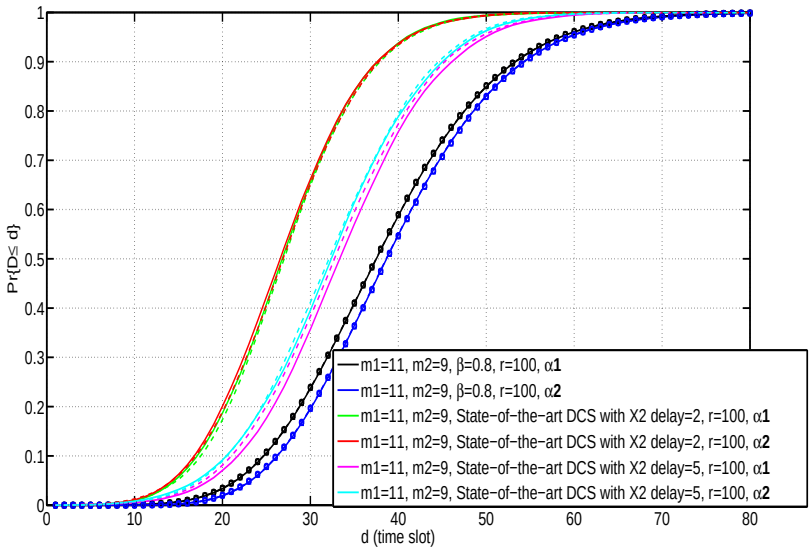

Figure 3.23: Delay CDF for various locations, packet scheduling, CQI feedback and packet arrival scenarios (Non-solid lines correspond to various CQI feedback scenarios and markers correspond to simulation results of the considered DCS scheme).

The delay CDF of various packet arrival and CQI feedback scenarios are shown in Fig. 3.23 for $r = 100$. The state-of-the-art DCS scheme outperforms the considered DCS scheme since these results are shown for a relatively short distance r.

Finally, we show the performance of the considered DCS scheme compared to the state-of-the-art DCS scheme when varying the number of UEs in the sleeping cell for various cases of packet arrival and amount of CQI feedback. The PLP and average queuing delay performances versus number of UEs in the sleeping cell are shown in Fig. 3.24 and Fig. 3.25, respectively. From Fig. 3.24, we can see that the considered DCS scheme provides better PLP performance compared to the state-of-the-art DCS scheme. On the other hand, average queuing delay performance of the state-of-the-art DCS scheme compared to the considered DCS scheme depends on the X2 interface delay and the various system and operating parameters as shown in Fig 3.25. For X2 interface delay of 2 time slots, the state-of-the-art DCS scheme outperforms the considered DCS scheme. However, for X2 interface delay of 5 time slots, the average queuing delay of the state-of-the-art DCS scheme compared to the considered DCS scheme depends on the number of UEs in the sleeping cell and the packet arrival scenario. For a higher sum transmission rate due to smaller number of UEs in the sleeping cell, the considered DCS scheme provides better average queuing delay performance for the first packet arrival scenario. Again this indicates that

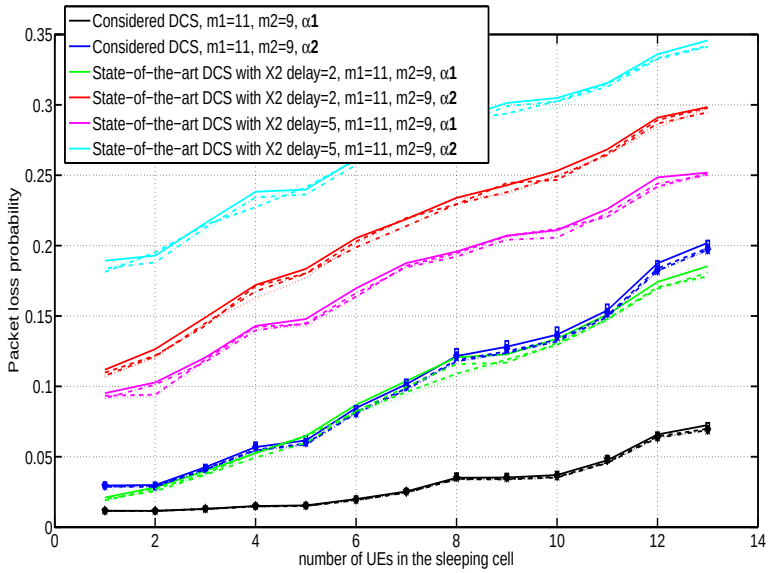

Figure 3.24: Packet loss probability vs. number of UEs in the sleeping cell (Non-solid lines correspond to various CQI feedback scenarios and markers correspond to simulation results of the considered DCS scheme)

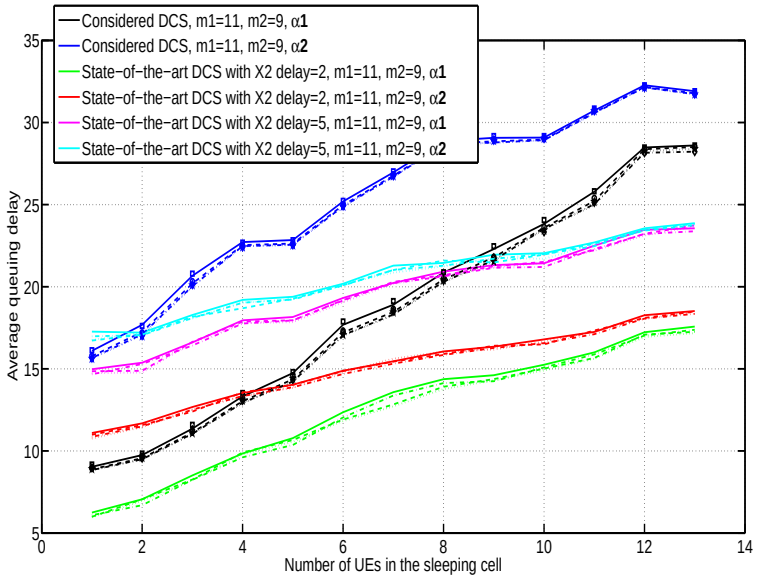

Figure 3.25: Average queuing delay vs. number of UEs in the sleeping cell (Non-solid lines correspond to various CQI feedback scenarios and markers correspond to simulation results of the considered DCS scheme).

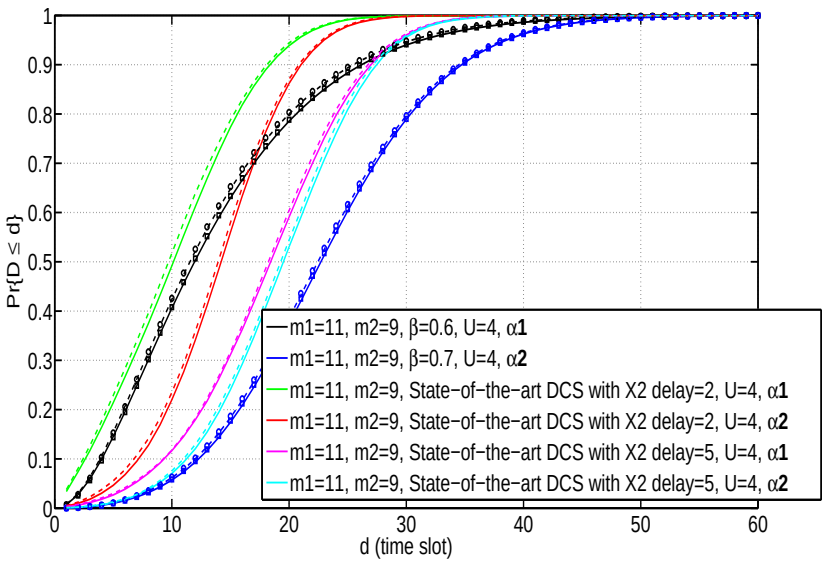

Figure 3.26: Delay CDF for various number of UEs in the sleeping cell, packet scheduling, CQI feedback and packet arrival scenarios (Non-solid lines correspond to various CQI feedback scenarios and markers correspond to simulation results of the considered DCS scheme).

the effect of out-of-sequence packet delivery in the considered DCS scheme is reduced for lower packet arrival rate and higher sum transmission rate.

The delay CDF of various packet arrival and CQI feedback scenarios are shown in Fig. 3.26. The queuing delay performance of the state-of-the-art DCS scheme compared to the considered DCS scheme depends on the value of X2 interface delay, the amount of CQI feedback and the packet arrival scenario.

From the above comparison between the considered DCS scheme and the state-of-the-art DCS scheme we can see that the considered DCS scheme provides better PLP performance mostly. On the other hand, queuing delay performance depends on the value of the X2 interface delay as well as other system and operating parameters. Also, the state-of-the-art DCS scheme suffers from a significant amount of additional backhaul resources due to packet duplication, which results in significant increase in cost and energy consumption.

3.4.6 Example applications of the developed queuing model

In what follows, we provide some example applications of our developed model. Our developed model can be used to gauge various packet level performance measures for the considered DCS scheme. Also, the developed model can be used to select various parame-

ters in order to achieve the QoS requirements of UEs in the sleeping cell. In particular, for given other system and operating parameters, the network operator can use our model to determine the values of β, m_1 and m_2 needed to maintain packet level QoS requirements of each UE in the sleeping cell. For example, for the packet arrival scenario with probability vector $\boldsymbol{\alpha_2}$, if the tagged UE QoS requirements are $\mathcal{P} = 0.1$, $\bar{\mathcal{D}} = 22$, $d_i = 20$ and $\zeta = 0.42$, these requirements can be satisfied with $m1 = 11$, $m2 = 9$ and $\beta = 0.7$ as obtained from Fig. 3.4, Fig. 3.5 and Fig. 3.6. Moreover, our model can be used to determine whether a particular UE in the sleeping cell should be served using the considered DCS scheme or using the conventional fixed cell selection based on the QoS requirements. For example, in Section IV-C for the first packet arrival scenario with probability vector $\boldsymbol{\alpha_1}$, it is obvious that at distance $r = 500$ between the tagged UE and the centre of the sleeping cell, fixed cell selection provides better average delay performance compared to the considered DCS scheme while the PLP performance of both schemes is similar due to low PLP in both cases. These can be observed from Fig. 3.10 and Fig. 3.11.

Also, our model can be used for cross-layer performance analysis with partial CQI feedback. In this chapter we consider partial CQI feedback and we develop a systematic procedure to incorporate this partial CQI feedback into the queuing analytical model. Even though our queuing model is specific to CoMP DCS, the procedure developed here to account for partial CQI feedback is comprehensive and can be used to analyze the cross-layer performance of wireless systems with best-m CQI feedback. Specifically, using eqs. (3.1)-(3.9) and the analytic procedure described in Section III-A, the states of the best m_h channels that are fed back to BS_h by the tagged UE, the probability that a particular channel, which has been fed back, is allocated to the tagged UE and the sum transmission rate allocated to the tagged UE by BS_h can be calculated.

In addition, our model can be used for CAC. CAC based on the packet level QoS requirements has been proposed in [58]. As shown in Section IV-D, our model can be used to measure the packet level performances of UEs in the sleeping cell for various numbers of UEs under the DCS scheme. So, based on these performances, the network operator can determine if the packet level QoS requirements of existing UEs as well as new UEs requesting service can be met if these new UEs are admitted in the system. If the QoS requirements of UEs are satisfied, new UE's request can be served. Otherwise, the request can be rejected.

Chapter 4

DL Multi-Flow CA in Heterogeneous Networks

4.1 Synopsis

We consider multi-flow CA with dedicated spectrum access for serving MUEs in the ER of the small cells. The main contributions and outcomes of this chapter are as follows.

1. We develop a cross-layer F/J queuing analytical model that takes into account the time varying channels, the channel scheduling algorithm, partial CQI feedback and the number of component carriers deployed at each tier. Our model also accounts for stochastic packet arrivals and the packet scheduling mechanism. The accuracy of the developed analytical model is validated through computer simulations.

2. The developed analytical model can be used to gauge various packet-level performance parameters e.g., PLP and queuing delay of MUEs in the ER of the small cells. For the queuing delay performance, our model takes out-of-sequence packet delivery into consideration.

3. Using numerical examples, we demonstrate that the developed model can also be used to select various system and operating parameters in order to offload as much traffic as possible from the macrocells to the small cells while maintaining the QoS requirements of MUEs in the ER of the small cells. For example, the packet scheduling parameter, the amount of CQI feedback, the number of deployed small cells and the ER of the small cells can be tuned to maintain the QoS requirements of MUEs in the ER of the small cells as demonstrated in Section IV.

The rest of this chapter is organized as follows. In Section 4.2 a detailed description of the system model is provided. Developing the queuing analytical model and deriving packet-level QoS measures are presented in Section 4.3. In Section 4.4, selected numerical results and example applications are presented.

4.2 System Model and Operating Assumptions

4.2.1 Overall system description

We consider a two-tier cellular network with the small cells randomly deployed within the macrocell following a uniform distribution as shown in Fig. 4.1. The coverage of the macrocells and the small cells is assumed to be circular with radii R_{M} and R_{S} respectively. Also, the ER of the small cells is denoted as R_{E} and is shown in Fig. 4.1. We consider dedicated carrier deployment where small cells utilize component carriers that are not used by the macrocells. One can also consider shared carrier deployment by accounting for cross-tier interference and employing a suitable ICIC technique, and then use the queuing model developed in this chapter to measure the performance of the MUEs in the ER of the small cells. It is noteworthy that this can result in performance degradation of SUEs since they already share the component carriers dedicated for them with nearby MUEs.

Different component carriers have distinct propagation characteristics depending on their frequency band. Without loss of generality, we consider that two component carriers F_{M1} and F_{M2} are deployed at the macro base station (MBS) while one component carrier F_{S1} is deployed at the SBSs. Moreover, each component carrier $F_{\mathrm{H}j}$ is assumed to be divided into $N_{\mathrm{H}j}$ channels, where $\mathrm{H} \in \{\mathrm{M}, \mathrm{S}\}$.

We assume that MUEs are uniformly distributed within the macrocell and SUEs are uniformly distributed within the small cells. MUEs that are not located within the ER of a small cell are only served by the macrocell. Similarly, SUEs are only served by the small cells[8]. On the other hand, a MUE that is located within the ER of a small cell is served by both the macrocell and the small cell through multi-flow CA. We consider a time slotted system and we are interested in the DL transmission. Our objective is to investigate the performance of a tagged MUE [9] in the ER of a reference small cell [10]. For notational convenience, we denote the number of MUEs as U_{M}, the number of MUEs in the ER of the reference small cell as U_{SM}, the number of MUEs in the ER of any small cell as U_{MS} and the number of SUEs in the reference small cell as U_{S}.

[8]It is also possible to consider multi-flow CA for SUEs, however, this can compromise the performance of the MUEs as this offloads traffic from the small cells to the macrocell.

[9]The overall system performance can be obtained by averaging the performance of all UEs in the network. However, this performance may not be interesting since the QoS requirements vary significantly among UEs depending on their applications/service classes.

[10]The performance of SUEs and MUEs that are not in the ER of any small cell can be obtained using traditional queuing models presented in [39, 40].

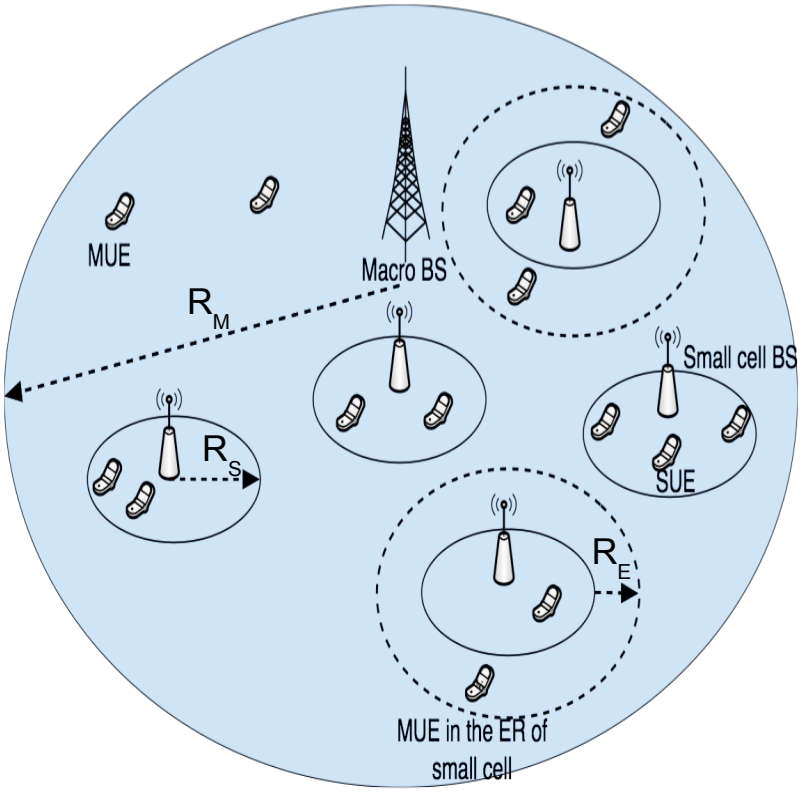

Figure 4.1: An example of a two-tier cellular network with CRE of the small cells.

4.2.2 Channel model, adaptive transmission, channel scheduling and partial CQI feedback

We model channel gain using the Gamma distribution, which is tractable, yet with a high accuracy, for modelling composite shadowing and fading channels [50]. The received SINR/SNR is mapped into a finite set of channel states $\mathcal{S} = \{0, 1, \cdots, K-1\}$, and adaptive transmission is utilized to take advantage of the time varying channels. In particular, let x denote the number of packets that can be transmitted over a particular channel at a given time slot. x is given by:

$$x = bk, \quad 0 \leq k \leq K-1, \tag{4.1}$$

where k is the channel state and b is an integer that depends on the network resource allocation.

Channel i from component carrier $F_{\mathrm{H}j}$ of UE l is considered to be in state k at time slot n if $\gamma_k \leq \gamma^{(n)}_{\mathrm{H},j,i,l} < \gamma_{k+1}$, where $\gamma^{(n)}_{\mathrm{H},j,i,l}$ is the received SINR/SNR and γ_k is the lower boundary threshold of channel state k [51], [52]. Also, the thresholds $\{\gamma_k\}_{k=0}^{K}$ take values that satisfy a target average bit error rate (BER_0) for all transmission modes (see for

example [53]). We denote the channel state of channel i from component carrier $F_{\mathrm{H}j}$ of UE l at time slot n as $s^{(n)}_{\mathrm{H},j,i,l}$, and the probabilities $\Pr\{s^{(n)}_{\mathrm{H},j,i,l} = k\}, k = 0, 1, \cdots, K-1$, can be calculated as follows:

$$\begin{aligned} &\Pr\{s^{(n)}_{\mathrm{H},j,i,l} = k\} = \Pr\{\gamma_k \leq \gamma^{(n)}_{\mathrm{H},j,i,l} < \gamma_{k+1}\} \\ &= \mathrm{P}_{\mathrm{th}}(\gamma_{k+1}) - \mathrm{P}_{\mathrm{th}}(\gamma_k), \quad k = 0, 1, \cdots, K-1, \end{aligned} \tag{4.2}$$

where $\mathrm{P}_{\mathrm{th}}(x)$ is essentially the outage probability. If no interferers are present, $\mathrm{P}_{\mathrm{th}}(\gamma_k)$ can be calculated as follows:

$$\mathrm{P}_{\mathrm{th}}(\gamma_k) = \frac{\Gamma_{\mathrm{L}}(\kappa_{\mathrm{H}j}, \gamma_k/(\bar{\gamma}_{\mathrm{H},j,l}\theta_{\mathrm{H}j}))}{\Gamma(\kappa_{\mathrm{H}j})}, \tag{4.3}$$

where $\Gamma_{\mathrm{L}}(y, x) = \int_0^x t^{y-1}\exp(-t)dt$, $\Gamma(y) = \int_0^\infty t^{y-1}\exp(-t)dt$, $\kappa_{\mathrm{H}j}$ and $\theta_{\mathrm{H}j}$ are respectively the first and the second parameters of the Gamma distribution for component carrier $F_{\mathrm{H}j}$ and $\bar{\gamma}_{\mathrm{H},j,l}$ is the average received SNR. $\bar{\gamma}_{\mathrm{H},j,l}$ depends on the distance between UE l and the serving BS, path loss exponent $\eta_{\mathrm{H}j}$ corresponding to component carrier $F_{\mathrm{H}j}$, thermal noise σ and transmission power p_{H}. On the other hand, in the presence of I interferers, $\mathrm{P}_{\mathrm{th}}(\gamma_k)$ can be calculated using the classical lemma presented in [54] as follows:

$$\mathrm{P}_{\mathrm{th}}(\gamma_k) = \frac{1}{\pi}\int_0^\infty \mathrm{Im}\left(\frac{\mathrm{e}^{j\gamma_k\sigma\omega}\Phi_D(-j\omega)\prod_{i=1}^{I}\Phi_i(j\gamma_k\omega)}{\omega}\right)d\omega + \frac{1}{2}, \tag{4.4}$$

where $\Phi_D(-j\omega)$ is the CF of the received desired signal D, and $\Phi_i(j\omega)$ is the CF of the received interference from interferer i. Since the desired signal as well as the interfering signals are modelled using the Gamma distribution, the CF of the Gamma distribution can be used in eq. (4.4) to calculate $\mathrm{P}_{\mathrm{th}}(\gamma_k)$.

We consider that all BSs utilize max-rate/opportunistic channel scheduling to maximize the overall throughput using multiuser diversity. Therefore, if there is a single UE that has the highest channel state in a particular channel at a given time slot, this UE is allocated with that particular channel. On the contrary, if multiple UEs have the highest channel state in a particular channel at a given time slot, then one of these UEs is randomly allocated with the channel. We also consider best-m partial CQI feedback for MUEs in the ER of the small cells in order to reduce CQI feedback overhead, especially for MUEs served by all component carriers through multi-flow CA. In particular, MUE l in the ER of a small cell is assumed to feed back its best $m_{\mathrm{M}l}$ channels with the MBS, where $m_{\mathrm{M}l} \in \{1, \cdots, N_{\mathrm{M1}} + N_{\mathrm{M2}}\}$. These channels could be from any component carrier deployed at the macrocell. Similarly, MUE l in the ER of a small cell is assumed to feed back its

best $m_{\mathrm{s}l}$ channels with the SBS, where $m_{\mathrm{s}l} \in \{1, \cdots, N_{\mathrm{s}1}\}$. In general, it is desirable to reduce the amount of CQI feedback to the MBS by MUEs in the ER of the small cells in order to offload more traffic to the small cells. The amount of CQI feedback to two BSs from both tiers that is needed for maintaining the QoS requirements of a particular MUE in the ER of a small cell can be determined using our analytical model. MUEs that are not in the ER of any small cell and SUEs are assumed to fully feed back their CQI to their BSs since they are served using only parts of the divided spectrum.

4.2.3 Packet arrival model and packet scheduling

We use the batch Bernoulli process, which is a general model that captures different levels of burstiness, to model random packet arrivals from the core network to the PSG. This process is specified by a probability vector $\boldsymbol{\alpha} = \{\alpha_0, \alpha_1, \cdots ., \alpha_Z\}$, where the probability of i packet arrivals at a particular time slot is denoted as α_i and the maximum possible packet arrival at a particular time slot is denoted as Z.

Then, packets of SUEs are forwarded to the SBSs and packets of MUEs that are not in the ER of any small cell are forwarded to the MBS. On the other hand, similar to the packet scheduling mechanism in [38], each packet of a particular MUE in the ER of a given small cell is randomly forwarded either to the MBS or to the SBS.

For the tagged MUE, we denote the packet scheduling parameter, which is the probability that a particular packet is forwarded to the MBS, as β. Therefore, the probability that the packet is forwarded to the SBS is $1 - \beta$. Also, we denote the joint probability of i packet arrivals to the MBS and j packet arrivals to the SBS at a given time slot as $\psi_{i,j}$, which can be calculated as follows [38]:

$$\psi_{i,j} = \begin{cases} \frac{(i+j)!}{i!j!}\alpha_{i+j}\beta^i(1-\beta)^j, i, j \geq 0, i+j \leq Z, \\ 0, \quad \text{otherwise}, \end{cases} \tag{4.5}$$

where ! denotes the factorial operator. The analytical model developed in this chapter can be used to find the optimal value of β with respect to a given performance measure. Also, the model can be used to find the minimum value of β for which the QoS requirements of the tagged MUE in the ER of the reference small cell are maintained while minimizing the macrocell load due to the tagged MUE's data packets.

We consider that each BS from either tier has a packet buffer dedicated for each UE that is being served by this BS. Since MUEs in the ER of the small cells are served by the macrocell as well as the small cells, each MUE in the ER of a small cell has two data buffers. The first buffer is located at the MBS and the second buffer is located at the SBS. Packets in a particular buffer are assumed to be served in the same order they arrive to

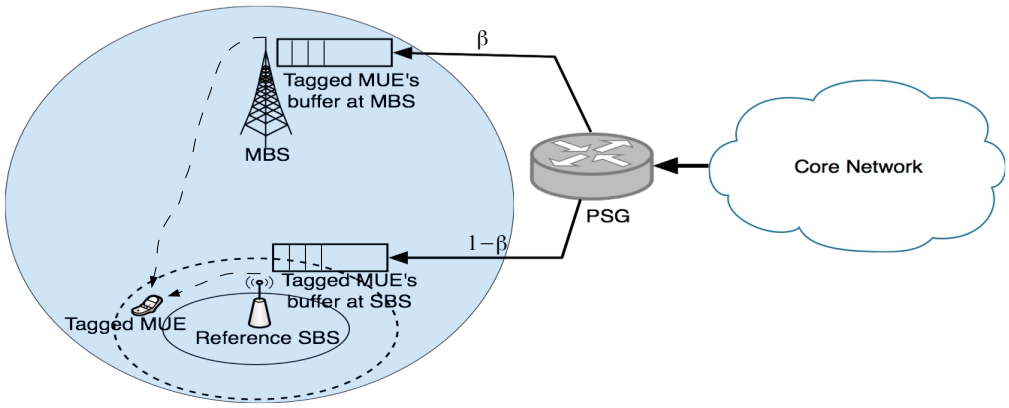

Figure 4.2: The resulting F/J queuing system (for clarity only tagged MUE and its serving SBS and MBS are shown).

that buffer. Also, a packet arriving to a given buffer at a given time slot can be served at the next time slot the earliest. It is noteworthy that packets can arrive to the MUEs in the ER of the small cells out-of-sequence since these packets are randomly forwarded to one of the two serving BSs and delivered to the MUEs by each BS independently. Fig. 4.2 shows the two data buffers of the tagged MUE. This buffer arrangement is often referred to as F/J queuing system.

4.3 Formulation of the Queueing Model

4.3.1 Tagged MUE joint sum transmission rate

The tagged MUE is allocated with a sum transmission rate by the serving MBS and a sum transmission rate by the serving SBS every time slot. These sum transmission rates depend on the number of component carriers deployed at each tier, partial CQI feedback and the employed max-rate/opportunistic channel scheduling. Here, we develop an analytic procedure to obtain the joint sum transmission rate of the tagged MUE from the serving MBS and the serving SBS. In particular, we define state variables to account for the joint sum transmission rate allocated to the tagged MUE by both BSs at a given time slot.

For the reference small cell, we denote the state of channel i of SUE l_{S} from component carrier $F_{\mathrm{S}j}$ at time slot n as $s^{(n)}_{\mathrm{S},j,i,l_{\mathrm{S}}}$. Then, the probabilities $\Pr\{s^{(n)}_{\mathrm{S},j,i,l_{\mathrm{S}}} = k\}, k = 0, 1, \cdots, K-1$, can be calculated using eq. (4.2). Also for MUEs in the ER of the reference small cell, channel i of MUE l_{SE} from component carrier $F_{\mathrm{S}j}$ is denoted as $s^{(n)}_{\mathrm{S},j,i,l_{\mathrm{SE}}}$ and the probabilities $\Pr\{s^{(n)}_{\mathrm{S},j,i,l_{\mathrm{SE}}} = k\}, k = 0, 1, \cdots, K-1$, can be calculated using eq. (4.2). Then we define random variable $v^{(n)}_{\mathrm{S},j,i,l_{\mathrm{SE}}}$, where $v^{(n)}_{\mathrm{S},j,i,l_{\mathrm{SE}}} \in \{0, 1\}$. $v^{(n)}_{\mathrm{S},j,i,l_{\mathrm{SE}}} = 1$ if

$$\Pr\{c^{(n)}_{\mathrm{S},1,1,l_{\mathrm{SE}}}=k\}=\begin{cases}\sum\limits_{k_{2_{\mathrm{S}1}}=0}^{K-1}\cdots\sum\limits_{k_{N_{\mathrm{S}1}}=0}^{K-1}\sum\limits_{k_{1_{\mathrm{S}2}}=0}^{K-1}\cdots\sum\limits_{k_{N_{\mathrm{S}C_{\mathrm{S}}}}=0}^{K-1} \\ (\min(1,\max(0,\frac{m_{\mathrm{S}l_{\mathrm{SE}}}-(g_k(k_{2_{\mathrm{S}1}})+\cdots+g_k(k_{N_{\mathrm{S}1}})+g_k(k_{1_{\mathrm{S}2}})+\cdots+g_k(k_{N_{\mathrm{S}C_{\mathrm{S}}}}))}{1+f_k(k_{2_{\mathrm{S}1}})+\cdots+f_k(k_{N_{\mathrm{S}1}})+f_k(k_{1_{\mathrm{S}2}})+\cdots+f_k(k_{N_{\mathrm{S}C_{\mathrm{S}}}})})) \\ \Pr\{s^{(n)}_{\mathrm{S},1,1,l_{\mathrm{SE}}}=k\}\prod\limits_{j=1}^{C_{\mathrm{S}}}\prod\limits_{\substack{i=1\\ i,j\neq 1}}^{N_{\mathrm{S}j}}\Pr\{s^{(n)}_{\mathrm{S},j,i,l_{\mathrm{SE}}}=k_{i_{\mathrm{S}j}}\}), \quad 1\le k\le K-1, \\ 1-\sum\limits_{k=1}^{K-1}\Pr\{c^{(n)}_{\mathrm{S},1,1,l_{\mathrm{SE}}}=k\}, \qquad\qquad k=0.\end{cases} \tag{4.6}$$

$$\Pr\{u^{(n)}_{\mathrm{S},j,i,1}=a\mid c^{(n)}_{\mathrm{S},j,i,1}=k\}=\begin{cases}\sum\limits_{k_{s1}=0}^{k}\cdot\cdot\sum\limits_{k_{sU_{\mathrm{S}}}=0}^{k}\sum\limits_{k_{e2}=0}^{k}\cdot\cdot\sum\limits_{k_{eU_{\mathrm{SM}}}=0}^{k} \\ (\frac{1}{1+f_k(k_{s1})+\cdots+f_k(k_{sU_{\mathrm{S}}})+f_k(k_{e2})+\cdots+f_k(k_{eU_{\mathrm{SM}}})} \\ \prod\limits_{l_{\mathrm{S}}=1}^{U_{\mathrm{S}}}\Pr\{s^{(n)}_{\mathrm{S},j,i,l_{\mathrm{S}}}=k_{sl_{\mathrm{S}}}\}\prod\limits_{l_{\mathrm{SE}}=2}^{U\mathrm{SM}}\Pr\{c^{(n)}_{\mathrm{S},j,i,l_{\mathrm{SE}}}=k_{el_{\mathrm{SE}}}\}), \quad a=1, \\ 1-\Pr\{u^{(n)}_{\mathrm{S},j,i,1}=1\mid c^{(n)}_{\mathrm{S},j,i,1}=k\}, \quad a=0.\end{cases} \tag{4.7}$$

the CQI of channel i of MUE l_{SE} from component carrier $F_{\mathrm{S}j}$ is fed back to the reference SBS at time slot n while $v^{(n)}_{\mathrm{S},j,i,l_{\mathrm{SE}}}=0$ otherwise. Moreover, we define state variable $c^{(n)}_{\mathrm{S},j,i,l_{\mathrm{SE}}}=v^{(n)}_{\mathrm{S},j,i,l_{\mathrm{SE}}}s^{(n)}_{\mathrm{S},j,i,l_{\mathrm{SE}}}, k=0,1,\cdots,K-1$. Let us consider that C_{S} component carriers are deployed at the small cells. Without loss of generality, for channel 1 from component carrier $F_{\mathrm{S}1}$ of MUE l_{SE} in the ER of the reference small cell, the probabilities $\Pr\{c^{(n)}_{\mathrm{S},1,1,l_{\mathrm{SE}}}=k\}, k=0,1,\cdots,K-1$, can be calculated using eq. (4.6) as shown in Appendix J. In eq. (4.6), function $f_x(y)$ is equal to 1 if $x=y$ and 0 otherwise, and function $g_x(y)$ is equal to 1 if $x<y$ and 0 otherwise.

Without loss of generality, we refer to the tagged MUE in the ER of the reference small cell as MUE 1. Assuming that channel i of the tagged MUE from component carrier $F_{\mathrm{S}j}$ is fed back to the reference SBS at time slot n, we define random variable $u^{(n)}_{\mathrm{S},j,i,1}\in\{0,1\}$, where $u^{(n)}_{\mathrm{S},j,i,1}=1$ if this particular channel is allocated to the tagged MUE in the ER of the reference small cell, and $u^{(n)}_{\mathrm{S},j,i,1}=0$ otherwise. Then, as shown in Appendix E, the conditional probabilities $\Pr\{u^{(n)}_{\mathrm{S},j,i,1}=a\mid c^{(n)}_{\mathrm{S},j,i,1}=k\}, a=0,1$, can be calculated using eq. (4.7). The proof of eq. (4.7) can be found in Appendix K.

Then, we denote the state space of the joint channel states of the best $m_{\mathrm{S}1}$ channels of the tagged MUE with the reference SBS as $\mathbf{\Lambda}_{\mathrm{S},1}=\{(s^{(n)}_{\mathrm{S},j_1,1,1},\cdots,s^{(n)}_{\mathrm{S},j_{m_{\mathrm{S}1}},m_{\mathrm{S}1},1})\mid 0\le s^{(n)}_{\mathrm{S},j_i,i,1}\le K-1\}$, where index j_i is to emphasize the fact that the best $m_{\mathrm{S}1}$ channels could be from any component carrier. State space $\mathbf{\Lambda}_{\mathrm{S},1}$ contains M_{S} unique states, where M_{S} can

$$\Pr\{s^{(n)}_{\mathrm{S},j_1,1,1}=k_1,\cdots,s^{(n)}_{\mathrm{S},j_{m_{\mathrm{S}1}},m_{\mathrm{S}1},1}=k_{m_{\mathrm{S}1}}\}=\sum_{k_{m_{\mathrm{S}1}+1}=0}^{k_l}\sum_{k_{m_{\mathrm{S}1}+2}=k_{m_{\mathrm{S}1}+1}}^{k_l}\cdots\sum_{k_{N_{\mathrm{S}}}=k_{N_{\mathrm{S}}-1}}^{k_l}\frac{N_{\mathrm{S}}!}{c_1!\times\cdots\times c_{K-1}!}\prod_{i=1}^{N_{\mathrm{S}}}\Pr\{s^{(n)}_{\mathrm{S},j_i,i,1}\}. \tag{4.9}$$

be calculated as follows [38]:

$$M_{\mathrm{S}}=\frac{(K+m_{\mathrm{S}1}-1)!}{m_{\mathrm{S}1}!(K-1)!}. \tag{4.8}$$

The probability of a particular element in $\mathbf{\Lambda}_{\mathrm{S},1}$, $\Pr\{s^{(n)}_{\mathrm{S},j_1,1,1}=k_1,\cdots,s^{(n)}_{\mathrm{S},j_{m_{\mathrm{S}1}},m_{\mathrm{S}1},1}=k_{m_{\mathrm{S}1}}\}$, can be calculated as shown in eq. (4.9), where $N_{\mathrm{S}}=\sum_{j=1}^{C_{\mathrm{S}}}N_{\mathrm{S}j}$, which is the total number of channels from all small cells' component carriers, $k_l=\min(k_1,\cdots,k_{m_{\mathrm{S}1}})$ and c_i's are to account only for unique elements in $\mathbf{\Lambda}_{\mathrm{S},1}$.

Next, we denote the state space of the joint channels states and channels allocation of the best $m_{\mathrm{S}1}$ channels of the tagged MUE with the reference SBS as: $\mathbf{\Upsilon}_{\mathrm{S},1}=\{(s^{(n)}_{\mathrm{S},j_1,1,1},\cdots,s^{(n)}_{\mathrm{S},j_{m_{\mathrm{S}1}},m_{\mathrm{S}1},1},u^{(n)}_{\mathrm{S},j_1,1,1},\cdots,u^{(n)}_{\mathrm{S},j_{m_{\mathrm{S}1}},m_{\mathrm{S}1},1})\mid 0\le s^{(n)}_{\mathrm{S},j_i,i,1}\le K-1,0\le u^{(n)}_{\mathrm{S},j_i,i,1}\le 1\}$. The probabilities of elements in state space $\mathbf{\Upsilon}_{\mathrm{S},1}$ can be calculated using eq. (4.9) along with the corresponding conditional probabilities in eq. (4.7). Next, we define state variable $t^{(n)}_{\mathrm{S}}=\sum_{i=1}^{m_{\mathrm{S}1}}s^{(n)}_{\mathrm{S},j_i,i,1}u^{(n)}_{\mathrm{S},j_i,i,1},0\le t^{(n)}_{\mathrm{S}}\le(K-1)m_{\mathrm{S}1}$, which is the sum of the channel states of all channels allocated to the tagged MUE by the reference SBS. Let y_t ($y_t\subset\mathbf{\Upsilon}_{\mathrm{S},1}$) denote the set of all elements for which $t^{(n)}_{\mathrm{S}}=t$. The probabilities $\Pr\{t^{(n)}_{\mathrm{S}}=t\},0\le t\le(K-1)m_{\mathrm{S}1}$, can be calculated as: $\Pr\{t^{(n)}_{\mathrm{S}}=t\}=\sum_{w\in y_t}\Pr\{w\}$. Finally, we define probability vector $\grave{\mathbf{T}}_{\mathrm{S}}$ whose elements are the probabilities $\Pr\{t^{(n)}_{\mathrm{S}}=t\},0\le t\le(K-1)m_{\mathrm{S}1}$, and matrix $\mathbf{T}_{\mathrm{S}}$ of identical rows with each row equals $\grave{\mathbf{T}}_{\mathrm{S}}$. The sum transmission rate allocated to the tagged MUE by the reference SBS at time slot n can readily be obtained using eq. (4.1).

Although the procedure needed to obtain the sum transmission rate allocated to the tagged MUE by the MBS is almost identical to the above, we include the details of this procedure for the sake of completeness. We also rewrite all equations with the corresponding state variables and parameters. At time slot n, we denote the state of channel i from component carrier $F_{\mathrm{M}j}$ of MUE l_{M} that is not in the ER of any small cell as $s^{(n)}_{\mathrm{M},j,i,l_{\mathrm{M}}}$. Also at time slot n, the state of channel i from component carrier $F_{\mathrm{M}j}$ of MUE l_{ME} that is in the ER of any small cell is denoted as $s^{(n)}_{\mathrm{M},j,i,l_{\mathrm{ME}}}$. The probabilities $\Pr\{s^{(n)}_{\mathrm{M},j,i,l_{\mathrm{M}}}=k\}$ and $\Pr\{s^{(n)}_{\mathrm{M},j,i,l_{\mathrm{ME}}}=k\},k=0,1,\cdots,K-1$, can be calculated using eq. (4.2). We define random variable $v^{(n)}_{\mathrm{M},j,i,l_{\mathrm{ME}}}\in\{0,1\}$, where $v^{(n)}_{\mathrm{M},j,i,l_{\mathrm{ME}}}=1$ if the CQI of channel i of MUE l_{ME} from

$$\Pr\{c^{(n)}_{\mathrm{M},1,1,l_{\mathrm{ME}}}=k\}=\begin{cases}\sum\limits_{k_{2_{\mathrm{M1}}}=0}^{K-1}\cdots\sum\limits_{k_{N_{\mathrm{M1}}}=0}^{K-1}\sum\limits_{k_{1_{\mathrm{M2}}}=0}^{K-1}\cdots\sum\limits_{k_{N_{\mathrm{M}C_{\mathrm{M}}}}=0}^{K-1} \\ (\min(1,\max(0,\frac{m_{\mathrm{M}l_{\mathrm{ME}}}-(g_k(k_{2_{\mathrm{M1}}})+\cdots+g_k(k_{N_{\mathrm{M1}}})+g_k(k_{1_{\mathrm{M2}}})+\cdots+g_k(k_{N_{\mathrm{M}C_{\mathrm{M}}}}))}{1+f_k(k_{2_{\mathrm{M1}}})+\cdots+f_k(k_{N_{\mathrm{M1}}})+f_k(k_{1_{\mathrm{M2}}})+\cdots+f_k(k_{N_{\mathrm{M}C_{\mathrm{M}}}})})) \\ \Pr\{s^{(n)}_{\mathrm{M},1,1,l_{\mathrm{ME}}}=k\}\prod\limits_{j=1}^{C_{\mathrm{M}}}\prod\limits_{\substack{i=1\\ i,j\neq 1}}^{N_{\mathrm{M}j}}\Pr\{s^{(n)}_{\mathrm{M},j,i,l_{\mathrm{ME}}}=k_{i_{\mathrm{M}j}}\}), & 1\le k\le K-1, \\ 1-\sum\limits_{k=1}^{K-1}\Pr\{c^{(n)}_{\mathrm{M},1,1,l_{\mathrm{ME}}}=k\}, & k=0.\end{cases} \tag{4.10}$$

$$\Pr\{u^{(n)}_{\mathrm{M},j,i,1}=a\mid c^{(n)}_{\mathrm{M},j,i,1}=k\}=\begin{cases}\sum\limits_{k_{m1}=0}^{k}\cdots\sum\limits_{k_{m(U_{\mathrm{M}}-U_{\mathrm{MS}})}=0}^{k}\sum\limits_{k_{e2}=0}^{k}\cdots\sum\limits_{k_{eU_{\mathrm{MS}}}=0}^{k} \\ (\frac{1}{1+f_k(k_{m1})+\cdots+f_k(k_{m(U_{\mathrm{M}}-U_{\mathrm{MS}})})+f_k(k_{e2})+\cdots+f_k(k_{eU_{\mathrm{MS}}})}) \\ (\prod\limits_{l_{\mathrm{M}}=1}^{U_{\mathrm{M}}-U_{\mathrm{MS}}}\Pr\{s^{(n)}_{\mathrm{M},j,i,l_{\mathrm{M}}}=k_{ml_{\mathrm{M}}}\}\prod\limits_{l_{\mathrm{ME}}=2}^{U_{\mathrm{MS}}}\Pr\{c^{(n)}_{\mathrm{M},j,i,l_{\mathrm{ME}}}=k_{el_{\mathrm{ME}}}\}), & a=1, \\ 1-\Pr\{u^{(n)}_{\mathrm{M},j,i,1}=1\mid c^{(n)}_{\mathrm{M},j,i,1}=k\}, & a=0.\end{cases} \tag{4.11}$$

component carrier $F_{\mathrm{M}j}$ is fed back to the MBS at time slot n while $v^{(n)}_{\mathrm{M},j,i,l_{\mathrm{ME}}}=0$ otherwise. We also define state variable $c^{(n)}_{\mathrm{M},j,i,l_{\mathrm{ME}}}=v^{(n)}_{\mathrm{M},j,i,l_{\mathrm{ME}}}s^{(n)}_{\mathrm{M},j,i,l_{\mathrm{ME}}}, k=0,1,\cdots,K-1$. Assuming that C_{M} component carriers are deployed at the macrocell and considering channel 1 from component carrier F_{M1} of MUE l_{ME} in the ER of any small cell, the probabilities $\Pr\{c^{(n)}_{\mathrm{M},1,1,l_{\mathrm{ME}}}=k\}, k=0,1,\cdots,K-1$, can be calculated as shown in eq. (4.10). We also refer to the tagged MUE in the ER of the reference small cell as MUE 1. Assuming that channel i of the tagged MUE from component carrier $F_{\mathrm{M}j}$ is fed back to the MBS at time slot n, we define random variable $u^{(n)}_{\mathrm{M},j,i,1}\in\{0,1\}$, where $u^{(n)}_{\mathrm{M},j,i,1}=1$ if this particular channel is allocated to the tagged MUE in the ER of the reference small cell, and $u^{(n)}_{\mathrm{M},j,i,1}=0$ otherwise. The conditional probabilities $\Pr\{u^{(n)}_{\mathrm{M},j,i,1}=a\mid c^{(n)}_{\mathrm{M},j,i,1}=k\}, a=0,1$, can be calculated as shown in eq. (4.11).

The state space of the joint channel states of the best m_{M1} channels of the tagged MUE with the MBS is denoted as $\mathbf{\Lambda}_{\mathrm{M},1}=\{(s^{(n)}_{\mathrm{M},j_1,1,1},\cdots,s^{(n)}_{\mathrm{M},j_{m_{\mathrm{M1}}},m_{\mathrm{M1}},1})\mid 0\le s^{(n)}_{\mathrm{M},j_i,i,1}\le K-1\}$ and contains M_{M} unique states, where M_{M} can be calculated as follows:

$$M_{\mathrm{M}}=\frac{(K+m_{\mathrm{M1}}-1)!}{m_{\mathrm{M1}}!(K-1)!}. \tag{4.12}$$

The probability of a particular element in $\mathbf{\Lambda}_{\mathrm{S},1}$ can be calculated as shown in eq. (4.13), where $N_{\mathrm{M}}=\sum\limits_{j=1}^{C_{\mathrm{M}}}N_{\mathrm{M}j}$. We then denote the state space of the joint channels states and channels allocation of the best m_{M1} channels of the tagged MUE with the MBS as: $\mathbf{\Upsilon}_{\mathrm{M},1}=\{(s^{(n)}_{\mathrm{M},j_1,1,1},\cdots,s^{(n)}_{\mathrm{M},j_{m_{\mathrm{M1}}},m_{\mathrm{M1}},1},u^{(n)}_{\mathrm{M},j_1,1,1},\cdots,u^{(n)}_{\mathrm{M},j_{m_{\mathrm{M1}}},m_{\mathrm{M1}},1})\mid 0\le s^{(n)}_{\mathrm{M},j_i,i,1}\le K-1, 0\le u^{(n)}_{\mathrm{M},j_i,i,1}\le 1\}$. The probabilities of elements in $\mathbf{\Upsilon}_{\mathrm{M},1}$ can be calculated using eq.

$$\Pr\{s^{(n)}_{\mathrm{M},j_1,1,1}=k_1,\cdots,s^{(n)}_{\mathrm{M},j_{m_{\mathrm{M1}}},m_{\mathrm{M1}},1}=k_{m_{\mathrm{M1}}}\}=\sum_{k_{m_{\mathrm{M1}}+1}=0}^{k_l}\sum_{k_{m_{\mathrm{M1}}+2}=k_{m_{\mathrm{M1}}+1}}^{k_l}\cdots\sum_{k_{N_{\mathrm{M}}}=k_{N_{\mathrm{M}}-1}}^{k_l}\frac{N_{\mathrm{M}}!}{c_1!\times\cdots\times c_{K-1}!}\prod_{i=1}^{N_{\mathrm{M}}}\Pr\{s^{(n)}_{\mathrm{M},j_i,i,1}\}. \tag{4.13}$$

(4.13) and eq. (4.11). Next, we define state variable $t^{(n)}_{\mathrm{M}}=\sum_{i=1}^{m_{\mathrm{M1}}}s^{(n)}_{\mathrm{M},j_i,i,1}u^{(n)}_{\mathrm{M},j_i,i,1}, 0\leq t^{(n)}_{\mathrm{M}}\leq (K-1)m_{\mathrm{M1}}$, which is the sum of the channel states of all channels allocated to the tagged MUE by the MBS. The probabilities $\Pr\{t^{(n)}_{\mathrm{M}}=t\}, 0\leq t\leq (K-1)m_{\mathrm{S1}}$, can be calculated as: $\Pr\{t^{(n)}_{\mathrm{M}}=t\}=\sum_{w\in y_t}\Pr\{w\}$, where y_t ($y_t\subset\boldsymbol{\Upsilon}_{\mathrm{M},1}$) denotes the set of all elements for which $t^{(n)}_{\mathrm{M}}=t$. Finally, we define probability vector $\grave{\mathbf{T}}_{\mathrm{M}}$ whose elements are the probabilities $\Pr\{t^{(n)}_{\mathrm{M}}=t\}, 0\leq t\leq (K-1)m_{\mathrm{M1}}$, and matrix $\mathbf{T}_{\mathrm{M}}$ of identical rows with each row equals $\grave{\mathbf{T}}_{\mathrm{M}}$. The sum transmission rate allocated to the tagged MUE by the macro BS at time slot n can readily be obtained using eq. (4.1).

Finally, we define matrix $\mathbf{W}$ whose elements are the joint probabilities $\Pr\{t^{(n)}_{\mathrm{M}}=t_1, t^{(n)}_{\mathrm{S}}=t_2\}, 0\leq t_1\leq (K-1)m_{\mathrm{M1}}, 0\leq t_2\leq (K-1)m_{\mathrm{S1}}$. $\mathbf{W}$ is then given by:

$$\mathbf{W}=\mathbf{T}_{\mathrm{M}}\otimes\mathbf{T}_{\mathrm{S}}, \tag{4.14}$$

where $\otimes$ denotes the Kronecker product.

4.3.2 System's state space and transition probability

Considering that all buffers have finite sizes, the joint system's state space is denoted as: $\boldsymbol{\Omega}=\{(q^{(n)}_{\mathrm{M}},q^{(n)}_{\mathrm{S}},t^{(n)}_{\mathrm{M}},t^{(n)}_{\mathrm{S}})\mid 0\leq q^{(n)}_{\mathrm{M}}\leq Q_{\mathrm{M}}, 0\leq q^{(n)}_{\mathrm{S}}\leq Q_{\mathrm{S}}, 0\leq t^{(n)}_{\mathrm{M}}\leq (K-1)m_{\mathrm{M1}}, 0\leq t^{(n)}_{\mathrm{S}}\leq (K-1)m_{\mathrm{S1}}\}$, where $q^{(n)}_{\mathrm{M}}$ and $q^{(n)}_{\mathrm{S}}$ are the number of packets in the tagged MUE's buffers at the MBS and the reference SBS respectively at time slot n. Also, Q_{M} and Q_{S} are the sizes of the tagged MUE's buffers at the MBS and the reference SBS respectively. The system can be modelled as a DTMC since it is time slotted with discrete state variables. We denote the transition probability matrix of the DTMC as $\mathbf{P}$, where the elements of $\mathbf{P}$ are the joint transition probabilities $\Pr\{q^{(n+1)}_{\mathrm{M}},q^{(n+1)}_{\mathrm{S}},t^{(n+1)}_{\mathrm{M}},t^{(n+1)}_{\mathrm{S}}\mid q^{(n)}_{\mathrm{M}},q^{(n)}_{\mathrm{S}},t^{(n)}_{\mathrm{M}},t^{(n)}_{\mathrm{S}}\}$. $\mathbf{P}$ is represented by its block sub-matrices in eq. (4.15), where $Y_{\mathrm{M}}=b(K-1)m_{\mathrm{M1}}$. Eq. (4.15)

$$
\mathbf{P} = \left[\begin{array}{c|ccccc|c}
\mathbf{A}_0^{(0)} & \mathbf{A}_{1^+}^{(0)} & \cdots & \mathbf{A}_{Z^+}^{(0)} & & & \\
\hline
\mathbf{A}_{1^-}^{(1)} & \mathbf{A}_0^{(1)} & \mathbf{A}_{1^+}^{(1)} & \cdots & \mathbf{A}_{Z^+}^{(1)} & & \\
\vdots & \vdots & & & \ddots & & \\
\mathbf{A}_{(Y_{\mathrm{M}}-Z+1)^-}^{(Y_{\mathrm{M}}-Z+1)} & \mathbf{A}_{(Y_{\mathrm{M}}-Z)^-}^{(Y_{\mathrm{M}}-Z+1)} & \cdots & \mathbf{A}_0^{(Y_{\mathrm{M}}-Z+1)} & \cdots & \mathbf{A}_{(Z-1)^+}^{(Y_{\mathrm{M}}-Z+1)} & \\
\vdots & \vdots & & & & \vdots & \\
\mathbf{A}_{Y_{\mathrm{M}}^-} & \mathbf{A}_{(Y_{\mathrm{M}}-1)^-} & \cdots & \cdots & \mathbf{A}_{1^-} & \mathbf{A}_0 & \\
\hline
 & \mathbf{A}_{Y_{\mathrm{M}}^-} & \cdots & \cdots & \cdots & \mathbf{A}_{1^-} & \\
 & & \ddots & & & \vdots & \\
 & & & \mathbf{A}_{Y_{\mathrm{M}}^-} & & \mathbf{A}_{(Y_{\mathrm{M}}-Z+1)^-} & \\
 & & & & \ddots & \vdots & \\
 & & & & & \mathbf{A}_{Y_{\mathrm{M}}^-} & \\
\hline
 & & & & \ddots & &
\end{array}\right.
$$

$$
\left.\begin{array}{ccccccc|cc}
 & & & & & & & & \\
\hline
 & & & & & & & & \\
 & & & & & & & & \\
\mathbf{A}_{Z^+}^{(Y_{\mathrm{M}}-Z+1)} & & & & & & & & \\
\vdots & \ddots & & & & & & & \\
\mathbf{A}_{1^+} & \cdots & \mathbf{A}_{Z^+} & & & & & & \\
\hline
\mathbf{A}_0 & \cdots & \cdots & \mathbf{A}_{Z^+} & & & & & \\
\vdots & & & \ddots & & & & & \\
\mathbf{A}_{(Y_{\mathrm{M}}-Z)^-} & \cdots & \cdots & \cdots & \mathbf{A}_{(Z-1)^+} & \mathbf{A}_{Z^+} & & & \\
\vdots & & & \ddots & \vdots & \vdots & \ddots & & \\
\mathbf{A}_{(Y_{\mathrm{M}}-1)^-} & \cdots & \cdots & \mathbf{A}_{1^-} & \mathbf{A}_0 & \mathbf{A}_{1^+} & \cdots & \mathbf{A}_{Z^+} & \\
\hline
 & & & \ddots & & & & \ddots &
\end{array}\right] . \tag{4.15}
$$

indicates that a QBD process can be obtained to represent $\mathbf{P}$ as follows:

$$\mathbf{P} = \begin{array}{c} 0 \\ 1 \\ 2 \\ 3 \\ \vdots \\ X-1 \\ X \end{array} \begin{bmatrix} \mathbf{C} & \mathbf{D} & & & & & \\ \mathbf{E} & \mathbf{F} & \mathbf{G} & & & & \\ & \mathbf{I_2} & \mathbf{I_1} & \mathbf{I_0} & & & \\ & & \mathbf{I_2} & \mathbf{I_1} & \mathbf{I_0} & & \\ & & & \ddots & \ddots & \ddots & \\ & & & & \mathbf{I_2} & \mathbf{I_1} & \mathbf{I_0}' \\ & & & & & \mathbf{I_2}' & \mathbf{I_1}' \end{bmatrix}, \tag{4.16}$$

where $X = \lfloor Q_{\mathrm{M}}/Y_{\mathrm{M}} \rfloor$.

Furthermore, each block sub-matrix $\mathbf{A}_{\delta_{\mathrm{M}}}^{(q_{\mathrm{M}})}$ is represented by its block sub-matrices in eq. (4.17), where $Y_{\mathrm{S}} = b(K-1)m_{\mathrm{S}1}$. block sub-matrix $\mathbf{A}_{\delta_{\mathrm{M}},\delta_{\mathrm{S}}}^{(q_{\mathrm{M}},q_{\mathrm{S}})}$ represents the transition of the system from states $(q_{\mathrm{M}}, q_{\mathrm{S}})$ at time slot n to states $(q_{\mathrm{M}}+\delta_{\mathrm{M}}, q_{\mathrm{S}}+\delta_{\mathrm{S}})$ at time slot $n+1$. In order to derive block sub-matrices $\mathbf{A}_{\delta_{\mathrm{M}},\delta_{\mathrm{S}}}^{(q_{\mathrm{M}},q_{\mathrm{S}})}$, we define matrices $\mathbf{J}_{\mathrm{M}}$ of size $(\frac{Y_{\mathrm{M}}}{b}+1)\times(\frac{Y_{\mathrm{M}}}{b}+1)$ and $\mathbf{J}_{\mathrm{S}}$ of size $(\frac{Y_{\mathrm{S}}}{b}+1)\times(\frac{Y_{\mathrm{S}}}{b}+1)$ whose elements are one. We also define set of matrices $\mathbf{O}_{\mathrm{M}}^{(l)}$ of size $(\frac{Y_{\mathrm{M}}}{b}+1)\times(\frac{Y_{\mathrm{M}}}{b}+1)$ as follows:

$$\mathbf{O}_{\mathrm{M}}^{(l)}(k,e) = \begin{cases} 1 & \text{if} \quad k = l \\ 0 & \text{if} \quad k \neq l \end{cases}, \quad 0 \leq l \leq Y_{\mathrm{M}}/b.$$

Similarly, we define set of matrices $\mathbf{O}_{\mathrm{S}}^{(l)}$ of size $(\frac{Y_{\mathrm{S}}}{b}+1)\times(\frac{Y_{\mathrm{S}}}{b}+1)$ as follows:

$$\mathbf{O}_{\mathrm{S}}^{(l)}(k,e) = \begin{cases} 1 & \text{if} \quad k = l \\ 0 & \text{if} \quad k \neq l \end{cases}, \quad 0 \leq l \leq Y_{\mathrm{S}}/b.$$

Then, we proceed to derive block sub-matrices of $\mathbf{P}$ as shown in eq. (H.1)-(H.9) in Appendix H, where $\circ$ denotes the Hadamard product and $\mathbf{B}_{\delta_{\mathrm{S}}}^{(q_{\mathrm{S}})}(i)$ is shown in eq. (I.1)-(I.9) in Appendix I.

4.3.3 Steady state solution and derivation of performance measures

We denote the steady state probability vector of the DTMC in the previous section as $\boldsymbol{\pi}$ which can be calculated using the matrix-analytic procedure in [46]. Steady state probability vector $\boldsymbol{\pi}$ can be written as: $\boldsymbol{\pi} = [\boldsymbol{\pi}_{(0,0)} \ \cdots \ \boldsymbol{\pi}_{(Q_{\mathrm{M}},Q_{\mathrm{S}})}]$, where $\boldsymbol{\pi}_{(i,j)}$ is steady state probability vector of states with $q_{\mathrm{M}}^{(n)} = i$ and $q_{\mathrm{S}}^{(n)} = j$. Using steady state probability vector $\boldsymbol{\pi}$, packet-level QoS measures can be derived as shown in the following subsections.

$$
\mathbf{A}_{\delta_{\mathrm{M}}}^{(q_{\mathrm{M}})} = \left[\begin{array}{c|c|ccc|cc}
\mathbf{A}_{\delta_{\mathrm{M}},0}^{(q_{\mathrm{M}},0)} & \mathbf{A}_{\delta_{\mathrm{M}},1^+}^{(q_{\mathrm{M}},0)} & \cdots & \mathbf{A}_{\delta_{\mathrm{M}},Z^+}^{(q_{\mathrm{M}},0)} & & & \\
\hline
\mathbf{A}_{\delta_{\mathrm{M}},1^-}^{(q_{\mathrm{M}},1)} & \mathbf{A}_{\delta_{\mathrm{M}},0}^{(q_{\mathrm{M}},1)} & \mathbf{A}_{\delta_{\mathrm{M}},1^+}^{(q_{\mathrm{M}},1)} & \cdots & \mathbf{A}_{\delta_{\mathrm{M}},Z^+}^{(q_{\mathrm{M}},1)} & & \\
\vdots & \vdots & & & \ddots & & \\
\mathbf{A}_{\delta_{\mathrm{M}},(Y_{\mathrm{S}}-Z+1)^-}^{(q_{\mathrm{M}},Y_{\mathrm{S}}-Z+1)} & \mathbf{A}_{\delta_{\mathrm{M}},(Y_{\mathrm{S}}-Z)^-}^{(q_{\mathrm{M}},Y_{\mathrm{S}}-Z+1)} & \cdots & \mathbf{A}_{\delta_{\mathrm{M}},0}^{(q_{\mathrm{M}})} & \cdots & \mathbf{A}_{\delta_{\mathrm{M}},(Z-1)^+}^{(q_{\mathrm{M}},Y_{\mathrm{S}}-Z+1)} & \\
\vdots & \vdots & & & & \vdots & \\
\mathbf{A}_{\delta_{\mathrm{M}},Y_{\mathrm{S}}^-}^{(q_{\mathrm{M}})} & \mathbf{A}_{\delta_{\mathrm{M}},(Y_{\mathrm{S}}-1)^-}^{(q_{\mathrm{M}})} & \cdots & \cdots & \mathbf{A}_{\delta_{\mathrm{M}},1^-}^{(q_{\mathrm{M}})} & \mathbf{A}_{\delta_{\mathrm{M}},0}^{(q_{\mathrm{M}})} & \\
\hline
 & \mathbf{A}_{\delta_{\mathrm{M}},Y_{\mathrm{S}}^-}^{(q_{\mathrm{M}})} & \cdots & \cdots & \cdots & \mathbf{A}_{\delta_{\mathrm{M}},1^-}^{(q_{\mathrm{M}})} & \\
 & & \ddots & & & \vdots & \\
 & & & \mathbf{A}_{\delta_{\mathrm{M}},Y_{\mathrm{S}}^-}^{(q_{\mathrm{M}})} & & \mathbf{A}_{\delta_{\mathrm{M}},(Y_{\mathrm{S}}-Z+1)^-}^{(q_{\mathrm{M}})} & \\
 & & & & \ddots & \vdots & \\
 & & & & & \mathbf{A}_{\delta_{\mathrm{M}},Y_{\mathrm{S}}^-}^{(q_{\mathrm{M}})} & \\
\hline
 & & & & \ddots & &
\end{array}\right.
$$

$$
\left.\begin{array}{c|cccc|cc}
 & & & & & & \\
\hline
 & & & & & & \\
\mathbf{A}_{\delta_{\mathrm{M}},Z^+}^{(q_{\mathrm{M}},Y_{\mathrm{S}}-Z+1)} & & & & & & \\
\vdots & \ddots & & & & & \\
\mathbf{A}_{\delta_{\mathrm{M}},1^+}^{(q_{\mathrm{M}})} & \cdots & \mathbf{A}_{\delta_{\mathrm{M}},Z^+}^{(q_{\mathrm{M}})} & & & & \\
\hline
\mathbf{A}_{\delta_{\mathrm{M}},0}^{(q_{\mathrm{M}})} & \cdots & \cdots & \mathbf{A}_{\delta_{\mathrm{M}},Z^+}^{(q_{\mathrm{M}})} & & & \\
\vdots & & & \ddots & & & \\
\mathbf{A}_{\delta_{\mathrm{M}},(Y_{\mathrm{S}}-Z)^-}^{(q_{\mathrm{M}})} & \cdots & \cdots & \cdots & \mathbf{A}_{\delta_{\mathrm{M}},(Z-1)^+}^{(q_{\mathrm{M}})} & \mathbf{A}_{\delta_{\mathrm{M}},Z^+}^{(q_{\mathrm{M}})} & \\
\vdots & & & \ddots & \vdots & \vdots & \ddots \\
\mathbf{A}_{\delta_{\mathrm{M}},(Y_{\mathrm{S}}-1)^-}^{(q_{\mathrm{M}})} & \cdots & \cdots & \mathbf{A}_{\delta_{\mathrm{M}},1^-}^{(q_{\mathrm{M}})} & \mathbf{A}_{\delta_{\mathrm{M}},0}^{(q_{\mathrm{M}})} & \mathbf{A}_{\delta_{\mathrm{M}},1^+}^{(q_{\mathrm{M}})} \cdots & \mathbf{A}_{\delta_{\mathrm{M}},Z^+}^{(q_{\mathrm{M}})} \\
\hline
 & & & \ddots & & & \ddots
\end{array}\right]. \tag{4.17}
$$

$$\boldsymbol{\omega}_{(q_{\mathrm{M}},q_{\mathrm{S}})} = \frac{1}{1-\alpha_0}\sum_{z=1}^{Z}\sum_{e_1=1}^{2}\cdots\sum_{e_z=1}^{2}\sum_{k=1}^{z}\frac{\psi_{\xi_{1z},\xi_{2z}}(\xi_{1z}!\xi_{2z}!)}{z(\xi_{1z}+\xi_{2z})!}\tilde{g}_{\xi_{1k}}(q_{\mathrm{M}})\tilde{g}_{\xi_{2k}}(q_{\mathrm{S}})(\tilde{g}_{q_{\mathrm{M}}}(Q_{\mathrm{M}}+f_1(e_k)\xi_{1k})$$
$$\tilde{g}_{q_{\mathrm{S}}}(Q_{\mathrm{S}}+f_2(e_k)\xi_{2k})\times\boldsymbol{\pi}_{0(q_{\mathrm{M}}-\xi_{1k},q_{\mathrm{S}}-\xi_{2k})}+f_{q_{\mathrm{M}}}(Q_{\mathrm{M}})f_2(e_k)\sum_{i=Q_{\mathrm{M}}-\xi_{1k}+1}^{Q_{\mathrm{M}}}\boldsymbol{\pi}_{0(i,q_{\mathrm{S}}-\xi_{2k})}$$
$$+f_{q_{\mathrm{S}}}(Q_{\mathrm{S}})f_1(e_k)\sum_{j=Q_{\mathrm{S}}-\xi_{2k}+1}^{Q_{\mathrm{S}}}\boldsymbol{\pi}_{0(q_{\mathrm{M}}-\xi_{1k},j)}). \tag{4.19}$$

Buffers' length distribution

The marginal joint steady state probability of finding i packets in the tagged MUE's buffer at the MBS and j packets at the tagged MUE's buffer at the SBS can be written as:

$$\Pr\{q_{\mathrm{M}}^{(n)}=i,q_{\mathrm{S}}^{(n)}=j\}=\boldsymbol{\pi}_{(i,j)}\mathbf{1},0\le i\le Q_{\mathrm{M}},0\le j\le Q_{\mathrm{S}}, \tag{4.18}$$

where $\mathbf{1}$ is a column vector of proper size with all elements equal 1.

Delay distribution

In this chapter we define the delay of a particular packet as the number of time slots that the packet takes to arrive at the tagged MUE along with all packets ahead of it in both buffers. This definition takes out-of-sequence packet delivery into consideration in parallel transmission schemes such as multi-flow CA, the DCS scheme in [38] and parallel transmission in multi-RATs [44].

Then, queuing delay and other packet-level QoS measures can be derived as follows. First an absorbing Markov chain $\mathbf{P}_{\mathrm{abs}}$ is obtained by following the same procedure to construct $\mathbf{P}$ while setting $\alpha_0 = 1$ and $\alpha_i = 0, 1 \le i \le Z$ [39]. Then, we define probability vector $\boldsymbol{\pi}_0$ as follows: $\boldsymbol{\pi}_0 = \boldsymbol{\pi}\mathbf{P}_{\mathrm{abs}}$. $\boldsymbol{\pi}_0$ can be written as: $\boldsymbol{\pi}_0 = [\boldsymbol{\pi}_{0(0,0)} \ \cdots \ \boldsymbol{\pi}_{0(Q_{\mathrm{M}},Q_{\mathrm{S}})}]$. We also define probability vector $\boldsymbol{\omega}$ whose elements are the joint probabilities of the states of the tagged MUE's buffers as seen by an arriving packet. $\boldsymbol{\omega}$ can be written as: $\boldsymbol{\omega} = [\boldsymbol{\omega}_{(0,0)} \ \cdots \ \boldsymbol{\omega}_{(Q_{\mathrm{M}},Q_{\mathrm{S}})}]$. Probability vector $\boldsymbol{\omega}_{(q_{\mathrm{M}},q_{\mathrm{S}})}$ can be calculated as shown in eq. (4.19), where $\xi_{ij} = \sum_{k=1}^{j} f_i(e_k)$, packet k is considered to be forwarded to the MBS if index e_k is equal to 1 and to the SBS otherwise, and function $\tilde{g}_x(y)$ is equal to 0 if $x > y$ and 1 otherwise.

A packet forwarded to one of the tagged MUE's buffers at either tier is dropped if that buffer is full. We denote the probability of dropping an arriving packet as ρ, which can be

calculated as follows:

$$\rho = \sum_{i=Q_{\mathrm{M}}+1}^{Q_{\mathrm{M}}+Z} \sum_{j=0}^{Q_{\mathrm{S}}} \boldsymbol{\omega}_{(i,j)}\mathbf{1} + \sum_{i=0}^{Q_{\mathrm{M}}} \sum_{j=Q_{\mathrm{S}}+1}^{Q_{\mathrm{S}}+Z} \boldsymbol{\omega}_{(i,j)}\mathbf{1}. \tag{4.20}$$

It is noteworthy that $\boldsymbol{\omega}$ represents the joint buffer states as seen by an arriving packet, whether this packet is admitted to its respective buffer or dropped due to buffer overflow at that buffer. Therefore $\boldsymbol{\omega}$ is not suitable for measuring queuing delay as queuing delay is not experienced by packets that are dropped due to buffer overflow. Hence, we define probability vector $\boldsymbol{\Delta}$ of the joint buffer state of the tagged MUE's buffers as seen by an admitted packet. $\boldsymbol{\Delta}$ can be written as $\boldsymbol{\Delta} = [\boldsymbol{\Delta}_{(0,0)} \ \cdots \ \boldsymbol{\Delta}_{(Q_{\mathrm{M}},Q_{\mathrm{S}})}]$, where probability vector $\boldsymbol{\Delta}_{(q_{\mathrm{M}},q_{\mathrm{S}})}$ is given by:

$$\boldsymbol{\Delta}_{(q_{\mathrm{M}},q_{\mathrm{S}})} = \frac{\boldsymbol{\omega}_{(q_{\mathrm{M}},q_{\mathrm{S}})}}{1-\rho}. \tag{4.21}$$

After d time slots, the joint buffer states of the tagged MUE's buffers as seen by an admitted packet is denoted as $\boldsymbol{\chi}(d)$. Then, $\boldsymbol{\chi}(d)$ can be calculated as: $\boldsymbol{\chi}(d) = \boldsymbol{\Delta}\mathbf{P}_{\mathrm{abs}}^{d}$. Also, $\boldsymbol{\chi}(d)$ can be written as $\boldsymbol{\chi}(d) = [\boldsymbol{\chi}(d)_{(0,0)} \ \cdots \ \boldsymbol{\chi}(d)_{(Q_{\mathrm{M}},Q_{\mathrm{S}})}]$. The queuing delay experienced by a packet that is admitted to one of the tagged MUE's buffers at either tier is denoted as D. The CDF of D is given by:

$$F_D(d) = \boldsymbol{\chi}(d)_{(0,0)}\mathbf{1}. \tag{4.22}$$

Eq. (4.22) suggests that an admitted packet is considered to have arrived to the tagged MUE only when all packets ahead of it in both buffers have also arrived. As such, this equation accounts for out-of-sequence packet delivery. Finally, the average queuing delay is denoted as $\bar{\mathcal{D}}$ and is given by:

$$\bar{\mathcal{D}} = \sum_{d=1}^{d_m} d(F_D(d) - F_D(d-1)), \tag{4.23}$$

where $F_D(d_m) = 1$. The average queuing delay in this chapter can only be calculated using the delay CDF since the Little's law, which is used to calculate the average queuing delay for traditional queuing systems, is not applicable for F/J queuing systems [59], [60]. Also, the delay CDF is a more elaborate measure of the tagged MUE's delay performance and is useful to guarantee statistical delay constraint. In particular, in addition to the average queuing delay requirement, the delay requirement of the tagged MUE can be in the form $F_D(d_i) \geq \zeta$, where d_i is a specific number of time slots and ζ is a given delay guarantee probability.

Table 4.1: Summary of parameter symbols and values.

Parameter Description	**Symbol**	**Value**
Number of interfering small cells	I	5
Macrocell radius	R_{M}	500 m
Small cell radius	R_{S}	50 m
ER of the small cells	R_{E}	30 m
Target average bit error rate	BER_0	10^{-5}
Tagged MUE's buffers sizes	$Q_{\mathrm{M}}, Q_{\mathrm{S}}$	$20, 20$
Packet size	ϵ	1024 bits
Packet arrival probability vector for first scenario	$\boldsymbol{\alpha_1}$	{0.2 0.1 0.4 0.3}
Packet arrival probability vector for second scenario	$\boldsymbol{\alpha_2}$	{0.1 0.2 0.3 0.4}
Number of channels in F_{M1}	N_{M1}	8
Number of channels in F_{M2}	N_{M2}	6
Number of channels in F_{S1}	N_{S1}	6
Shadowing-fading parameters of F_{M1}	$\kappa_{\mathrm{M1}}, \theta_{\mathrm{M1}}$	1.6, 2.3
Shadowing-fading parameters of F_{M2}	$\kappa_{\mathrm{M2}}, \theta_{\mathrm{M2}}$	1.4, 2
Shadowing-fading parameters of F_{S1}	$\kappa_{\mathrm{S1}}, \theta_{\mathrm{S1}}$	1.5, 2.1
Path loss exponents	η_{M1}, η_{M2}, η_{S1}	2.8, 3.1, 2.9
Values of transmission power	p_{M}, p_{S}	43 dBm, 25 dBm
Thermal noise power	σ	-121 dBm
Adaptive transmission parameter	b	1
Number of channel states	K	3

Packet loss probability

Packet loss can occur either due to buffer overflow or due to link error and the overall PLP is given by:

$$\mathcal{P} = 1 - (1 - \rho)(1 - \mathrm{PER}_0), \tag{4.24}$$

where PER_0 is the average packet error rate which is given by: $\mathrm{PER}_0 = 1 - (1 - \mathrm{BER}_0)^{\epsilon}$, where ϵ is the packet size.

4.4 Numerical Results and Example Applications

In this section, using the analytical model developed in Section 3.3, we present some selected numerical results. We validate all numerical results via computer simulations. We also demonstrate some example applications of our developed analytical model. We generate locations of small cells, MUEs and SUEs randomly at the beginning of simulations. The number of MUEs $U_{\mathrm{M}} = 21$ and the number of MUEs in the ER of any small cell

$U_{\mathrm{MS}} = 11$. Also, the number of MUEs in the ER of the reference small cell $U_{\mathrm{SM}} = 3$ and the number of SUEs in the reference small cell $U_{\mathrm{S}} = 4$. Two packet arrival scenarios are considered with probability vectors $\boldsymbol{\alpha_1}$ and $\boldsymbol{\alpha_2}$ as shown in Table I. Other system parameters are also specified in Table I.

4.4.1 Effect of the packet forwarding probability

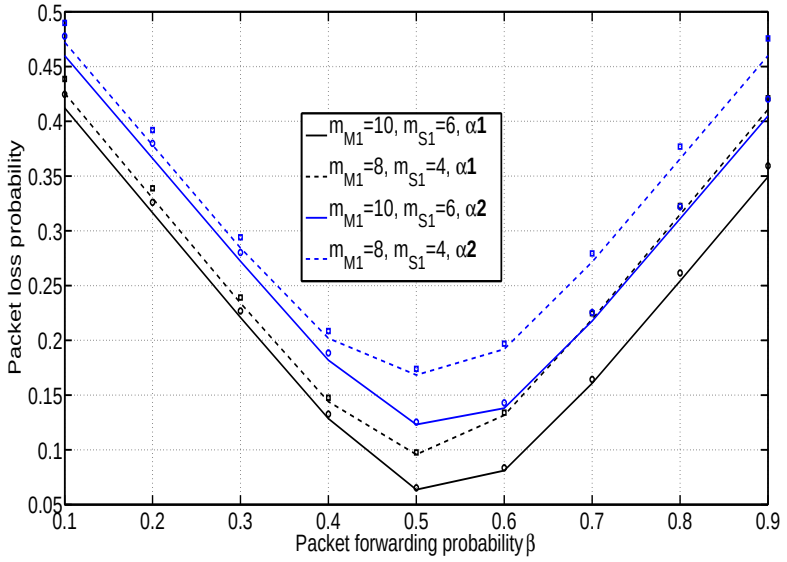

Figure 4.3: PLP vs. packet forwarding probability (markers correspond to simulation results).

Here, the effect of varying the packet forwarding probability β on the performance of the tagged MUE in the ER of the reference small cell is investigated for several cases of packet arrival and amount of CQI feedback. Fig. 4.3 shows the PLP performance versus β, whereas Fig. 4.4 shows the average queuing delay performance versus β. In these figures, for a particular case of packet arrival and amount of CQI feedback, there is a value of β that minimizes the PLP and a value of β that minimizes the average queuing delay. The value of β that minimizes the PLP and the value of β that minimizes the average queuing delay are not necessarily unique for the same case of packet arrival and amount of CQI feedback as shown in Fig. 4.3 and Fig. 4.4.

Next, the CDF of delay is investigated for various cases of packet arrival and amount of CQI feedback using various values of β as shown in Fig. 4.5. In this figure, for a particular case of packet arrival and amount of CQI feedback, we plot the CDF of delay using the value of β that minimizes the average queuing delay. As expected, the delay performance

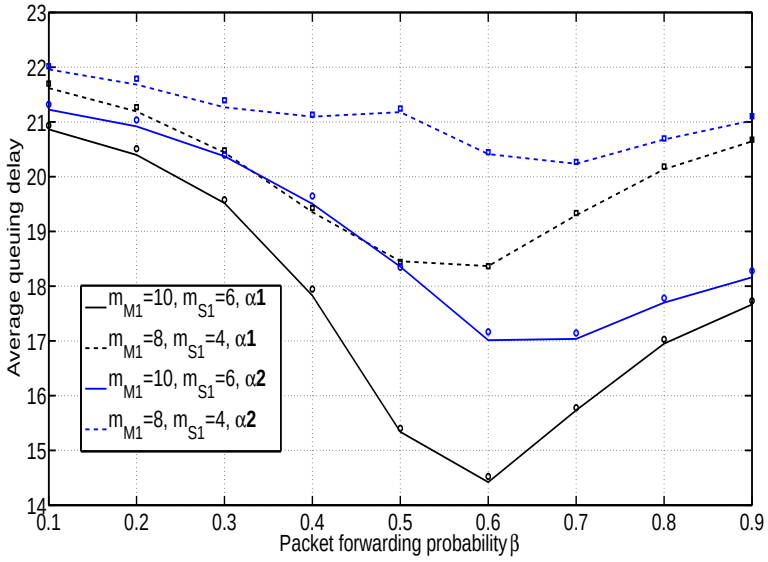

Figure 4.4: Average queuing delay vs. packet forwarding probability (markers correspond to simulation results).

of the tagged MUE is improved for a particular case of packet arrival and packet scheduling parameter when increasing the amount of CQI feedback.

4.4.2 Effect of varying the number of small cells

Next, we investigate the performance of the tagged MUE in the reference small cell when varying the number of interfering small cells. The PLP and the average queuing delay versus the number of interfering small cells are shown in Fig. 4.6 and Fig. 4.7 respectively. In Fig. 4.6, for a given case of packet arrival, amount of CQI feedback and number of interfering small cells, we plot the PLP using the value of β that minimizes the PLP. Similarly in Fig. 4.7, for a given case of packet arrival, amount of CQI feedback, and number of interfering small cells, we plot the average queuing delay using the value of β that minimizes the average queuing delay. It is obvious from these figures that the PLP and the average queuing delay vary significantly when varying the number of interfering small cells. This is due to the fact that deploying additional small cells has several effects on the performance of the tagged MUE. In particular, increasing the number of small cells increases the interference at the tagged MUE, and hence the sum transmission rate offered to the tagged MUE by the SBS decreases. However, traffic can be offloaded from the macrocell to the small cells as the number of small cells increases, which increases the sum transmission rate offered to the tagged MUE by the MBS.

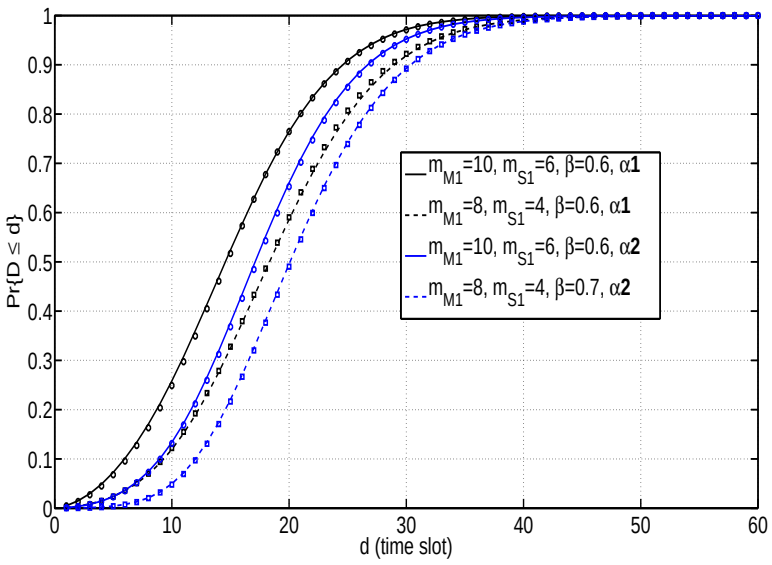

Figure 4.5: Delay CDF of various cases of packet arrival, amount of CQI feedback and packet scheduling parameter (markers correspond to simulation results).

The delay CDF of various cases of packet arrival, amount of CQI feedback and number of interfering small cells is shown in Fig. 4.8. In this figure, for a given case of packet arrival, amount of CQI feedback and number of interfering small cells, we plot the delay CDF using the value of β that minimizes the average queuing delay. Improvement in the delay performance due to increasing the amount of CQI feedback varies significantly with the number of interfering small cells. For example, for both packet arrival scenarios in Fig. 4.8, increasing the amount of CQI feedback significantly improves the delay performance for $I = 8$. On the other hand, only limited improvement in the delay performance is achieved when increasing the amount of CQI feedback for $I = 3$.

4.4.3 Effect of varying the number of MUEs

Here, we investigate the performance of the tagged MUE when varying the number of MUEs. The PLP and the average queuing delay versus the number of MUEs are shown in Fig. 4.9 and Fig. 4.10 respectively. In Fig. 4.9, for a given case of packet arrival, amount of CQI feedback and number of MUEs, we plot the PLP using the value of β that minimizes the PLP. Similarly in Fig. 4.10, for a given case of packet arrival, amount of CQI feedback and number of MUEs, we plot the average queuing delay using the value of β that minimizes the average queuing delay. It is obvious from these figures that the improvement in the PLP due to increasing the amount of CQI feedback becomes more significant when

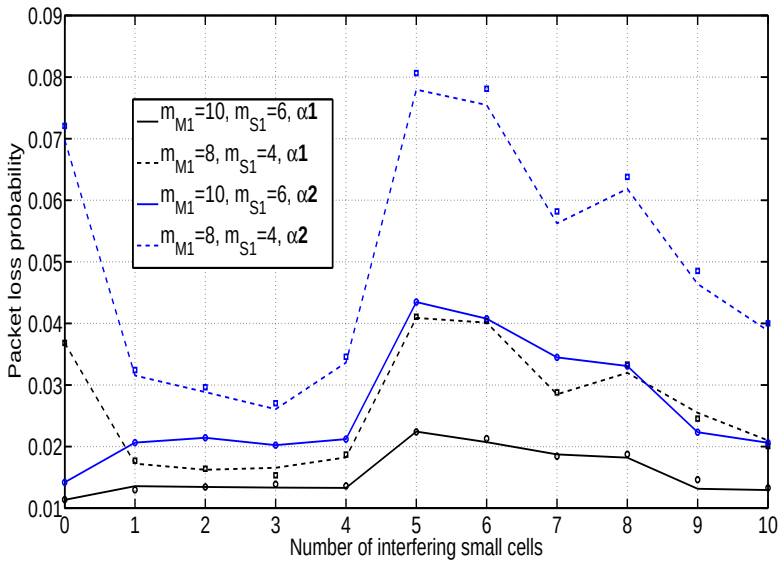

Figure 4.6: Packet loss probability vs. the number of interfering small cells (markers correspond to simulation results).

the number of MUEs increases. On the other hand, significant improvement in the average queuing delay due to increasing the amount of CQI feedback is achieved for any number of MUEs. The effect of varying the number of SUEs on the performance of the tagged MUE can also be readily obtained using our model, however, we do not include numerical results in this chapter for brevity.

The delay CDF of various cases of packet arrival, amount of CQI feedback and number of MUEs is shown in Fig. 4.11. In this figure, for a given case of packet arrival, amount of CQI feedback and number of MUEs, we plot the delay CDF using the value of β that minimizes the average queuing delay. This figure shows that increasing the amount of CQI feedback significantly improves the queuing delay performance for any number of MUEs in the system.

4.4.4 Effect of varying the ER of the reference small cell

Here, we investigate the performance of the tagged MUE when varying the ER of the reference small cell. The PLP and the average queuing delay versus R_{E} are shown in Fig. 4.12 and Fig. 4.13 respectively. In Fig. 4.12, for a given case of packet arrival, amount of CQI feedback and ER of the reference small cell, we plot the PLP using the value of β that minimizes the PLP. Similarly in Fig. 4.13, for a given case of packet arrival, amount of CQI feedback and ER of the reference small cell, we plot the average queuing delay using the

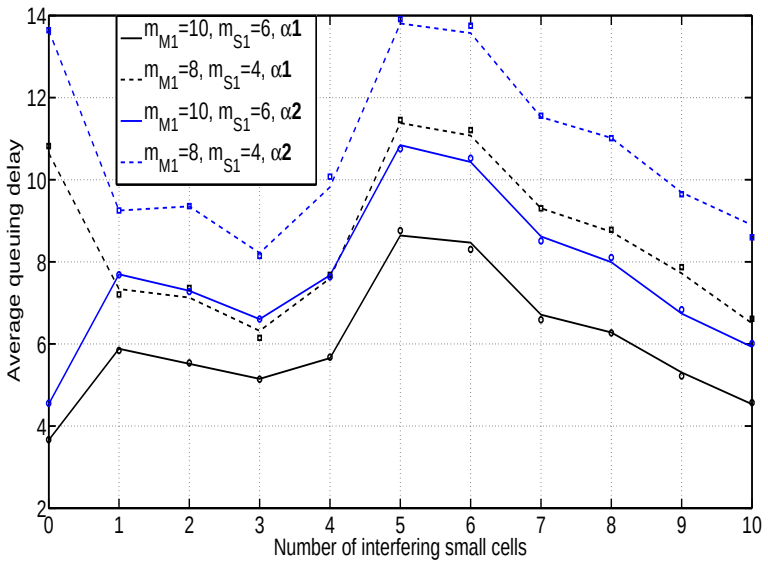

Figure 4.7: Average queuing delay vs. the number of interfering small cells (markers correspond to simulation results).

value of β that minimizes the average queuing delay. We consider that the tagged MUE is located at a distance $R_{\mathrm{M}} + R_{\mathrm{E}}$ from the reference SBS. As such, the PLP and average queuing delay performances shown in Fig. 4.12 and Fig. 4.13 are the worst case scenario performances when varying the ER of the reference small cell.

The delay CDF of various cases of packet arrival, amount of CQI feedback and ER of the reference small cell is shown in Fig. 4.14. In this figure, for a given case of packet arrival, amount of CQI feedback and ER of the reference small cell, we plot the delay CDF using the value of β that minimizes the average queuing delay. For both packet arrival scenarios in Fig. 4.14, increasing the amount of CQI feedback significantly improves the delay performance for $R_{\mathrm{E}} = 20$. On the other hand, limited improvement in the delay performance is achieved when increasing the amount of CQI feedback for $R_{\mathrm{E}} = 10$.

4.4.5 Example applications of the developed queuing model

In what follows, we provide some example applications of the developed queuing analytical model.

- *Cross-layer performance analysis:* Our model can be used to measure various packet level performance parameters for MUEs served by multiple tiers through multi-flow CA. In particular, the network operator can implement the steps for the queuing

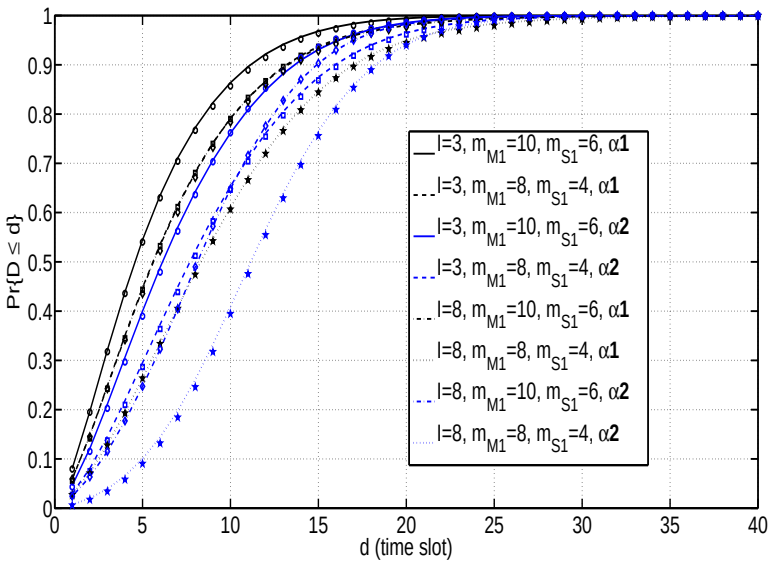

Figure 4.8: Delay CDF for several cases of packet arrival, amount of CQI feedback and number of interfering small cells (markers correspond to simulation results).

model developed in Section III that takes system parameters (packet arrival statistics, number of component carriers in each tier, coverage of BSs from different tiers, number of interfering small cells, etc.) as inputs and provides QoS parameters (e.g., PLP and queuing delay) as outputs for a given case of packet scheduling parameter and amount of CQI feedback.

- *Parameter selection:* Our model can be used to tune various parameters in order to offload as much traffic as possible from the macrocell to the small cells while maintaining the QoS requirements of MUEs in the ER of the small cells. For example, for given other system and operating parameters, the network operator can use our model to determine the minimum value of β and the amount of CQI feedback to the MBS and the SBSs needed to maintain the packet level QoS requirements of MUEs in the ER of the small cells. If the tagged MUE's QoS requirements are $\mathcal{P} = 0.14$, $\bar{\mathcal{D}} = 18.5$, $d_i = 20$ and $\zeta = 0.6$ for packet arrival described by $\boldsymbol{\alpha_1}$, these requirements are maintained with $m_{\mathrm{M1}} = 8$, $m_{\mathrm{S1}} = 4$ and $\beta = 0.6$ as shown in Fig. 4.3, Fig. 4.4 and Fig. 4.5. In this particular example, 40% of the tagged MUE's data packets are delivered by the reference SBS. Also, for given other system and operating parameters, the network operator can use our model to tune the number of small cells and the ER of each small cell based on the QoS requirements of MUEs in the ER of the small cells as shown in Section IV-B and Section IV-D.

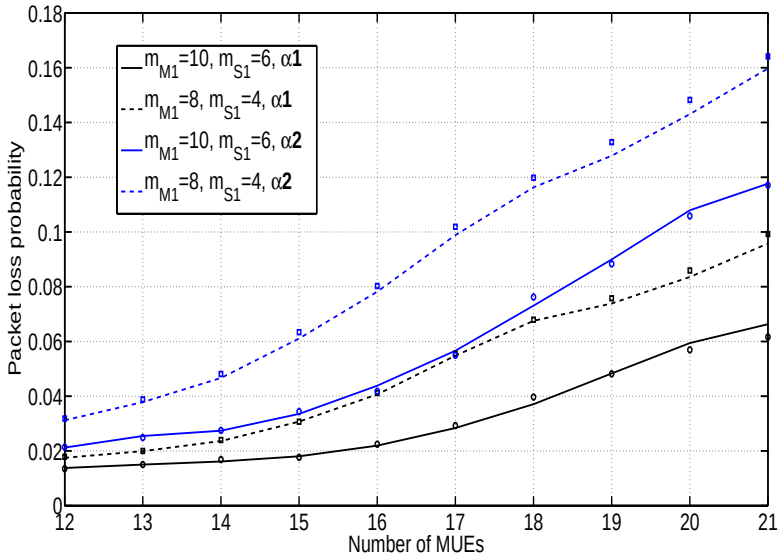

Figure 4.9: Packet loss probability vs. number of MUEs (markers correspond to simulation results).

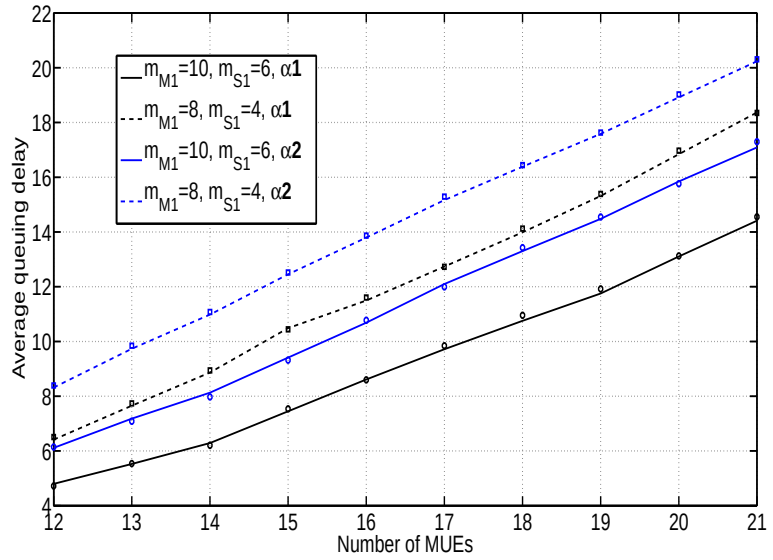

Figure 4.10: Average queuing delay vs. number of MUEs (markers correspond to simulation results).

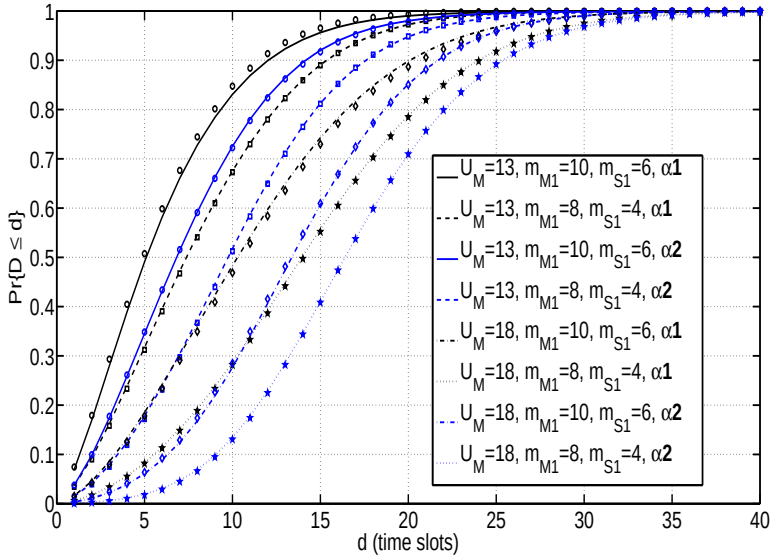

Figure 4.11: Delay CDF for several cases of packet arrival, amount of CQI feedback and number of MUEs (markers correspond to simulation results).

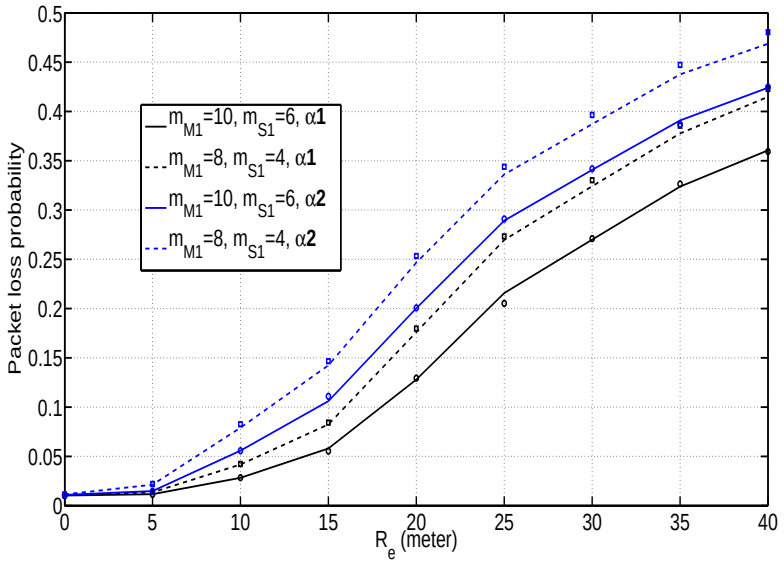

Figure 4.12: Packet loss probability vs. the ER of the reference small cell (markers correspond to simulation results).

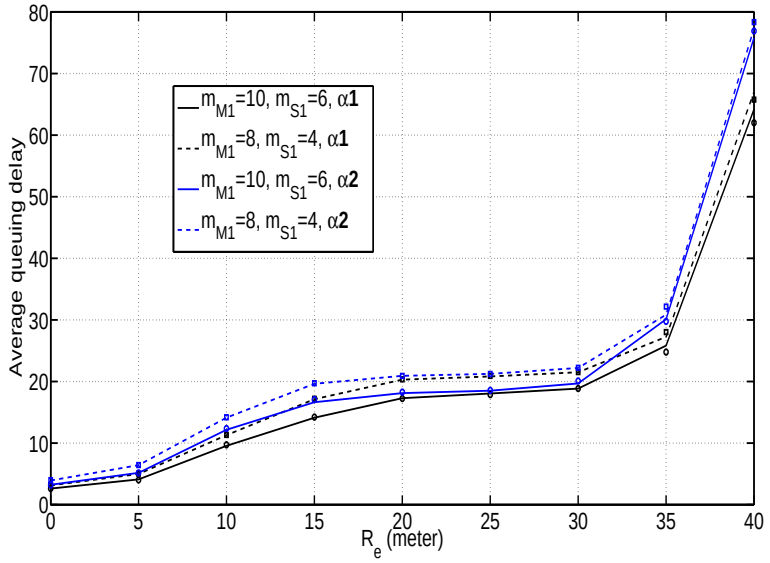

Figure 4.13: Average queuing delay vs. the ER of the reference small cell (markers correspond to simulation results).

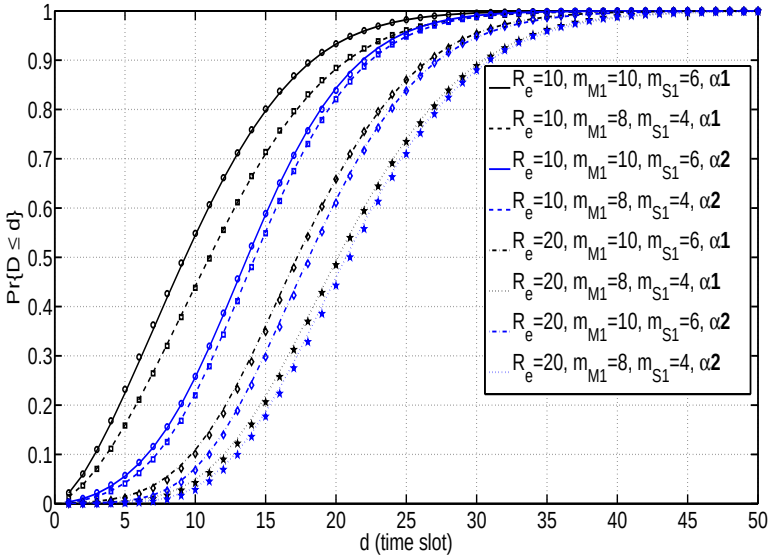

Figure 4.14: Delay CDF for several cases of packet arrival, amount of CQI feedback and ER of the reference small cell (markers correspond to simulation results).

- *CAC:* In [58], CAC based on the packet level QoS requirements has been proposed. As shown in Section IV-C, the performance of the MUEs in the ER of the small cells can be measured when varying the number of UEs using our developed analytical model. Therefore, using our model, the network operator can determine whether the QoS requirements of MUEs that are served using multi-flow CA are maintained if new UEs are admitted in the system. As for UEs that are served by a single tier, the traditional queuing models developed in [39], [40] can be used to determine if their QoS requirements are maintained. Then, based on the QoS requirements of all UEs in the system (including new UEs requesting service), the new service requests can be either admitted or rejected. Also, our model can be used along with the traditional queuing models to determine if it is necessary to serve a particular MUE in the ER of a small cell using multi-flow CA or if serving this MUE by a single tier is sufficient to maintain its QoS requirements.

Chapter 5

Conclusion

In this thesis, we have investigated QoS performances of resource allocation mechanisms in various state-of-the-art wireless systems by developing cross-layer analytical models. These models are useful for gauging the QoS performances of UEs in emerging wireless networks and tuning various system and operating parameters to maintain QoS requirements. The resource allocation mechanisms considered in this thesis include channel scheduling, packet scheduling and cell selection and the QoS parameters include PLP and queuing delay. The state-of-the-art wireless systems investigated in this thesis are: SCNs with non-line-of-sight wireless backhaul links, DL DCS in wireless networks with cell sleeping, and DL multi-flow CA in HetNets.

In Chapter 2, we have investigated the channel scheduling mechanism for the access link and the backhaul link in SCNs. For the access link we have considered the so-called max rate/opportunistic channel scheduling mechanism in order to exploit multiuser diversity, while for the backhaul link we have considered three different channel scheduling mechanisms, namely, fixed channel scheduling, round robin channel scheduling and access link dependent channel scheduling. We have developed an elaborate cross-layer analytical model to analyze various data link layer performances e.g., PLP and average queuing delay jointly capturing the time varying nature of the channels in both links, channel scheduling mechanisms in both links, stochastic packet arrivals, and network topology. We have demonstrated through numerical examples how the developed cross-layer analytical model can assist network designers to measure and compare beforehand various data link layer QoS performances e.g., end-to-end PLP and average queuing delay of packets for the considered channel scheduling mechanisms. We also have shown how the developed model can facilitate cross-layer design to select various design parameters such that the data link layer QoS requirements of the small cells' UEs are maintained. For instance, the developed model can be used to determine whether it is feasible to deploy an additional SBS for given QoS requirements.

In Chapter 3, for a given BS inactivation scheme/pattern, we have considered a CoMP DCS scheme for serving sleeping cell UEs. According to this DCS scheme, each packet of a particular UE in a sleeping cell arriving from the core network to the PSG is randomly forwarded to one of the potential active BSs and the UE in the sleeping cell dynamically

selects its serving BS from these active BSs. Unlike the conventional DCS scheme, the considered packet scheduling/forwarding mechanism does not require additional backhaul resources since a particular packet is forwarded only to one particular active BS. For the CoMP DCS scheme under consideration, we have modelled the system as a F/J queuing system and developed a cross-layer analytical model that considers the time varying nature of the channels, channel scheduling mechanism, partial CQI feedback, cell selection mechanism, bursty packet arrivals and packet scheduling mechanism. The developed analytical model can be used to measure various packet level performance parameters such as PLP and queuing delay while accounting for out-of-sequence packet delivery. The model is also useful to tune the amount of CQI feedback and to find the optimal packet scheduling by the PSG such that the packet level QoS requirements of the UEs in the sleeping cell are maintained. We have compared the performance of the DCS scheme under consideration with the conventional fixed cell selection and with the state-of-the-art DCS. Presented numerical results show that the DCS scheme under consideration significantly improves the PLP performance. Queuing delay performance, on the other hand, depends on the system and operating parameters.

In Chapter 4, we have considered multi-flow CA with dedicated spectrum access for serving MUEs in the ER of the small cells. We have developed a cross-layer F/J queuing analytical model that takes into account the time varying channels, the channel scheduling mechanism, partial CQI feedback and the number of component carriers deployed at each tier. Our model also accounts for stochastic packet arrivals and the packet scheduling mechanism. The developed analytical model can be used to gauge various packet-level performance parameters e.g., PLP and queuing delay of MUEs in the ER of the small cells. For the queuing delay performance, our model takes out-of-sequence packet delivery into consideration. Also, using numerical examples, we have demonstrated that the developed model can be used to select various system and operating parameters in order to offload as much traffic as possible from the macrocells to the small cells while maintaining the QoS requirements of MUEs in the ER of the small cells. For example, the packet scheduling parameter, the amount of CQI feedback, the number of deployed small cells and the ER of the small cells can be tuned to maintain the QoS requirements of MUEs in the ER of the small cells.

Bibliography

[1] Y. Qi, M. Hunukumbure, M. Nekovee, J. Lorca, and V. Sgardoni, "Quantifying data rate and bandwidth requirements for immersive 5g experience," in *IEEE Intl. Conf. Commun. Wksps (ICC Wksps)*, May 2016, pp. 455–461. → pages 1

[2] G. Fettweis and E. Zimmermann, "ICT energy consumption-trends and challenges," in *Intl. symp. on wireless prsnl. mmd. commun. (WPMC)*. → pages 1

[3] "Breaking the backhaul bottleneck: How to meet your backhaul capacity needs while maximizing revenue," White Paper, SKYFIBER, May 2013. → pages 1, 6

[4] E. Hossain, L. B. Le, and D. Niyato, *Radio resource management in multi-tier cellular wireless networks*. John Wiley & Sons, 2013. → pages 1

[5] X. Lin, J. G. Andrews, and A. Ghosh, "Modeling, analysis and design for carrier aggregation in heterogeneous cellular networks," *IEEE Trans. Commun.*, vol. 61, no. 9, pp. 4002–4015, Sep. 2013. → pages 2, 7

[6] S. Parkvall, E. Dahlman, A. Furuskar, Y. Jading, M. Olsson, S. Wanstedt, and K. Zangi, "LTE-Advanced - evolving LTE towards IMT-Advanced," in *IEEE Veh. Technol. Conf. (VTC)*, Sep. 2008, pp. 1–5. → pages 2

[7] H. Wang, C. Rosa, and K. I. Pedersen, "Dedicated carrier deployment in heterogeneous networks with inter-site carrier aggregation," in *IEEE Wireless Commun. and Ntwk Conf. (WCNC)*, Apr. 2013, pp. 756–760. → pages 2, 6, 7

[8] E. Oh, B. Krishnamachari, X. Liu, and Z. Niu, "Toward dynamic energy-efficient operation of cellular network infrastructure," *IEEE Commun. Mag.*, vol. 49, no. 6, pp. 56–61, Jun. 2011. → pages 2

[9] J. Louhi, "Energy efficiency of modern cellular base stations," in *Intl. Telecomm. Energy Conf. (INTELEC)*, Sep. 2007, pp. 475–476. → pages 2

[10] J. Hoydis, M. Kobayashi, and M. Debbah, "Green small-cell networks," *IEEE Veh. Technol. Mag.*, vol. 6, no. 1, pp. 37–43, Mar. 2011. → pages 4

[11] Small Cell Forum, "Backhaul technologies for small cells: Use cases, requirements and solutions," Tech. Rep. Rel. 5, Feb. 2013. → pages 4, 5

[12] J. Robson, "Small cell backhaul requirements," *NGMN White Paper*, pp. 1–40, Jun. 2012. → pages 4, 11

[13] Y. Sun, R. Jover, and X. Wang, "Uplink interference mitigation for OFDMA femtocell networks," *IEEE Trans. Wireless Commun.*, vol. 11, no. 2, pp. 614–625, Feb. 2012. → pages 5

[14] A. Hatoum, R. Langar, N. Aitsaadi, and G. Pujolle, "Q-FCRA: QoS-based OFDMA femtocell resource allocation algorithm," in *IEEE Intl. Conf. Commun. (ICC)*, Jun. 2012, pp. 5151–5156. → pages 5

[15] H. Tabassum, Z. Dawy, E. Hossain, and M.-S. Alouini, "Interference statistics and capacity analysis for uplink transmission in two-tier small cell networks: A geometric probability approach," *IEEE Trans. Wireless Commun.*, vol. 13, no. 7, pp. 3837–3852, Jul. 2014. → pages 5, 11, 13, 15

[16] H.-S. Jo, Y. J. Sang, P. Xia, and J. Andrews, "Heterogeneous cellular networks with flexible cell association: A comprehensive downlink SINR analysis," *IEEE Trans. Wireless Commun.*, vol. 11, no. 10, pp. 3484–3495, Oct. 2012. → pages

[17] V. Chandrasekhar, M. Kountouris, and J. Andrews, "Coverage in multi-antenna two-tier networks," *IEEE Trans. Wireless Commun.*, vol. 8, no. 10, pp. 5314–5327, Oct. 2009. → pages 5

[18] H. Dhillon and G. Caire, "Wireless backhaul networks: Capacity bound, scalability analysis and design guidelines," *IEEE Trans. Wireless Commun.*, vol. 14, no. 11, pp. 6043 – 6056, Jun. 2015. → pages 5

[19] D. Tsilimantos, J.-M. Gorce, and E. Altman, "Stochastic analysis of energy savings with sleep mode in OFDMA wireless networks," in *IEEE Intl. Conf. Comp. Commun. (INFOCOM)*, Apr. 2013, pp. 1097–1105. → pages 5

[20] Y. S. Soh, T. Quek, M. Kountouris, and H. Shin, "Energy efficient heterogeneous cellular networks," *IEEE J. Sel. Areas Commun.*, vol. 31, no. 5, pp. 840–850, May 2013. → pages 6

[21] D. Cao, S. Zhou, and Z. Niu, "Optimal combination of base station densities for energy-efficient two-tier heterogeneous cellular networks," *IEEE Trans. Wireless Commun.*, vol. 12, no. 9, pp. 4350–4362, Sep. 2013. → pages 6

[22] A. Bousia, A. Antonopoulos, L. Alonso, and C. Verikoukis, "Green distance-aware base station sleeping algorithm in LTE-Advanced," in *IEEE Intl. Conf. Commun. (ICC)*, Jun. 2012, pp. 1347–1351. → pages 6

[23] F. Han, Z. Safar, and K. Liu, "Energy-efficient base-station cooperative operation with guaranteed QoS," *IEEE Trans. Commun.*, vol. 61, no. 8, pp. 3505–3517, Aug. 2013. → pages 6

[24] H. Tabassum, U. Siddique, E. Hossain, and M. Hossain, "Downlink performance of cellular systems with base station sleeping, user association, and scheduling," *IEEE Trans. Wireless Commun.*, vol. 13, no. 10, pp. 5752–5767, Oct. 2014. → pages 5, 6

[25] M. Sawahashi, Y. Kishiyama, A. Morimoto, D. Nishikawa, and M. Tanno, "Coordinated multipoint transmission/reception techniques for LTE-Advanced [coordinated and distributed MIMO]," *IEEE Trans. Wireless Commun.*, vol. 17, no. 3, pp. 26–34, June 2010. → pages 6

[26] S. Tombaz, P. Monti, F. Farias, M. Fiorani, L. Wosinska, and J. Zander, "Is backhaul becoming a bottleneck for green wireless access networks?" in *IEEE Intl. Conf. Commun. (ICC)*, Jun. 2014, pp. 4029–4035. → pages 6

[27] Y. Yang, B. Bai, W. Chen, and L. Hanzo, "A low-complexity cross-layer algorithm for coordinated downlink scheduling and robust beamforming under a limited feedback constraint," *IEEE Trans. Veh. Technol.*, vol. 63, no. 1, pp. 107–118, Jan. 2014. → pages 37

[28] B. Bai, W. Chen, Z. Cao, and K. B. Letaief, "Max-matching diversity in OFDMA systems," *IEEE Trans. Commun.*, vol. 58, no. 4, pp. 1161–1171, Apr. 2010. → pages 6, 37

[29] L. Surez, M. A. Bouraoui, M. A. Mertah, M. Morvan, and L. Nuaymi, "Energy efficiency and cost issues in backhaul architectures for high data-rate green mobile heterogeneous networks," in *IEEE Prsnl, Indr, and Mob. Radio Commun. (PIMRC)*, Aug. 2015, pp. 1563–1568. → pages 6

[30] Y. J. Zhang and K. Letaief, "Multiuser adaptive subcarrier-and-bit allocation with adaptive cell selection for OFDM systems," *IEEE Trans. Wireless Commun.*, vol. 3, no. 5, pp. 1566–1575, Sep. 2004. → pages 6

[31] J. Chen, R. Berry, and M. Honig, "Limited feedback schemes for downlink OFDMA based on sub-channel groups," *IEEE J. Sel. Areas Commun.*, vol. 26, no. 8, pp. 1451–1461, Oct. 2008. → pages 6, 7

[32] Y. Lu, N. Yang, M. Elkashlan, and J. Yuan, "Partial channel quality information feedback in multiuser relay networks over Nakagami-m fading," *IEEE Trans. Wireless Commun.*, vol. 14, no. 9, pp. 4783–4796, Sep. 2015. → pages 6, 7

[33] G. Boudreau, J. Panicker, N. Guo, R. Chang, N. Wang, and S. Vrzic, "Interference coordination and cancellation for 4G networks," *IEEE Commun. Mag.*, vol. 47, no. 4, pp. 74–81, April 2009. → pages 6

[34] D. Lopez-Perez, X. Chu, and . Guvenc, "On the expanded region of picocells in heterogeneous networks," *IEEE J. Sel. Top. Sign. Proces.*, vol. 6, no. 3, pp. 281–294, Jun. 2012. → pages 6, 7

[35] I. Guvenc, M. R. Jeong, I. Demirdogen, B. Kecicioglu, and F. Watanabe, "Range expansion and inter-cell interference coordination (ICIC) for picocell networks," in *IEEE Veh. Technol. Conf. (VTC)*, Sep. 2011, pp. 1–6. → pages 6, 7

[36] C. Rosa, K. Pedersen, H. Wang, P. H. Michaelsen, S. Barbera, E. Malkamaki, T. Henttonen, and B. Sebire, "Dual connectivity for LTE small cell evolution: functionality and performance aspects," *IEEE Commun. Mag.*, vol. 54, no. 6, pp. 137–143, June 2016. → pages 7

[37] A. Hatoum, R. Langar, N. Aitsaadi, and G. Pujolle, "Q-FCRA: QoS-based OFDMA femtocell resource allocation algorithm," in *IEEE Intl. Conf. Commun. (ICC)*, Jun. 2012, pp. 5151–5156. → pages 7

[38] A. Alorainy and M. J. Hossain, "Downlink dynamic cell selection in wireless networks with cell sleeping: Cross layer performance analysis," in *IEEE Glob. Commun. Conf. (GLOBECOM)*, Dec. 2015, pp. 1–7. → pages 7, 75, 78, 84

[39] M. Rashid, J. Hossain, E. Hossain, and V. Bhargava, "Opportunistic spectrum access in cognitive radio networks: A queueing analytic model and admission controller design," in *IEEE Glob. Commun. Conf. (GLOBECOM)*, Nov. 2007, pp. 4647–4652. → pages 8, 16, 41, 52, 72, 84, 96

[40] H. C. Yang and S. Sasankan, "Analysis of channel-adaptive packet transmission over fading channels with transmit buffer management," *IEEE Trans. Veh. Technol.*, vol. 57, no. 1, pp. 404–413, Jan. 2008. → pages 8, 72, 96

[41] A. Alorainy and M. J. Hossain, "Cross-layer performance of channel scheduling mechanisms in small-cell networks with non-line-of-sight wireless backhaul links," *IEEE Trans. Wireless Commun.*, vol. 14, no. 9, pp. 4907–4922, Sep. 2015. → pages 8, 41

[42] L. B. Le, A. T. Nguyen, and E. Hossain, "A tandem queue model for performance analysis in multihop wireless networks," in *Proc. IEEE Wireless Communications and Networking Conference (WCNC)*, Mar. 2007, pp. 2981–2985. → pages 27

[43] T. Issariyakul and V. Krishnamurthy, "Amplify-and-forward cooperative diversity wireless networks: Model, analysis, and monotonicity properties," *IEEE/ACM Transactions on Networking*, vol. 17, no. 1, pp. 225–238, Feb. 2009. → pages 8

[44] Y. Choi, H. Kim, S. wook Han, and Y. Han, "Joint resource allocation for parallel multi-radio access in heterogeneous wireless networks," *IEEE Trans. Wireless Commun.*, vol. 9, no. 11, pp. 3324–3329, Nov. 2010. → pages 8, 49, 84

[45] H. d. M. G. Bolch, S. Greiner and K. Trivedi, *Queueing networks and Markov chains: modeling and performance evaluation with computer science applications.* John Wiley and Sons, 2006. → pages 8

[46] M. F. Neuts, *Matrix-geometric solutions in stochastic models: an algorithmic approach.* Courier Corporation, 1981. → pages 9, 25, 48, 82

[47] K. B. Baltzis, *Hexagonal vs circular cell shape: a comparative analysis and evaluation of the two popular modeling approximations.* INTECH Open Access Publisher, 2011. → pages 11

[48] I. Marić, B. Boštjančič, and A. Goldsmith, "Resource allocation for constrained backhaul in picocell networks," in *Info. Theory and Appl. Workshop (ITA)*, Feb. 2011, pp. 1–6. → pages 11, 12

[49] P. Bithas, N. Sagias, P. Mathiopoulos, G. Karagiannidis, and A. Rontogiannis, "On the performance analysis of digital communications over generalized-K fading channels," *IEEE Commun. Lett.*, vol. 10, no. 5, pp. 353–355, May 2006. → pages 13, 38

[50] S. Al-Ahmadi and H. Yanikomeroglu, "On the approximation of the generalized-K distribution by a gamma distribution for modeling composite fading channels," *IEEE Trans. Wireless Commun.*, vol. 9, no. 2, pp. 706–713, Feb. 2010. → pages 13, 38, 73

[51] Q. Liu, S. Zhou, and G. Giannakis, "Queuing with adaptive modulation and coding over wireless links: Cross-layer analysis and design," *IEEE Trans. Wireless Commun.*, vol. 4, no. 3, pp. 1142–1153, May 2005. → pages 14, 39, 73

[52] H. S. Wang and N. Moayeri, "Finite-state markov channel-a useful model for radio communication channels," *IEEE Trans. Veh. Technol.*, vol. 44, no. 1, pp. 163–171, Feb. 1995. → pages 14, 39, 73

[53] M. Hassan, M. Hossain, and J. Cheng, "Performance of non-adaptive and adaptive subcarrier intensity modulations in gamma-gamma turbulence," *IEEE Trans. Commun.*, vol. 61, no. 7, pp. 2946–2957, Jul. 2013. → pages 14, 39, 74

[54] Q. T. Zhang, "Outage probability of cellular mobile radio in the presence of multiple nakagami interferers with arbitrary fading parameters," *IEEE Trans. Veh. Technol.*, vol. 44, no. 3, pp. 661–667, Aug. 1995. → pages 14, 39, 74

[55] F. Berggren and R. Jantti, "Asymptotically fair transmission scheduling over fading channels," *IEEE Trans. Wireless Commun.*, vol. 3, no. 1, pp. 326–336, Jan. 2004. → pages 15

[56] H. Son, S. Lee, S.-C. Kim, and Y.-S. Shin, "Soft load balancing over heterogeneous wireless networks," *IEEE Trans. Veh. Technol.*, vol. 57, no. 4, pp. 2632–2638, Jul. 2008. → pages 49

[57] L. Le, E. Hossain, and A. Alfa, "Delay statistics and throughput performance for multi-rate wireless networks under multiuser diversity," *IEEE Trans. Wireless Commun.*, vol. 5, no. 11, pp. 3234–3243, Nov. 2006. → pages 52

[58] D. Niyato and E. Hossain, "Call admission control for QoS provisioning in 4G wireless networks: issues and approaches," *IEEE Network*, vol. 19, no. 5, pp. 5–11, Sep. 2005. → pages 70, 96

[59] F. Alomari and D. A. Menasc, "Efficient response time approximations for multiclass fork and join queues in open and closed queuing networks," *IEEE Trans. Parallel Distrib. Syst.*, vol. 25, no. 6, pp. 1437–1446, Jun. 2014. → pages 85

[60] A. Thomasian, "Analysis of fork/join and related queueing systems," *ACM Comput. Surv.*, vol. 47, no. 2, pp. 17:1–17:71, Aug. 2014. → pages 85

Appendices

Appendix A

Derivation of Block Sub-Matrices of P in Chapter 2

$$\mathbf{A}_{0,\delta_2}^{(0,q_{\mathrm{A}})} = (\alpha_0 \mathbf{J}_1 \otimes \mathbf{B2}_{\delta_2}^{(q_{\mathrm{A}})}(0)) \circ \mathbf{W} \tag{A.1}$$

$$\mathbf{A}_{\delta_1^+,\delta_2}^{(0,q_{\mathrm{A}})} = (\alpha_{\delta_1} \mathbf{J}_1 \otimes \mathbf{B2}_{\delta_2}^{(q_{\mathrm{A}})}(0)) \circ \mathbf{W}, \quad \delta_1 \leq Z \tag{A.2}$$

$$\mathbf{A}_{0,\delta_2}^{(q_{\mathrm{C}},q_{\mathrm{A}})} = \begin{cases} [\sum\limits_{\substack{0\leq i\leq q_{\mathrm{C}}-1 \\ i \mod b=0}} (\alpha_i \mathbf{O}_1^{(\frac{i}{b})} \otimes \mathbf{B2}_{\delta_2}^{(q_{\mathrm{A}})}(\min(q_{\mathrm{C}}, i)) \circ \mathbf{W} \\ +\alpha_{q_{\mathrm{C}}} \sum\limits_{\lceil q_{\mathrm{C}}/b\rceil \leq i\leq Y_1/b} (\mathbf{O}_1^{(i)} \otimes \mathbf{B2}_{\delta_2}^{(q_{\mathrm{A}})}(\min(q_{\mathrm{C}}, b.i)) \circ \mathbf{W}], \text{ if } q_{\mathrm{C}} \leq Z \\ \sum\limits_{\substack{0\leq i\leq Z \\ i \mod b=0}} (\alpha_i \mathbf{O}_1^{(\frac{i}{b})} \otimes \mathbf{B2}_{\delta_2}^{(q_{\mathrm{A}})}(\min(q_{\mathrm{C}}, i)) \circ \mathbf{W}, \text{ if } Z < q_{\mathrm{C}} < Q_{\mathrm{C,max}} \end{cases} \tag{A.3}$$

$$\mathbf{A}_{0,\delta_2}^{(Q_{\mathrm{C,max}},q_{\mathrm{A}})} = \sum_{0\leq i\leq Z} \sum_{\substack{0\leq l\leq i \\ l \mod b=0}} (\alpha_i \mathbf{O}_1^{(\frac{l}{b})} \otimes \mathbf{B2}_{\delta_2}^{(q_{\mathrm{A}})}(l)) \circ \mathbf{W} \tag{A.4}$$

$$\mathbf{A}_{(Q_{\mathrm{C,max}}-q_{\mathrm{C}})^+,\delta_2}^{(q_{\mathrm{C}},q_{\mathrm{A}})} = \sum_{\delta_1\leq i\leq Z} \sum_{\substack{0\leq l\leq i-\delta_1 \\ l \mod b=0}} (\alpha_i \mathbf{O}_1^{(\frac{l}{b})} \otimes \mathbf{B2}_{\delta_2}^{(q_{\mathrm{A}})}(l)) \circ \mathbf{W}, \delta_1 \leq Z \tag{A.5}$$

For $1 \leq q_{\mathrm{C}} \leq Y_1 - 1$ we can write:

$$\mathbf{A}_{\delta_1^-,\delta_2}^{(q_{\mathrm{C}},q_{\mathrm{A}})} = \begin{cases} [\sum\limits_{\substack{0\leq i\leq q_{\mathrm{C}}-\delta_1-1 \\ (i+\delta_1) \mod b=0}} (\alpha_i \mathbf{O}_1^{(\frac{i+\delta_1}{b})} \otimes \mathbf{B2}_{\delta_2}^{(q_{\mathrm{A}})}(\min(q_{\mathrm{C}}, i+\delta_1)) \circ \mathbf{W} \\ +\alpha_{q_{\mathrm{C}}-\delta_1} \sum\limits_{\lceil q_{\mathrm{C}}/b\rceil \leq i\leq Y_1/b} (\mathbf{O}_1^{(i)} \otimes \mathbf{B2}_{\delta_2}^{(q_{\mathrm{A}})}(\min(q_{\mathrm{C}}, b.i)) \circ \mathbf{W}], \text{ if } q_{\mathrm{C}} - Z \leq \delta_1 \leq q_{\mathrm{C}} - 1 \\ \alpha_0 \sum\limits_{\lceil q_{\mathrm{C}}/b\rceil \leq i\leq Y_1/b} (\mathbf{O}_1^{(i)} \otimes \mathbf{B2}_{\delta_2}^{(q_{\mathrm{A}})}(\min(q_{\mathrm{C}}, b.i)) \circ \mathbf{W}, \text{ if } \delta_1 = q_{\mathrm{C}} \\ \sum\limits_{\substack{0\leq i\leq Z \\ (i+\delta_1) \mod b=0}} (\alpha_i \mathbf{O}_1^{(\frac{i+\delta_1}{b})} \otimes \mathbf{B2}_{\delta_2}^{(q_{\mathrm{A}})}(\min(q_{\mathrm{C}}, i+\delta_1)) \circ \mathbf{W}, \text{ otherwise} \end{cases} \tag{A.6}$$

$$\mathbf{A}_{\delta_1^+,\delta_2}^{(q_\mathrm{C},q_\mathrm{A})} = \left[\begin{array}{l} \sum\limits_{\substack{\delta_1 \le i \le q_\mathrm{C}+\delta_1-1 \\ (i-\delta_1) \bmod b=0}} (\alpha_i \mathbf{O}_1^{(\frac{i-\delta_1}{b})} \otimes \mathbf{B2}_{\delta_2}^{(q_\mathrm{A})}(\min(q_\mathrm{C}, i-\delta_1)) \circ \mathbf{W} \\ +\alpha_{q_\mathrm{C}+\delta_1} \sum\limits_{\lceil q_\mathrm{C}/b \rceil \le i \le Y_1/b} (\mathbf{O}_1^{(i)} \otimes \mathbf{B2}_{\delta_2}^{(q_\mathrm{A})}(\min(q_\mathrm{C}, b.i)) \circ \mathbf{W} \end{array} \right], \delta_1 \le Z \quad \text{(A.7)}$$

For $q_\mathrm{C} \ge Y_1$ we can write:

$$\mathbf{A}_{\delta_1^-,\delta_2}^{(q_\mathrm{A})} = \begin{cases} \sum\limits_{\substack{0 \le i \le Z \\ (i+\delta_1) \bmod b=0}} (\alpha_i \mathbf{O}_1^{(\frac{i+\delta_1}{b})} \otimes \mathbf{B2}_{\delta_2}^{(q_\mathrm{A})}(i+\delta_1)) \circ \mathbf{W} & \text{if} \quad 1 \le \delta_1 < Y_1 - Z \\ \sum\limits_{\substack{0 \le i \le Y_1-\delta_1 \\ (i+\delta_1) \bmod b=0}} (\alpha_i \mathbf{O}_1^{(\frac{i+\delta_1}{b})} \otimes \mathbf{B2}_{\delta_2}^{(q_\mathrm{A})}(i+\delta_1)) \circ \mathbf{W} & \text{if} \quad Y_1 - Z \le \delta_1 \le Y_1 \end{cases} \quad \text{(A.8)}$$

$$\mathbf{A}_{\delta_1^+,\delta_2}^{(q_\mathrm{A})} = \sum_{\substack{\delta_1 \le i \le Z \\ (i-\delta_1) \bmod b=0}} (\alpha_i \mathbf{O}_1^{(\frac{i-\delta_1}{b})} \otimes \mathbf{B2}_{\delta_2}^{(q_\mathrm{A})}(i-\delta_1)) \circ \mathbf{W}, \delta_1 \le Z \quad \text{(A.9)}$$

Appendix B

Derivation of Block Sub-Matrices $\mathbf{B2}_{\delta 2}^{(q2)}(\lambda)$ in Chapter 2

$$\mathbf{B2}_0^{(0)}(\lambda) = f_\lambda(0)\mathbf{J}_2 \tag{B.1}$$

$$\mathbf{B2}_{\delta_2^+}^{(0)}(\lambda) = f_\lambda(\delta_2)\mathbf{J}_2 \tag{B.2}$$

$$\mathbf{B2}_0^{(Q_{\mathrm{A,max}})}(\lambda) = \sum_{\substack{0\le j\le\lambda \\ j \mod b=0}} \mathbf{O}_2^{(\frac{j}{b})} \tag{B.3}$$

$$\mathbf{B2}_{(Q_{\mathrm{A,max}}-q_{\mathrm{A}})^+}^{(q_{\mathrm{A}})}(\lambda) = \sum_{\substack{0\le j\le\lambda-\delta_2 \\ j \mod b=0}} \mathbf{O}_2^{(\frac{j}{b})}, \quad \delta_2 \le \lambda \tag{B.4}$$

For $1 \le q_{\mathrm{A}} \le \lambda$ we can write:

$$\mathbf{B2}_0^{(q_{\mathrm{A}})}(\lambda) = \sum_{\substack{0\le j\le q_{\mathrm{A}}-1 \\ j \mod b=0}} f_\lambda(j)\mathbf{O}_2^{(\frac{j}{b})} + f_\lambda(q_{\mathrm{A}}) \sum_{\lceil q_{\mathrm{A}}/b\rceil \le j\le Y_2/b} \mathbf{O}_2^{(j)} \tag{B.5}$$

For $\lambda < q_{\mathrm{A}} < Q_{\mathrm{A,max}}$ we can write:

$$\mathbf{B2}_0(\lambda) = \mathbf{O}_2^{(\frac{\lambda}{b})}|_{\lambda \mod b=0} \tag{B.6}$$

For $1 \leq q_{\mathrm{A}} \leq Y_2 - 1$ we can write:

$$\mathbf{B2}_{\delta_2^-}^{(q_{\mathrm{A}})}(\lambda) = \begin{cases} \sum\limits_{\substack{0 \leq j \leq q_{\mathrm{A}} - \delta_2 - 1 \\ (j+\delta_2) \mod b = 0}} f_\lambda(j) \mathbf{O}_2^{(\frac{j+\delta_2}{b})} \\ \quad + f_\lambda(q_{\mathrm{A}} - \delta_2) \sum\limits_{\lceil q_{\mathrm{A}}/b \rceil \leq j \leq Y_2/b} \mathbf{O}_2^{(j)}, & \text{if } \; q_{\mathrm{A}} - \lambda \leq \delta_2 \leq q_{\mathrm{A}} - 1 \\ f_\lambda(0) \sum\limits_{\lceil q_{\mathrm{A}}/b \rceil \leq j \leq Y_2/b} \mathbf{O}_2^{(j)}, & \text{if } \; \delta_2 = q_{\mathrm{A}} \\ \mathbf{O}_2^{(\frac{\lambda+\delta_2}{b})}|_{(\lambda+\delta_2) \mod b = 0}, & \text{otherwise} \end{cases} \tag{B.7}$$

$$\mathbf{B2}_{\delta_2^+}^{(q_{\mathrm{A}})}(\lambda) = \sum_{\substack{\delta_2 \leq j \leq q_{\mathrm{A}} + \delta_2 - 1 \\ (j-\delta_2) \mod b = 0}} f_\lambda(j) \mathbf{O}_2^{(\frac{j-\delta_2}{b})} + f_\lambda(q_{\mathrm{A}} + \delta_2) \sum_{\lceil q_{\mathrm{A}}/b \rceil \leq j \leq Y_2/b} \mathbf{O}_2^{(j)} \quad , \; \delta_2 \leq \lambda \tag{B.8}$$

For $q_{\mathrm{A}} \geq Y_2$ we can write:

$$\mathbf{B2}_{\delta_2^-}(\lambda) = \begin{cases} \mathbf{O}_2^{(\frac{\lambda+\delta_2}{b})}|_{(\lambda+\delta_2) \mod b = 0}, & \text{if } \; \delta_2 < Y_2 - \lambda \\ \sum\limits_{\substack{0 \leq j \leq Y_2 - \delta_2 \\ (j+\delta_2) \mod b = 0}} f_\lambda(j) \mathbf{O}_2^{(\frac{j+\delta_2}{b})}, & \text{if } \; Y_2 - \lambda \leq \delta_2 \leq Y_2 \end{cases} \tag{B.9}$$

$$\mathbf{B2}_{\delta_2 +}(\lambda) = \mathbf{O}_2^{(\frac{\lambda-\delta_2}{b})}|_{(\lambda-\delta_2) \mod b = 0}, \quad \delta_2 \leq \lambda \tag{B.10}$$

Appendix C

Derivation of Block Sub-Matrices of P in Chapter 3

When a BS is not selected as the serving BS, tagged UE's packets at that BS cannot be transmitted. Therefore, for $\delta_{\bar{i}}^{-} < 0$ (which is equivalent to decreasing number of packets in tagged UE's buffer at the non-serving BS):

$$\mathbf{A}_{\delta_i,\delta_{\bar{i}}^{-}}^{(q_i,q_{\bar{i}})}(i,j) = \mathbf{0} \tag{C.1}$$

Increasing the number of packets at the non-serving BS by less than $(Q_{\bar{i}} - q_{\bar{i}})$: for $0 \leq \delta_{\bar{i}}^{+} < (Q_{\bar{i}} - q_{\bar{i}})^{+}$, $\delta_{\bar{i}}^{+} \leq Z$:

$$\mathbf{A}_{\delta_i^{+},\delta_{\bar{i}}^{+}}^{(0,q_{\bar{i}})}(i,j) = \psi_{\delta_i,\delta_{\bar{i}}}\mathbf{T}_{ij}, \quad 0 \leq \delta_i \leq Z \tag{C.2}$$

$$\mathbf{A}_{0,\delta_{\bar{i}}^{+}}^{(q_i,q_{\bar{i}})}(i,j) = \begin{cases} \sum\limits_{\substack{0\leq k\leq q_i-1 \\ k \mod b=0}} \psi_{k,\delta_{\bar{i}}}\mathbf{O}_{ij}^{(\frac{k}{b})} + \psi_{q_i,\delta_{\bar{i}}} \sum\limits_{\lceil q_i/b\rceil \leq k\leq Y_i/b} \mathbf{O}_{ij}^{(k)}, \text{ if } q_i \leq Z \\ \sum\limits_{\substack{0\leq k\leq Z \\ k \mod b=0}} \psi_{k,\delta_{\bar{i}}}\mathbf{O}_{ij}^{(\frac{k}{b})}, \text{ if } Z < q_i < Q_i \end{cases} \tag{C.3}$$

$$\mathbf{A}_{0,\delta_{\bar{i}}^{+}}^{(Q_i,q_{\bar{i}})}(i,j) = \sum_{0\leq k\leq Z} \sum_{\substack{0\leq l\leq k \\ l \mod b=0}} \psi_{k,\delta_{\bar{i}}}\mathbf{O}_{ij}^{(\frac{l}{b})} \tag{C.4}$$

$$\mathbf{A}_{(Q_i-q_i)^{+},\delta_{\bar{i}}^{+}}^{(q_i,q_{\bar{i}})}(i,j) = \sum_{\delta_i^{+}\leq k\leq Z} \sum_{\substack{0\leq l\leq k-\delta_i^{+} \\ l \mod b=0}} \psi_{k,\delta_{\bar{i}}}\mathbf{O}_{ij}^{(\frac{l}{b})}, \ \delta_i \leq Z \tag{C.5}$$

For $1 \leq q_i \leq Y_i - 1$ we can write:

$$\mathbf{A}^{(q_i,q_{\bar{i}})}_{\delta_i^-,\delta_i^+}(i,j) = \begin{cases} \sum\limits_{\substack{0\leq k\leq q_i-\delta_i-1 \\ (k+\delta_i) \mod b=0}} \psi_{k,\delta_{\bar{i}}} \mathbf{O}_{ij}^{(\frac{k+\delta_i}{b})} \\ +\psi_{q_i-\delta_i,\delta_{\bar{i}}} \sum\limits_{\lceil q_i/b\rceil \leq k\leq Y_i/b} \mathbf{O}_{ij}^{(k)}, \text{ if } q_i - Z \leq \delta_i \leq q_i - 1 \\ \psi_{0,\delta_{\bar{i}}} \sum\limits_{\lceil q_i/b\rceil \leq k\leq Y_i/b} \mathbf{O}_{ij}^{(k)}, \text{ if } \delta_i = q_i \\ \sum\limits_{\substack{0\leq k\leq Z \\ (k+\delta_i) \mod b=0}} \psi_{k,\delta_{\bar{i}}} \mathbf{O}_{ij}^{(\frac{k+\delta_i}{b})}, \text{ otherwise} \end{cases} \tag{C.6}$$

$$\mathbf{A}^{(q_i,q_{\bar{i}})}_{\delta_i^+,\delta_i^+}(i,j) = \sum_{\substack{\delta_i\leq k\leq q_i+\delta_i-1 \\ (k-\delta_i) \mod b=0}} \psi_{k,\delta_{\bar{i}}} \mathbf{O}_{ij}^{(\frac{k-\delta_i}{b})} + \psi_{q_i+\delta_i,\delta_{\bar{i}}} \sum_{\lceil q_i/b\rceil \leq k\leq Y_i/b} \mathbf{O}_{ij}^{(k)}, \ \delta_i \leq Z \tag{C.7}$$

For $q_i \geq Y_i$ we can write:

$$\mathbf{A}^{(q_{\bar{i}})}_{\delta_i^-,\delta_i^+}(i,j) = \begin{cases} \sum\limits_{\substack{0\leq k\leq Z \\ (k+\delta_i) \mod b=0}} \psi_{k,\delta_{\bar{i}}} \mathbf{O}_{ij}^{(\frac{k+\delta_i}{b})} \quad \text{if} \quad 1 \leq \delta_i < Y_i - Z \\ \sum\limits_{\substack{0\leq k\leq Y_i-\delta_i \\ (k+\delta_i) \mod b=0}} \psi_{k,\delta_{\bar{i}}} \mathbf{O}_{ij}^{(\frac{k+\delta_i}{b})} \quad \text{if} \quad Y_i - Z \leq \delta_i \leq Y_i \end{cases} \tag{C.8}$$

$$\mathbf{A}^{(q_{\bar{i}})}_{\delta_i^+,\delta_{\bar{i}}^+}(i,j) = \sum_{\substack{\delta_i\leq k\leq Z \\ (k-\delta_i) \mod b=0}} \psi_{k,\delta_{\bar{i}}} \mathbf{O}_{ij}^{(\frac{k-\delta_i}{b})}, \delta_i \leq Z \tag{C.9}$$

Increasing the number of packets at the non-serving BS by $(Q_{\bar{i}} - q_{\bar{i}})$:
for $\delta_{\bar{i}}^+ = (Q_{\bar{i}} - q_{\bar{i}})^+$, $0 \leq \delta_{\bar{i}}^+ \leq Z$:

$$\mathbf{A}^{(0,q_{\bar{i}})}_{\delta_i^+,\delta_{\bar{i}}^+}(i,j) = \sum_{e=\delta_{\bar{i}}}^{Z} \psi_{\delta_i,e} \mathbf{T}_{ij}, \quad 0 \leq \delta_i \leq Z \tag{C.10}$$

$$\mathbf{A}^{(q_i,q_{\bar{i}})}_{0,\delta_{\bar{i}}^+}(i,j) = \begin{cases} \sum\limits_{e=\delta_{\bar{i}}}^{Z} \Big(\sum\limits_{\substack{0\leq k\leq q_i-1 \\ k \mod b=0}} \psi_{k,e} \mathbf{O}_{ij}^{(\frac{k}{b})} + \psi_{q_i,e} \sum\limits_{\lceil q_i/b\rceil \leq k\leq Y_i/b} \mathbf{O}_{ij}^{(k)} \Big), \text{ if } q_i \leq Z \\ \sum\limits_{e=\delta_{\bar{i}}}^{Z} \sum\limits_{\substack{0\leq k\leq Z \\ k \mod b=0}} \psi_{k,e} \mathbf{O}_{ij}^{(\frac{k}{b})}, \text{ if } Z < q_i < Q_i \end{cases} \tag{C.11}$$

$$\mathbf{A}_{0,\delta_{\bar{i}}^{+}}^{(Q_i,q_{\bar{i}})}(i,j)=\sum_{e=\delta_{\bar{i}}^{-}}^{Z}\sum_{0\leq k\leq Z}\sum_{\substack{l\\ 0\leq l\leq k\\ \text{mod } b=0}}\psi_{k,e}\mathbf{O}_{ij}^{(\frac{l}{b})} \tag{C.12}$$

$$\mathbf{A}_{(Q_i-q_i)^{+},\delta_{\bar{i}}^{+}}^{(q_i,q_{\bar{i}})}(i,j)=\sum_{e=\delta_{\bar{i}}^{-}}^{Z}\sum_{\delta_i^{+}\leq k\leq Z}\sum_{\substack{l\\ 0\leq l\leq k-\delta_i^{+}\\ \text{mod } b=0}}\psi_{k,e}\mathbf{O}_{ij}^{(\frac{l}{b})},\ \delta_i\leq Z \tag{C.13}$$

For $1\leq q_i\leq Y_i-1$ we can write:

$$\mathbf{A}_{\delta_i^{-},\delta_{\bar{i}}^{+}}^{(q_i,q_{\bar{i}})}(i,j)=\begin{cases}\sum_{e=\delta_{\bar{i}}^{-}}^{Z}\Big(\sum_{\substack{0\leq k\leq q_i-\delta_i-1\\ (k+\delta_i)\ \text{mod } b=0}}\psi_{k,e}\mathbf{O}_{ij}^{(\frac{k+\delta_i}{b})}\\ +\psi_{q_i-\delta_i,e}\sum_{\lceil q_i/b\rceil\leq k\leq Y_i/b}\mathbf{O}_{ij}^{(k)}\Big),\ \text{if } q_i-Z\leq\delta_i\leq q_i-1\\ \psi_{0,\delta_{\bar{i}}}\sum_{\lceil q_i/b\rceil\leq k\leq Y_i/b}\mathbf{O}_{ij}^{(k)},\ \text{if } \delta_i=q_i\\ \sum_{e=\delta_{\bar{i}}^{-}}^{Z}\sum_{\substack{0\leq k\leq Z\\ (k+\delta_i)\ \text{mod } b=0}}\psi_{k,e}\mathbf{O}_{ij}^{(\frac{k+\delta_i}{b})},\ \text{otherwise}\end{cases} \tag{C.14}$$

$$\mathbf{A}_{\delta_i^{+},\delta_{\bar{i}}^{+}}^{(q_i,q_{\bar{i}})}(i,j)=\sum_{e=\delta_{\bar{i}}^{-}}^{Z}\Big(\sum_{\substack{\delta_i\leq k\leq q_i+\delta_i-1\\ (k-\delta_i)\ \text{mod } b=0}}\psi_{k,e}\mathbf{O}_{ij}^{(\frac{k-\delta_i}{b})}+\psi_{q_i+\delta_i,e}\sum_{\lceil q_i/b\rceil\leq k\leq Y_i/b}\mathbf{O}_{ij}^{(k)}\Big),\ \delta_i\leq Z \tag{C.15}$$

For $q_i\geq Y_i$ we can write:

$$\mathbf{A}_{\delta_i^{-},\delta_{\bar{i}}^{+}}^{(q_{\bar{i}})}(i,j)=\begin{cases}\sum_{e=\delta_{\bar{i}}^{-}}^{Z}\sum_{\substack{0\leq k\leq Z\\ (k+\delta_i)\ \text{mod } b=0}}\psi_{k,e}\mathbf{O}_{ij}^{(\frac{k+\delta_i}{b})} & \text{if} \quad 1\leq\delta_i<Y_i-Z\\ \sum_{e=\delta_{\bar{i}}^{-}}^{Z}\sum_{\substack{0\leq k\leq Y_i-\delta_i\\ (k+\delta_i)\ \text{mod } b=0}}\psi_{k,e}\mathbf{O}_{ij}^{(\frac{k+\delta_i}{b})} & \text{if} \quad Y_i-Z\leq\delta_i\leq Y_i\end{cases} \tag{C.16}$$

$$\mathbf{A}_{\delta_i^{+},\delta_{\bar{i}}^{+}}^{(q_{\bar{i}})}(i,j)=\sum_{e=\delta_{\bar{i}}^{-}}^{Z}\sum_{\substack{\delta_i\leq k\leq Z\\ (k-\delta_i)\ \text{mod } b=0}}\psi_{k,e}\mathbf{O}_{ij}^{(\frac{k-\delta_i}{b})},\delta_i\leq Z \tag{C.17}$$

Appendix D

Proof of Eq. (3.6)

- *For* $0 < k \leq K-1$*:*

  The conditional probability $\Pr\{c_{1,h,j}^{(n)} = k \mid s_{2,h,j}^{(n)} = k_2, \cdots, s_{N,h,j}^{(n)} = k_N\}$ can be written as:

$$\Pr\{c_{1,h,j}^{(n)} = k \mid s_{2,h,j}^{(n)} = k_2, \cdots, s_{N,h,j}^{(n)} = k_N\} = \Pr\{s_{1,h,j}^{(n)} = k, v_{1,h,j}^{(n)} = 1 \mid s_{2,h,j}^{(n)} = k_2, \cdots, s_{N,h,j}^{(n)} = k_N\} = \Pr\{s_{1,h,j}^{(n)} = k\}\Pr\{v_{1,h,j}^{(n)} = 1 \mid s_{2,h,j}^{(n)} = k_2, \cdots, s_{N,h,j}^{(n)} = k_N\}. \tag{D.1}$$

  Let $k_{\min}$ denote the minimum state of the states of the best m_{jh} channels fed back by UE j in the sleeping cell to BS_h. There are three different cases:

  1. If $k > k_{\min}$: $\Pr\{v_{1,h,j}^{(n)} = 1 \mid s_{2,h,j}^{(n)} = k_2, \cdots, s_{N,h,j}^{(n)} = k_N\} = 1$.
  2. If $k < k_{\min}$: $\Pr\{v_{1,h,j}^{(n)} = 1 \mid s_{2,h,j}^{(n)} = k_2, \cdots, s_{N,h,j}^{(n)} = k_N\} = 0$.
  3. If $k = k_{\min}$:
     (a) The number of channels with channel state k is: $1 + f_k(k_2) + \cdots + f_k(k_N)$.
     (b) The number of fed back channels with channel state k is: $m_{jh} - (g_k(k_2) + \cdots + g_k(k_N))$.

     So, we can write:
     $\Pr\{v_{1,h,j}^{(n)} = 1 \mid s_{2,h,j}^{(n)} = k_2, \cdots, s_{N,h,j}^{(n)} = k_N\} = \frac{m_{jh} - (g_k(k_2) + \cdots + g_k(k_N))}{1 + f_k(k_2) + \cdots + f_k(k_N)}$.

  From the above three cases, we can write: $\Pr\{v_{1,h,j}^{(n)} = 1 \mid s_{2,h,j}^{(n)} = k_2, \cdots, s_{N,h,j}^{(n)} = k_N\} = \min(1, \max(0, \frac{m_{jh} - (g_k(k_2) + \cdots + g_k(k_N))}{1 + f_k(k_2) + \cdots + f_k(k_N)}))$.

  Finally, the probabilities $\Pr\{c_{1,h,j}^{(n)} = k\}$ can be calculated by the sum of all conditional probabilities as follows:

$$\Pr\{c_{1,h,j}^{(n)} = k\} = \sum_{k_2=0}^{K-1} \cdots \sum_{k_N=0}^{K-1} \min(1, \max(0, \frac{m_{jh} - (g_k(k_2) + \cdots + g_k(k_N))}{1 + f_k(k_2) + \cdots + f_k(k_N)})) \Pr\{s_{1,h,j}^{(n)} = k\} \prod_{i=2}^{N} \Pr\{s_{i,h,j}^{(n)} = k_i\}.$$

- *For* $k = 0$*:*

$$Pr\{c_{1,h,j}^{(n)} = 0\} = 1 - Pr\{c_{1,h,j}^{(n)} \neq 0\} \implies Pr\{c_{1,h,j}^{(n)} = 0\} = 1 - \sum_{k=1}^{K-1} Pr\{c_{1,h,j}^{(n)} = k\}.$$

Appendix E

Proof of Eq. (3.7)

- *For $a = 1$:*

  According to the considered channel scheduling mechanism, a particular channel is allocated to the UE with the highest channel state. If there are multiple UEs with the highest channel state, one of these UEs is randomly selected and allocated with the channel. In other words, the probability that a given UE is allocated with a particular channel assuming that this UE has the highest channel state in that particular channel at a given time slot is: $\frac{1}{\#\textit{of UEs having the highest channel state}}$.

  Therefore, the conditional probability $\Pr\{u_{i,h,1}^{(n)} = a \mid c_{i,h,1}^{(n)} = k, \cdots, c_{i,h,U_{sh}}^{(n)} = l_{U_{sh}}, s_{i,1}^{(n)} = k_1, \cdots, s_{i,U_h}^{(n)} = k_{U_h}\}$ is given by:

$$\begin{aligned}&\Pr\{u_{i,h,1}^{(n)} = a \mid c_{i,h,1}^{(n)} = k, \cdots, c_{i,h,U_{sh}}^{(n)} = l_{U_{sh}}, s_{i,1}^{(n)} = k_1, \cdots, s_{i,U_h}^{(n)} = k_{U_h}\} \\ &= \begin{cases} \frac{1}{1+f_k(k_1)+\cdots+f_k(k_{U_h})+f_k(l_2)+\cdots+f_k(l_{U_{sh}})}, 0 \le k_1, \cdots, k_{U_h}, l_2, \cdots, l_{U_{sh}} \le k \\ 0, \qquad\qquad \text{otherwise.} \end{cases}\end{aligned} \tag{E.1}$$

  As a result, the probability $\Pr\{u_{i,h,1}^{(n)} = a \mid c_{i,h,1}^{(n)} = k\}$ can be calculated by summing the conditional probabilities as follows:

$$\begin{aligned}\Pr\{u_{i,h,1}^{(n)} = a \mid c_{i,h,1}^{(n)} = k\} = \sum_{k_1=0}^{k} \cdots \sum_{k_{U_h}=0}^{k} \sum_{l_2=0}^{k} \cdots \sum_{l_{U_{sh}}=0}^{k} \frac{1}{1+f_k(k_1)+\cdots+f_k(k_{U_h})+f_k(l_2)+\cdots+f_k(l_{U_{sh}})} \\ \prod_{j=1}^{U_h} \Pr\{s_{i,j}^{(n)} = k_j\} \prod_{j=2}^{U_{sh}} \Pr\{c_{i,h,j}^{(n)} = l_j\}.\end{aligned}$$

- *For $a = 0$:*

$$Pr\{u_{i,h,1}^{(n)} = a \mid c_{i,h,1}^{(n)} = k\} = 1 - Pr\{u_{i,h,1}^{(n)} = 1 \mid c_{i,h,1}^{(n)} = k\}.$$

Appendix F

Proof of Eq. (3.10)

According to the considered DCS mechanism, the tagged UE selects the BS offering the highest sum transmission rate at a given time slot. If both BSs offer equal sum transmission rate at a given time slot, the tagged UE selects either BS randomly.

Therefore, the joint probabilities $\Pr\{h^{(n)} = i, t^{(n)} = j\}, 1 \leq i \leq 2, 0 \leq j \leq (K-1)m_{1i}$, are given by:

$$\Pr\{h^{(n)} = i, t^{(n)} = j\} = \Pr\{t_i^{(n)} = j\}(\Pr\{t_{\bar{i}}^{(n)} < j\} + \frac{1}{2}\Pr\{t_{\bar{i}}^{(n)} = j\}).$$

So, we can write: $\Pr\{h^{(n)} = i, t^{(n)} = j\} = \sum_{k=0}^{j} \frac{1}{1+f_j(k)} \Pr\{t_{\bar{i}}^{(n)} = k\},\ 1 \leq i \leq 2, 0 \leq j \leq (K-1)m_{1i}$.

Appendix G

Proof of Eq. (3.17)

Let us consider z packet arrivals to the tagged UE's queues at time slot n. The probability of the joint tagged UE's queues states as seen by arriving packet $k, 1 \leq k \leq z$, for a given packet scheduling scenario can be calculated as follows. Without loss of generality, let $h^{(n)} = 1$. Also, let $q_{0,1}^{(n+1)} = \min(q_1^{(n)} - t^{(n)}, 0)$. Then, the tagged UE's queues states at the next time slot before dropping packets due to queue overflow is: $q_1^{(n+1)} = q_{0,1}^{(n+1)} + \xi_{1k}, 0 \leq q_1^{(n+1)} \leq Q_1 + Z$. On the other hand, $q_2^{(n+1)} = q_2^{(n)} + \xi_{2k}, 0 \leq q_2^{(n+1)} \leq Q_2 + Z$. Note that for 0 packet arrivals to the tagged UE's queues at time slot n, the probability $\Pr\{q_1^{(n+1)} = q_1, q_2^{(n+1)} = q_2\}$ is given by:

$$\Pr\{q_1^{(n+1)} = q_1, q_2^{(n+1)} = q_2\} = \boldsymbol{\pi}_{0(i,j)}^{(1)} \mathbf{1}. \tag{G.1}$$

Now let $q_1^{(k,n+1)}$ and $q_2^{(k,n+1)}$ denote tagged UE's queues states as seen by arriving packet k. If $e_k = 1$ (i.e., packet k is forwarded to BS_1), we define $q_1^{(k,n+1)}$ and $q_2^{(k,n+1)}$ as:

$$\begin{aligned} q_1^{(k,n+1)} &= q_1^{(n+1)} \\ q_2^{(k,n+1)} &= \min(q_2^{(n+1)}, Q_2). \end{aligned}$$

On the other hand, if $e_k = 2$, we define $q_1^{(k,n+1)}$ and $q_2^{(k,n+1)}$ as:

$$\begin{aligned} q_2^{(k,n+1)} &= q_2^{(n+1)} \\ q_1^{(k,n+1)} &= \min(q_1^{(n+1)}, Q_1). \end{aligned}$$

Next, we proceed to deriving the probabilities $\Pr\{q_1^{(k,n+1)} = q_1, q_2^{(k,n+1)} = q_2\}$ for a given packet arrival and packet scheduling scenario. There are three different cases which are explained as follows.

1. *If* $e_k = 1$ *and* $q_2 = Q_2$*:* $\Pr\{q_1^{(k,n+1)} = q_1, q_2^{(k,n+1)} = q_2\} = \sum_{j=Q_2-\xi_{2k}}^{Q_2} \boldsymbol{\pi}_{0(q_1-\xi_{1k},j)}^{(1)}, \xi_{1k} \leq q_1 \leq Q_1 + \xi_{1k}$.

2. *If* $e_k = 2$ *and* $q_1 = Q_1$*:* $\Pr\{q_1^{(k,n+1)} = q_1, q_2^{(k,n+1)} = q_2\} = \sum_{i=Q_1-\xi_{1k}}^{Q_1} \boldsymbol{\pi}_{0(i,q_2-\xi_{2k})}^{(1)}, \xi_{2k} \leq q_2 \leq Q_2 + \xi_{2k}$

3. *If* $e_k = 1$ *and* $q_2 < Q_2$*:* $\Pr\{q_1^{(k,n+1)} = q_1, q_2^{(k,n+1)} = q_2\} = \boldsymbol{\pi}^{(h)}_{0(q_1-\xi_{1k},q_2-\xi_{2k})}, \xi_{1k} \leq q_1 \leq Q_1 + \xi_{1k}$.

4. *If* $e_k = 2$ *and* $q_1 < Q_1$*:* $\Pr\{q_1^{(k,n+1)} = q_1, q_2^{(k,n+1)} = q_2\} = \boldsymbol{\pi}^{(h)}_{0(q_1-\xi_{1k},q_2-\xi_{2k})}, \xi_{2k} \leq q_2 \leq Q_2 + \xi_{2k}$.

Using functions $f_x(y)$ and $\tilde{g}_x(y)$ defined earlier in the chapter, we combine these different cases in a single expression as follows:

$$\begin{aligned}\Pr\{q_1^{(k,n+1)} = q_1, q_2^{(k,n+1)} = q_2\} = \tilde{g}_{\xi_{1k}}(q_1)\tilde{g}_{\xi_{2k}}(q_2)(\tilde{g}_{q_1}(Q_1 + f_1(e_k)\xi_{1k}) \\ \tilde{g}_{q_2}(Q_2 + f_2(e_k)\xi_{2k})\boldsymbol{\pi}^{(h)}_{0(q_1-\xi_{1k},q_2-\xi_{2k})} + f_{q_1}(Q_1)f_2(e_k)\sum_{i=Q_1-\xi_{1k}+1}^{Q_1}\boldsymbol{\pi}^{(h)}_{0(i,q_2-\xi_{2k})} \\ +f_{q_2}(Q_2)f_1(e_k)\sum_{j=Q_2-\xi_{2k}+1}^{Q_2}\boldsymbol{\pi}^{(h)}_{0(q_1-\xi_{1k},j)}).\end{aligned} \tag{G.2}$$

In order to see that eq. (G.2) accounts for all the different cases, one can use the values of e_k, q_1 and q_2 in eq. (G.2) to see that the resulting terms correspond to the particular case. The same can be done for $h^{(n)} = 2$.

Finally, the probability vector of the joint probabilities of the tagged UE's queues states as seen by an arriving packet for any packet arrival and scheduling scenario (given that there is packet arrival in that particular time slot) is given by:

$$\begin{aligned}\boldsymbol{\omega}^{(h)}_{(q_1,q_2)} = \tfrac{1}{1-\alpha_0}\sum_{z=1}^{Z}\sum_{e_1=1}^{2}\cdots\sum_{e_z=1}^{2}\sum_{k=1}^{z}\tfrac{\psi_{\xi_{1z},\xi_{2z}}(\xi_{1z}!\xi_{2z}!)}{z(\xi_{1z}+\xi_{2z})!}\tilde{g}_{\xi_{1k}}(q_1)\tilde{g}_{\xi_{2k}}(q_2)(\tilde{g}_{q_1}(Q_1 + f_1(e_k)\xi_{1k}) \\ \tilde{g}_{q_2}(Q_2 + f_2(e_k)\xi_{2k})\boldsymbol{\pi}^{(h)}_{0(q_1-\xi_{1k},q_2-\xi_{2k})} + f_{q_1}(Q_1)f_2(e_k)\sum_{i=Q_1-\xi_{1k}+1}^{Q_1}\boldsymbol{\pi}^{(h)}_{0(i,q_2-\xi_{2k})} \\ +f_{q_2}(Q_2)f_1(e_k)\sum_{j=Q_2-\xi_{2k}+1}^{Q_2}\boldsymbol{\pi}^{(h)}_{0(q_1-\xi_{1k},j)}),\end{aligned}$$

where factor $\frac{1}{1-\alpha_0}$ is due to the fact that probability vector $\boldsymbol{\omega}^{(h)}_{(q_1,q_2)}$ is calculated given that $z \neq 0$. Also, factor $\frac{\psi_{\xi_{1z},\xi_{2z}}(\xi_{1z}!\xi_{2z}!)}{z(\xi_{1z}+\xi_{2z})!}$ is the probability of a given packet arrival and scheduling scenario as evident from eq. (3.5).

Appendix H

Derivation of Block Sub-Matrices of P in Chapter 4

$$\mathbf{A}_{0,\delta_{\mathrm{S}}}^{(0,q_{\mathrm{S}})} = (\mathbf{J}_{\mathrm{M}} \otimes \mathbf{B}_{\delta_{\mathrm{S}}}^{(q_{\mathrm{S}})}(0)) \circ \mathbf{W} \tag{H.1}$$

$$\mathbf{A}_{\delta_{\mathrm{M}}^{+},\delta_{\mathrm{S}}}^{(0,q_{\mathrm{S}})} = (\mathbf{J}_{\mathrm{M}} \otimes \mathbf{B}_{\delta_{\mathrm{S}}}^{(q_{\mathrm{S}})}(\delta_{\mathrm{M}})) \circ \mathbf{W}, \quad \delta_{\mathrm{M}} \leq Z \tag{H.2}$$

$$\mathbf{A}_{0,\delta_{\mathrm{S}}}^{(q_{\mathrm{M}},q_{\mathrm{S}})} = \begin{cases} [\sum\limits_{\substack{0\leq i\leq q_{\mathrm{M}}-1 \\ i \mod b=0}} (\mathbf{O}_{\mathrm{M}}^{(\frac{i}{b})} \otimes \mathbf{B}_{\delta_{\mathrm{S}}}^{(q_{\mathrm{S}})}(i)) \circ \mathbf{W} \\ + \sum\limits_{\lceil q_{\mathrm{M}}/b \rceil \leq i \leq Y_{\mathrm{M}}/b} (\mathbf{O}_{\mathrm{M}}^{(i)} \otimes \mathbf{B}_{\delta_{\mathrm{S}}}^{(q_{\mathrm{S}})}(q_{\mathrm{M}})) \circ \mathbf{W}], \text{ if } q_{\mathrm{M}} \leq Z \\ \sum\limits_{\substack{0\leq i\leq Z \\ i \mod b=0}} (\mathbf{O}_{\mathrm{M}}^{(\frac{i}{b})} \otimes \mathbf{B}_{\delta_{\mathrm{S}}}^{(q_{\mathrm{S}})}(i)) \circ \mathbf{W}, \text{ if } Z < q_{\mathrm{M}} < Q_{\mathrm{M}} \end{cases} \tag{H.3}$$

$$\mathbf{A}_{0,\delta_{\mathrm{S}}}^{(Q_{\mathrm{M}},q_{\mathrm{S}})} = \sum_{0\leq i\leq Z} \sum_{\substack{0\leq l\leq i \\ l \mod b=0}} (\mathbf{O}_{\mathrm{M}}^{(\frac{l}{b})} \otimes \mathbf{B}_{\delta_{\mathrm{S}}}^{(q_{\mathrm{S}})}(i)) \circ \mathbf{W} \tag{H.4}$$

$$\mathbf{A}_{(Q_{\mathrm{M}}-q_{\mathrm{M}})^{+},\delta_{\mathrm{S}}}^{(q_{\mathrm{M}},q_{\mathrm{S}})} = \sum_{(Q_{\mathrm{M}}-q_{\mathrm{M}})\leq i\leq Z} \sum_{\substack{0\leq l\leq i-(Q_{\mathrm{M}}-q_{\mathrm{M}}) \\ l \mod b=0}} (\mathbf{O}_{\mathrm{M}}^{(\frac{l}{b})} \otimes \mathbf{B}_{\delta_{\mathrm{S}}}^{(q_{\mathrm{S}})}(i)) \circ \mathbf{W}, \quad (Q_{\mathrm{M}}-q_{\mathrm{M}}) \leq Z \tag{H.5}$$

For $1 \leq q_{\mathrm{M}} \leq Y_{\mathrm{M}} - 1$ we can write:

$$\mathbf{A}^{(q_{\mathrm{M}},q_{\mathrm{S}})}_{\delta^{-}_{\mathrm{M}},\delta_{\mathrm{S}}} = \begin{cases} [\sum\limits_{\substack{0\leq i\leq q_{\mathrm{M}}-\delta_{\mathrm{M}}-1 \\ (i+\delta_{\mathrm{M}}) \mod b=0}} (\mathbf{O}_{\mathrm{M}}^{(\frac{i+\delta_{\mathrm{M}}}{b})} \otimes \mathbf{B}^{(q_{\mathrm{S}})}_{\delta_{\mathrm{S}}}(i)) \circ \mathbf{W} \\ + \sum\limits_{\lceil q_{\mathrm{M}}/b\rceil \leq i\leq Y_{\mathrm{M}}/b} (\mathbf{O}^{(i)}_{\mathrm{M}} \otimes \mathbf{B}^{(q_{\mathrm{S}})}_{\delta_{\mathrm{S}}}(q_{\mathrm{M}}-\delta_{\mathrm{M}})) \circ \mathbf{W}], \text{ if } q_{\mathrm{M}} - Z \leq \delta_{\mathrm{M}} \leq q_{\mathrm{M}} - 1 \\ \sum\limits_{\lceil q_{\mathrm{M}}/b\rceil \leq i\leq Y_{\mathrm{M}}/b} (\mathbf{O}^{(i)}_{\mathrm{M}} \otimes \mathbf{B}^{(q_{\mathrm{S}})}_{\delta_{\mathrm{S}}}(0)) \circ \mathbf{W}, \text{ if } \delta_{\mathrm{M}} = q_{\mathrm{M}} \\ \sum\limits_{\substack{0\leq i\leq Z \\ (i+\delta_{\mathrm{M}}) \mod b=0}} (\mathbf{O}_{\mathrm{M}}^{(\frac{i+\delta_{\mathrm{M}}}{b})} \otimes \mathbf{B}^{(q_{\mathrm{S}})}_{\delta_{\mathrm{S}}}(i)) \circ \mathbf{W}, \text{ otherwise} \end{cases} \tag{H.6}$$

$$\mathbf{A}^{(q_{\mathrm{M}},q_{\mathrm{S}})}_{\delta^{+}_{\mathrm{M}},\delta_{\mathrm{S}}} = [\begin{array}{c} \sum\limits_{\substack{\delta_{\mathrm{M}}\leq i\leq q_{\mathrm{M}}+\delta_{\mathrm{M}}-1 \\ (i-\delta_{\mathrm{M}}) \mod b=0}} (\mathbf{O}_{\mathrm{M}}^{(\frac{i-\delta_{\mathrm{M}}}{b})} \otimes \mathbf{B}^{(q_{\mathrm{S}})}_{\delta_{\mathrm{S}}}(i)) \circ \mathbf{W} \\ + \sum\limits_{\lceil q_{\mathrm{M}}/b\rceil \leq i\leq Y_{\mathrm{M}}/b} (\mathbf{O}^{(i)}_{\mathrm{M}} \otimes \mathbf{B}^{(q_{\mathrm{S}})}_{\delta_{\mathrm{S}}}(q_{\mathrm{M}}+\delta_{\mathrm{M}})) \circ \mathbf{W} \end{array}], \delta_{\mathrm{M}} \leq Z \tag{H.7}$$

For $q_{\mathrm{M}} \geq Y_{\mathrm{M}}$ we can write:

$$\mathbf{A}^{(q_{\mathrm{S}})}_{\delta^{-}_{\mathrm{M}},\delta_{\mathrm{S}}} = \begin{cases} \sum\limits_{\substack{0\leq i\leq Z \\ (i+\delta_{\mathrm{M}}) \mod b=0}} (\mathbf{O}_{\mathrm{M}}^{(\frac{i+\delta_{\mathrm{M}}}{b})} \otimes \mathbf{B}^{(q_{\mathrm{S}})}_{\delta_{\mathrm{S}}}(i)) \circ \mathbf{W} \quad \text{if} \quad 1 \leq \delta_{\mathrm{M}} < Y_{\mathrm{M}} - Z \\ \sum\limits_{\substack{0\leq i\leq Y_{\mathrm{M}}-\delta_{\mathrm{M}} \\ (i+\delta_{\mathrm{M}}) \mod b=0}} (\mathbf{O}_{\mathrm{M}}^{(\frac{i+\delta_{\mathrm{M}}}{b})} \otimes \mathbf{B}^{(q_{\mathrm{S}})}_{\delta_{\mathrm{S}}}(i)) \circ \mathbf{W} \quad \text{if} \quad Y_{\mathrm{M}} - Z \leq \delta_{\mathrm{M}} \leq Y_{\mathrm{M}} \end{cases} \tag{H.8}$$

$$\mathbf{A}^{(q_{\mathrm{S}})}_{\delta^{+}_{\mathrm{M}},\delta_{\mathrm{S}}} = \sum_{\substack{\delta_{\mathrm{M}}\leq i\leq Z \\ (i-\delta_{\mathrm{M}}) \mod b=0}} (\mathbf{O}_{\mathrm{M}}^{(\frac{i-\delta_{\mathrm{M}}}{b})} \otimes \mathbf{B}^{(q_{\mathrm{S}})}_{\delta_{\mathrm{S}}}(i)) \circ \mathbf{W}, \delta_{\mathrm{M}} \leq Z \tag{H.9}$$

Appendix I

Derivation of Block Sub-Matrices $\mathbf{B}_{\delta_{\mathrm{s}}}^{(q_{\mathrm{s}})}(i)$ in Chapter 4

$$\mathbf{B}_0^{(0)}(i) = \psi_{i,0}\mathbf{J}_{\mathrm{S}} \tag{I.1}$$

$$\mathbf{B}_{\delta_{\mathrm{S}}^+}^{(0)}(i) = \psi_{i,\delta_{\mathrm{S}}}\mathbf{J}_{\mathrm{S}}, \quad \delta_{\mathrm{S}} \leq Z \tag{I.2}$$

$$\mathbf{B}_0^{(q_{\mathrm{S}})}(i) = \begin{cases} [\sum\limits_{\substack{0\leq j\leq q_{\mathrm{S}}-1 \\ j \mod b=0}} \psi_{i,j}\mathbf{O}_{\mathrm{S}}^{(\frac{j}{b})} + \psi_{i,q_{\mathrm{S}}} \sum\limits_{\lceil q_{\mathrm{S}}/b\rceil \leq j\leq Y_{\mathrm{S}}/b} \mathbf{O}_{\mathrm{S}}^{(j)}], \text{ if } q_{\mathrm{S}} \leq Z \\ \sum\limits_{\substack{0\leq j\leq Z \\ j \mod b=0}} \psi_{i,j}\mathbf{O}_{\mathrm{S}}^{(\frac{j}{b})}, \text{ if } Z < q_{\mathrm{S}} < Q_{\mathrm{S}} \end{cases} \tag{I.3}$$

$$\mathbf{B}_0^{(Q_{\mathrm{S}})}(i) = \sum_{0\leq j\leq Z} \sum_{\substack{0\leq l\leq j \\ l \mod b=0}} \psi_{i,j}\mathbf{O}_{\mathrm{S}}^{(\frac{l}{b})} \tag{I.4}$$

$$\mathbf{B}_{(Q_{\mathrm{S}}-q_{\mathrm{S}})^+}^{(q_{\mathrm{S}})}(i) = \sum_{(Q_{\mathrm{S}}-q_{\mathrm{S}})\leq j\leq Z} \sum_{\substack{0\leq l\leq j-(Q_{\mathrm{S}}-q_{\mathrm{S}}) \\ l \mod b=0}} \psi_{i,j}\mathbf{O}_{\mathrm{S}}^{(\frac{l}{b})}, \quad (Q_{\mathrm{S}}-q_{\mathrm{S}}) \leq Z \tag{I.5}$$

For $1 \leq q_{\mathrm{S}} \leq Y_{\mathrm{S}} - 1$ we can write:

$$\mathbf{B}_{\delta_{\mathrm{S}}^-}^{(q_{\mathrm{S}})}(i) = \begin{cases} [\sum\limits_{\substack{0\leq j\leq q_{\mathrm{S}}-\delta_{\mathrm{S}}-1 \\ (j+\delta_{\mathrm{S}}) \mod b=0}} \psi_{i,j}\mathbf{O}_{\mathrm{S}}^{(\frac{j+\delta_{\mathrm{S}}}{b})} + \psi_{i,(q_{\mathrm{S}}-\delta_{\mathrm{S}})} \sum\limits_{\lceil q_{\mathrm{S}}/b\rceil \leq j\leq Y_{\mathrm{S}}/b} \mathbf{O}_{\mathrm{S}}^{(j)}], \text{ if } q_{\mathrm{S}} - Z \leq \delta_{\mathrm{S}} \leq q_{\mathrm{S}} - 1 \\ \psi_{i,0} \sum\limits_{\lceil q_{\mathrm{S}}/b\rceil \leq j\leq Y_{\mathrm{S}}/b} \mathbf{O}_{\mathrm{S}}^{(j)}, \text{ if } \delta_{\mathrm{S}} = q_{\mathrm{S}} \\ \sum\limits_{\substack{0\leq j\leq Z \\ (j+\delta_{\mathrm{S}}) \mod b=0}} \psi_{i,j}\mathbf{O}_{\mathrm{S}}^{(\frac{j+\delta_{\mathrm{S}}}{b})}, \text{ otherwise} \end{cases} \tag{I.6}$$

$$\mathbf{B}_{\delta_{\mathrm{S}}^{+}}^{(q_{\mathrm{S}})}(i) = [\sum_{\substack{\delta_{\mathrm{S}} \le j \le q_{\mathrm{S}}+\delta_{\mathrm{S}}-1 \\ (j-\delta_{\mathrm{S}}) \mod b=0}} \psi_{i,j} \mathbf{O}_{\mathrm{S}}^{(\frac{j-\delta_{\mathrm{S}}}{b})} + \psi_{i,(q_{\mathrm{S}}+\delta_{\mathrm{S}})} \sum_{\lceil q_{\mathrm{S}}/b \rceil \le j \le Y_{\mathrm{S}}/b} \mathbf{O}_{\mathrm{S}}^{(j)}], \delta_{\mathrm{S}} \le Z \tag{I.7}$$

For $q_{\mathrm{S}} \ge Y_{\mathrm{S}}$ we can write:

$$\mathbf{B}_{\delta_{\mathrm{S}}^{-}}(i) = \begin{cases} \sum_{\substack{0 \le j \le Z \\ (j+\delta_{\mathrm{S}}) \mod b=0}} \psi_{i,j} \mathbf{O}_{\mathrm{S}}^{(\frac{j+\delta_{\mathrm{S}}}{b})} & \text{if} \quad 1 \le \delta_{\mathrm{S}} < Y_{\mathrm{S}} - Z \\ \sum_{\substack{0 \le j \le Y_{\mathrm{S}}-\delta_{\mathrm{S}} \\ (j+\delta_{\mathrm{S}}) \mod b=0}} \psi_{i,j} \mathbf{O}_{\mathrm{S}}^{(\frac{j+\delta_{\mathrm{S}}}{b})} & \text{if} \quad Y_{\mathrm{S}} - Z \le \delta_{\mathrm{S}} \le Y_{\mathrm{S}} \end{cases} \tag{I.8}$$

$$\mathbf{B}_{\delta_{\mathrm{S}}^{+}}(i) = \sum_{\substack{\delta_{\mathrm{S}} \le j \le Z \\ (j-\delta_{\mathrm{S}}) \mod b=0}} \psi_{i,j} \mathbf{O}_{\mathrm{S}}^{(\frac{j-\delta_{\mathrm{S}}}{b})}, \delta_{\mathrm{S}} \le Z \tag{I.9}$$

Appendix J

Proof of Eq. (4.6)

- *For* $0 < k \leq K-1$*:*

  The conditional probability $Pr\{c^{(n)}_{S,1,1,l_{SE}} = k \mid s^{(n)}_{S,1,2,l_{SE}} = k_{2_{S1}}, \cdots, s^{(n)}_{S,1,N,l_{SE}} = k_{N_{S1}}, s^{(n)}_{S,2,1,l_{SE}} = k_{1_{S2}}, \cdots, s^{(n)}_{S,C_S,N,l_{SE}} = k_{N_{SC_S}}\}$ *can be written as:*

$$\begin{smallmatrix} Pr\{c^{(n)}_{S,1,1,l_{SE}} = k \mid s^{(n)}_{S,1,2,l_{SE}} = k_{2_{S1}}, \cdots, s^{(n)}_{S,1,N,l_{SE}} = k_{N_{S1}}, s^{(n)}_{S,2,1,l_{SE}} = k_{1_{S2}}, \cdots, s^{(n)}_{S,C_S,N,l_{SE}} = k_{N_{SC_S}}\} = \\ Pr\{s^{(n)}_{S,1,1,l_{SE}} = k, v^{(n)}_{S,1,1,l_{SE}} = 1 \mid s^{(n)}_{S,1,1,l_{SE}} = k_{2_{S1}}, \cdots, s^{(n)}_{S,1,N,l_{SE}} = k_{N_{S1}}, s^{(n)}_{S,2,1,l_{SE}} = k_{1_{S2}}, \cdots, s^{(n)}_{S,C_S,N,l_{SE}} = k_{N_{SC_S}}\} = \\ Pr\{s^{(n)}_{S,1,1,l_{SE}} = k\} Pr\{v^{(n)}_{S,1,1,l_{SE}} = 1 \mid s^{(n)}_{S,1,1,l_{SE}} = k_{2_{S1}}, \cdots, s^{(n)}_{S,1,N,l_{SE}} = k_{N_{S1}}, s^{(n)}_{S,2,1,l_{SE}} = k_{1_{S2}}, \cdots, s^{(n)}_{S,C_S,N,l_{SE}} = k_{N_{SC_S}}\}. \end{smallmatrix} \tag{J.1}$$

  Let k_{min} *denote the minimum state of the states of the best* $m_{Sl_{SE}}$ *channels fed back by MUE* l_{SE} *to the reference SBS. There are three different cases:*

  1. *If* $k > k_{min}$*:* $Pr\{v^{(n)}_{S,1,1,l_{SE}} = 1 \mid s^{(n)}_{S,1,1,l_{SE}} = k_{2_{S1}}, \cdots, s^{(n)}_{S,1,N,l_{SE}} = k_{N_{S1}}, s^{(n)}_{S,2,1,l_{SE}} = k_{1_{S2}}, \cdots, s^{(n)}_{S,C_S,N,l_{SE}} = k_{N_{SC_S}}\} = 1$
  2. *If* $k < k_{min}$*:* $Pr\{v^{(n)}_{S,1,1,l_{SE}} = 1 \mid s^{(n)}_{S,1,1,l_{SE}} = k_{2_{S1}}, \cdots, s^{(n)}_{S,1,N,l_{SE}} = k_{N_{S1}}, s^{(n)}_{S,2,1,l_{SE}} = k_{1_{S2}}, \cdots, s^{(n)}_{S,C_S,N,l_{SE}} = k_{N_{SC_S}}\} = 0$
  3. *If* $k = k_{min}$*:*
     (a) *The number of channels with channel state* k *is:*
     $1 + f_k(k_{2_{S1}}) + \cdots + f_k(k_{N_{S1}}) + f_k(k_{1_{S2}}) + \cdots + f_k(k_{N_{SC_S}})$.
     (b) *The number of fed back channels with channel state* k *is:*
     $m_{Sl_{SE}} - (g_k(k_{2_{S1}}) + \cdots + g_k(k_{N_{S1}}) + g_k(k_{1_{S2}}) + \cdots + g_k(k_{N_{SC_S}}))$.

     So, we can write:
     $Pr\{v^{(n)}_{S,1,1,l_{SE}} = 1 \mid s^{(n)}_{S,1,1,l_{SE}} = k_{2_{S1}}, \cdots, s^{(n)}_{S,1,N,l_{SE}} = k_{N_{S1}}, s^{(n)}_{S,2,1,l_{SE}} = k_{1_{S2}}, \cdots, s^{(n)}_{S,C_S,N,l_{SE}} = k_{N_{SC_S}}\} = \frac{m_{Sl_{SE}} - (g_k(k_{2_{S1}}) + \cdots + g_k(k_{N_{S1}}) + g_k(k_{1_{S2}}) + \cdots + g_k(k_{N_{SC_S}}))}{1 + f_k(k_{2_{S1}}) + \cdots + f_k(k_{N_{S1}}) + f_k(k_{1_{S2}}) + \cdots + f_k(k_{N_{SC_S}})}$

  From the above three cases, we can write:

  $Pr\{v^{(n)}_{S,1,1,l_{SE}} = 1 \mid s^{(n)}_{S,1,1,l_{SE}} = k_{2_{S1}}, \cdots, s^{(n)}_{S,1,N,l_{SE}} = k_{N_{S1}}, s^{(n)}_{S,2,1,l_{SE}} = k_{1_{S2}}, \cdots, s^{(n)}_{S,C_S,N,l_{SE}} = k_{N_{SC_S}}\} = (min(1, max(0, \frac{m_{Sl_{SE}} - (g_k(k_{2_{S1}}) + \cdots + g_k(k_{N_{S1}}) + g_k(k_{1_{S2}}) + \cdots + g_k(k_{N_{SC_S}}))}{1 + f_k(k_{2_{S1}}) + \cdots + f_k(k_{N_{S1}}) + f_k(k_{1_{S2}}) + \cdots + f_k(k_{N_{SC_S}})}))$.

Finally, the probabilities $Pr\{c^{(n)}_{S,1,1,l_{SE}} = k\}$ *can be calculated by the sum of all conditional probabilities as follows:*

$$Pr\{c^{(n)}_{S,1,1,l_{SE}} = k\} = \sum_{k_{2_{S1}}=0}^{K-1} \cdots \sum_{k_{N_{S1}}=0}^{K-1} \sum_{k_{1_{S2}}=0}^{K-1} \cdots \sum_{k_{N_{SC_S}}=0}^{K-1}$$
$$(min(1, max(0, \frac{{}^{m}Sl_{SE} - (g_k(k_{2_{S1}}) + \cdots + g_k(k_{N_{S1}}) + g_k(k_{1_{S2}}) + \cdots + g_k(k_{N_{SC_S}}))}{1 + f_k(k_{2_{S1}}) + \cdots + f_k(k_{N_{S1}}) + f_k(k_{1_{S2}}) + \cdots + f_k(k_{N_{SC_S}})})) Pr\{s^{(n)}_{S,1,1,l_{SE}} = k\} \prod_{j=1}^{C_S} \prod_{\substack{i=1 \\ i,j \neq 1}}^{N_{Sj}} Pr\{s^{(n)}_{S,j,i,l_{SE}} = k_{i_{Sj}}\})$$

- *For* $k = 0$*:*

  $Pr\{c^{(n)}_{S,1,1,l_{SE}} = 0\} = 1 - Pr\{c^{(n)}_{S,1,1,l_{SE}} \neq 0\} \implies Pr\{c^{(n)}_{S,1,1,l_{SE}} = 0\} = 1 - \sum_{k=1}^{K-1} Pr\{c^{(n)}_{S,1,1,l_{SE}} = k\}$

Appendix K

Proof of Eq. (4.7)

- *For $a = 1$:*

  According to the considered channel scheduling algorithm, a particular channel is allocated to the UE with the highest channel state. If there are multiple UEs with the highest channel state, one of these UEs is randomly selected and allocated with the channel. In other words, the probability that a given UE is allocated with a particular channel assuming that this UE has the highest channel state in that particular channel at a given time slot is: $\frac{1}{\#\textit{of UEs having the highest channel state}}$.

  Therefore, the conditional probability $\Pr\{u^{(n)}_{\mathrm{S},j,i,1} = a \mid c^{(n)}_{\mathrm{S},j,i,1} = k, \cdots, c^{(n)}_{\mathrm{S},j,i,U_{\mathrm{SM}}} = k_{eU_{\mathrm{SM}}}, s^{(n)}_{\mathrm{S},j,i,1} = k_{s1}, \cdots, s^{(n)}_{\mathrm{S},j,i,U_{\mathrm{S}}} = k_{sU_{\mathrm{S}}}\}$ is given by:

$$\begin{aligned}&\Pr\{u^{(n)}_{\mathrm{S},j,i,1} = a \mid c^{(n)}_{\mathrm{S},j,i,1} = k, \cdots, c^{(n)}_{\mathrm{S},j,i,U_{\mathrm{SM}}} = k_{eU_{\mathrm{SM}}}, s^{(n)}_{\mathrm{S},j,i,1} = k_{s1}, \cdots, s^{(n)}_{\mathrm{S},j,i,U_{\mathrm{S}}} = k_{sU_{\mathrm{S}}}\}\\ &= \begin{cases} \frac{1}{1+f_k(k_{s1})+\cdots+f_k(k_{sU_{\mathrm{S}}})+f_k(k_{e2})+\cdots+f_k(k_{eU_{\mathrm{SM}}})}, 0 \le k_{s1}, \cdots, k_{sU_{\mathrm{S}}}, k_{e2}, \cdots, k_{eU_{\mathrm{SM}}} \le k \\ 0, \qquad\qquad \text{otherwise.} \end{cases}\end{aligned} \tag{K.1}$$

  As a result, the probability $\Pr\{u^{(n)}_{\mathrm{S},j,i,1} = a \mid c^{(n)}_{\mathrm{S},j,i,1} = k\}$ can be calculated by summing the conditional probabilities as follows:

$$\Pr\{u^{(n)}_{\mathrm{S},j,i,1} = a \mid c^{(n)}_{\mathrm{S},j,i,1} = k\} = \sum_{k_{s1}=0}^{k} \cdots \sum_{k_{sU_{\mathrm{S}}}=0}^{k} \sum_{k_{e2}=0}^{k} \cdots \sum_{k_{eU_{\mathrm{SM}}}=0}^{k}$$
$$\left(\frac{1}{1+f_k(k_{s1})+\cdots+f_k(k_{sU_{\mathrm{S}}})+f_k(k_{e2})+\cdots+f_k(k_{eU_{\mathrm{SM}}})} \prod_{l_{\mathrm{S}}=1}^{U_{\mathrm{S}}} \Pr\{s^{(n)}_{\mathrm{S},j,i,l_{\mathrm{S}}} = k_{sl_{\mathrm{S}}}\} \prod_{l_{\mathrm{SE}}=2}^{U_{\mathrm{SM}}} \Pr\{c^{(n)}_{\mathrm{S},j,i,l_{\mathrm{SE}}} = k_{el_{\mathrm{SE}}}\}\right).$$

- *For $a = 0$:*

$$Pr\{u^{(n)}_{S,j,i,1} = a \mid c^{(n)}_{S,j,i,1} = k\} = 1 - Pr\{u^{(n)}_{S,j,i,1} = 1 \mid c^{(n)}_{S,j,i,1} = k\}.$$